Development of recombinant immunotoxins targeting overexpressed cell surface biomarkers trophoblast cell-surface antigen 2 and mesothelin for cervical cancer treatment.

Dissertation submitted in fulfilment for the degree of

Master of Science (Medicine)

Sizalobuhle Masuku

Supervisor

Prof. Dr. Dr. Stefan Barth

Medical Biotechnology and Immunotherapy Research Unit

Institute of Infectious Disease and Molecular Medicine

SARChI Chair in Cancer Biotechnology

Department of Integrative Biomedical Sciences

Faculty of Health Science

February 2025

Plagiarism Declaration

I, **Sizalobuhle Masuku** hereby declare that the work in this dissertation is my original work except where acknowledgements indicate otherwise. I know that Plagiarism is wrong. Plagiarism is to use ideas or work from another source as your own. Neither the substance nor any part of this dissertation has been in the past, currently being, or is to be submitted for a degree at this University, or any other university other than this Master of Science at the University of Cape Town. Each significant contribution to, and quotation in this thesis from the works of other authors and collaborators has been attributed, cited, and referenced.

This dissertation has been submitted to the Turnitin module. I empower the University of Cape Town authority to reproduce the content of this dissertation, for the purpose of research.

Signature: Signed by candidate

Date : 17 February 2025

Acknowledgments

First and foremost, I give all glory and honour to God, whose grace, love, and unfailing guidance have carried me through this journey. Without His strength, I would not have reached this milestone, and for that, I am deeply grateful.

I extend my deepest gratitude to Prof. Stefan Barth for his invaluable mentorship, unwavering support, and wealth of knowledge. His guidance has shaped my growth as a researcher and inspired me to push myself beyond my limits.

I want to express my gratitude to the Sturrock, Blackburn, H3D, and MCB research groups for generously allowing me to use their equipment. Your support has been instrumental in the success of my research.

To Prof. Dirk, I cannot express enough gratitude for your patience, encouragement, and willingness to go the extra mile. Your guidance in capturing beautiful images during my binding assays made a significant difference.

A special thank you to Marc, Emmanuel, Dr. Dogbey, and Dr. Lekena; you have been nothing short of amazing. Your constant assistance brings joy and light during dark times, along with encouragement and unwavering support that kept me going, especially through the most challenging moments in my research. I deeply appreciate your kindness and motivation.

To everyone in MB&I, meeting and working alongside such brilliant and kind-hearted individuals has truly been a privilege. You made the lab feel like a welcoming home.

To my dear friends Amanda, Tatenda, Munyaradzi, Siko, Jabu, and Nontokozo, thank you for being my pillars of strength. Through the highs and lows of this journey, you stood by me in different ways that enabled me to stay sane and gave me strength. You also shared the heavy load of navigating motherhood and research work. Thank you for your support, love, and encouragement; they have meant the world to me.

To my beloved family, Rejoice, Everjoy, Ndabezinhle, and my mother, Nigel Masuku, thank you for your unwavering love and financial support. Your faith in me provided the strength to persevere.

To my beloved daughter, Nina, thank you for your understanding, patience, and for allowing Mama to complete her research studies. Your love has been my greatest motivation, and I dedicate this achievement to you. We accomplished this together!

Dad, I wish you were still here to witness this moment. I miss you deeply, and your memory continues to inspire me every day.

Finally, I would like to express my gratitude to the National Research Foundation (NRF) for their financial support, which made this research possible.

List of Abbreviations

ADC	Antibody-drug conjugate
CDR	Complementary determining region
CIN	Cervical Intraepithelial Neoplasia
CV	Column Volume
DTT	Dithiothreitol
ETA	*Pseudomonas* Exotoxin A immunotoxin
Fab	Antigen binding fragment
FBS	Foetal bovine serum albumin
FP	Fusion protein
HPV	Human papillomavirus
His	Histidine
HIV	Human Immunodeficiency Virus
HRP	Horseradish peroxidase
IEC	Ion-exchange chromatography
Ig	Immunoglobulin
IMAC	Immobilised metal affinity chromatography
LB	Luria – Bertani
MB&I	Medical Biotechnology and Immunotherapy Research Unit
MWCO	Molecular weight cut off
NEB	New England Biolabs
ORF	Open reading frame
PBS	Phosphate-buffered saline
PVDF	Polyvinylidene difluoride

Rcf	Relative centrifugal force
RPMI	Roswell Park Memorial Institute (Medium)
ScFv	Single chain variable fragment
SDS	Sodium dodecyl sulphate
SDS -PAGE	Sodium dodecyl sulphate polyacrylamide gel electrophoresis
SEC	Size exclusion chromatography
SOC	Super Optimal Broth with Catabolite repression
TAA	Tumour-associated antigen
TBS-T	Tris-buffered saline – Tween
TCR	T-cell receptor
VH	Variable heavy chain
VL	Variable light chain
WHO	World Health Organisation

List of Figures

Figure 1.1: Cervical cancer estimated cumulative risk (%) **2**
Figure 1.2: HPV genome and virion structure **6**
Figure 1.3: Schematic diagram demonstrating the progression of cervical cancer **8**
Figure 1.4: The signalling pathways that are activated by mesothelin **15**
Figure 1.5: Structure of a complete antibody and an scFv antibody fragment **20**
Figure 1.6: The progression of immunotoxin development over three generations **. 22**
Figure 1.7: ETA Structural and functional domains of the *Pseudomonas* exotoxin A **..... 24**
Figure 1.8: *Pseudomonas* exotoxin A (PE) mechanism of action **26**
Figure 1.9: Study workflow..... **31**
Figure 3.1: Plasmid maps showing the molecular cloning process and key features of the pMT-ETA and pUC57- vector **52**
Figure 3.2: Plasmid maps showing the molecular cloning process and key features of the pMT-dETA and pUC57- vector..... **54**
Figure 3.3: Cloning of the anti-MSLN (scFv) and anti-TROP2 (scFv) genes into pMT-ETA and dETA plasmids..... **56**
Figure 3.4: Confirmation of selected colonies to contain the pMT-anti-MSLN (scFv)-ETA/dETA and pMT-anti-TROP2(scFv)-ETA/dETA plasmids by restriction endonuclease mapping **59**
Figure 3.5: SDS-PAGE analysis of the anti-MSLN rITs expression and extraction **. 61**
Figure 3.6: SDS-PAGE and western blot analysis of purified rITs following 2-step IMAC purification **63**
Figure 3.7: Estimation of TROP2(scFv)-dETA and ETA using densitometry..... **64**
Figure 3.8: Fixed cell imaging using a confocal microscope **67**
Figure 3.9: Dose-response curves **69**

List of Tables

Table 2.1: pMT expression vector critical features and their function **34**

Table 2.2: Agarose gel and buffer recipes **38**

Table 2.3: Restriction digestion reaction mixture of pU57 and pMT-(scFv)-dETA/ETA **39**

Table 2.4: Ligation reaction setup **40**

Table 2.5: First IMAC purification **43**

Table 2.6: Second IMAC purification **44**

Table 2.7: 10% SDS PAGE composition **45**

Table 2.8: The components for the conjugation of the anti-His-Alexa-Fluor-488 to rIT **48**

Table 3.1: Quantification of plasmid DNA concentrations following a midi prep **55**

Table 3.2: *E. coli* colonies transformed with pMT-MSLN-ETA/dETA and pMT-TROP2-ETA/dETA **57**

Table 3.4: Protein quantification and yields of bacterially expressed recombinant immunotoxins **65**

Table 7.1: Equipment used for the experimental process of this study **124**

Table 7.2: The composition of media used for bacterial transformation in molecular cloning **126**

Table 7.3: Restriction digestion of pUC57 and pMT-“x”(scFv)-dETA/ETA **127**

Table 7.4: Buffer recipes and composition for agarose gel electrophoresis **127**

Table 7.5: Reaction reagents for ligation of the scFv inserted into the pMT-scFv-ETA/dETA vector **127**

Table 7.6: Restriction mapping reagents **128**

Table 7.7: *E.coli* strain used for the entire **129**

Table 7.8: Buffer recipes for bacterial expression **129**

Table 7.9: First IMAC purification buffers recipes..... **130**

Table 7.10: Second IMAC purification buffer recipes..... **131**

Table 7.11: Cell lines for in vitro studies..... **131**

Table 7.12: Reagents for conjugation of the anti-His PE antibody Fluorophore to an rIT..... **132**

Table 7.13: Reagent and equipment for rIT functionality testing **132**

Abstract

Cervical cancer is a devastating disease that raises significant health concerns in Sub-Saharan Africa. In South Africa, cervical cancer is considered the second most common cause of cancer-related deaths, with high incidence rates. The disease is strongly linked to persistent infection by high-risk strains of the human papillomavirus (HPV). Despite the availability of HPV vaccines and early detection methods such as Pap smears and HPV testing, many women remain undiagnosed or only receive treatment in advanced stages of the disease in low- and middle-income countries (LMIC). The high costs associated with cervical cancer screening and the ineffectiveness of current conventional treatments, which often result in severe side effects, exacerbate this public health crisis. Addressing these challenges necessitates innovative therapeutic approaches, such as recombinant immunotoxins, which may offer targeted treatment options with reduced side effects compared to traditional therapies.

In this study, we focused on developing a target-specific next-generation recombinant immunotoxin (rIT) to improve treatment outcomes. The rITs were targeting cell surface biomarkers, Trophoblast cell surface antigen 2 (TROP2) and mesothelin (MSLN), which are overexpressed in cervical cancer cells. Targeting TROP2 and MSLN presents a promising therapeutic approach. The study aimed to develop novel recombinant anti-TROP2 and anti-MSLN immunotoxin candidates based on truncated *Pseudomonas* exotoxin A (ETA) or its deimmunized version (dETA) with an R456T point mutation to compare their cytotoxicity activity towards cancer cells.

ETA represents the wild type (wt) of *Pseudomonas* exotoxin A, a highly cytotoxic protein toxin produced by a bacterium that inhibits protein synthesis in host cells leading to cell death. dETA version of ETA being the modified form of the toxin generated using a supercomputing-based molecular dynamics simulation model to identify point mutations that minimize the risk of an immune response in patients while maintaining the cytotoxic activity of the wild type (wt) ETA.

In this study, to generate anti-TROP2/MSLN-specific rIT, corresponding single-chain antibody fragment (αTROP2/MSLN (scFv)) genes were cloned into either a pMT ETA or dETA expression vectors to create pMT-TROP2/MSLN-ETA/dETA constructs. The constructs were expressed under osmotic stress in the presence of compatible solutes

in *Escherichia coli* (BL21 DE3) cells. The rITs were extracted using sonication in a lysis buffer with protease inhibitors to recover soluble active proteins. Once expression was confirmed, purification was performed using two-step immobilized metal affinity chromatography (IMAC) and quantified. Purified proteins were characterized by sodium dodecyl-sulfate polyacrylamide gel electrophoresis (SDS-PAGE) and western blot analysis.

The rITs were subsequently tested for their ability to bind to antigen-positive cervical cancer cell lines, and their cytotoxic effects were evaluated. The results of this study demonstrated that such difficult-to-express rITs can be successfully generated using the unique periplasmic stress expression protocol. This was illustrated by the SDS- PAGE results from the first IMAC purification showing full-length protein of anti- TROP2(scFv)-ETA, anti-TROP2(scFv)-dETA, anti-MSLN(scFv)-ETA, and anti- MSLN(scFv)-dETA at around 72 kDa. Despite initial success in purifying the MSLN rITs using IMAC, significant degradation of both anti-MSLN(scFv)-ETA and anti- MSLN(scFv)-dETA during the second purification limited their further characterisation. Future work needs to be conducted to reduce degradation.

In contrast, the TROP2 rIT average protein yield from a 2L culture volume was calculated to be approximately 1.66 and 3.735 mg of anti-TROP2(scFv)-ETA and anti-TROP2(scFv)-dETA, respectively and these purified proteins demostrated excellent performance in downstream functionality assays. Both anti-TROP2(scFv)-ETA and anti-TROP2(scFv)-dETA showed strong antigen-dependent binding and internalisation, which were confirmed by confocal microscopy. Furthermore, cytotoxicity results demonstrated dose-dependent killing of target cervical cancer cells. The anti-TROP2(scFv)-ETA (wild type) showed greater cytotoxicity activity than the anti-TROP2(scFv)-dETA, with a two-fold difference in IC_{50} values, representing an improvement in the deimmunised version compared to previous studies.

This study demonstrated the potential of recombinant immunotoxins (rITs) as a targeted strategy for treating cervical cancer in vitro, due to their specificity and cytotoxic activity against cancerous cells. However, the immunogenicity and therapeutic efficacy of the rITs described in this work still require validation through preclinical in vivo studies. Overall, the preliminary proof-of-concept experiments presented in this thesis provide a promising foundation for the development of rIT-based therapies aimed at selectively targeting and eliminating cervical cancer cells.

Table of contents

Plagiarism Declaration ..... **i**

Acknowledgments ..... **ii**

List of Abbreviations ..... **iv**

List of Figures ..... **vi**

List of Tables ..... **vii**

Abstract ..... **ix**

Table of contents ..... **xii**

1. CHAPTER 1 ..... ***1***

LITERATURE REVIEW ***1***

1.1 Cervical Cancer **1**

1.1.1 Disparities in Cervical Cancer Incidences and Mortality 1

1.1.2 The Impact of Cervical Cancer in South Africa 4

1.1.3 Types of Cervical Cancer 5

1.1.4 Aetiology of Cervical Cancer 5

1.2 Management of Cervical Cancer **8**

1.2.1 Vaccination 8

1.2.2 Diagnosis 9

1.3 Treatments **10**

1.3.1 Current Standard Treatment Options 10

1.3.2 Immunotherapy 12

1.4 Antibody-Based Cancer Immunotherapy **13**

1.4.1 Tumour Associated Antigens for Cervical Cancer Immunotherapy 14

1.4.2 Monoclonal Antibodies 17

1.5 Antibody Drug-Conjugates (ADCs) **20**

1.6 Development of Immunotoxins for Anticancer Therapy **21**

1.6.1 *Pseudomonas* Exotoxin A (ETA/PE) 23

1.6.2 The mechanism of action of the *Pseudomonas* exotoxin A (ETA) 24

1.6.3 Advances in Recombinant Immunotoxins with *Pseudomonas* Exotoxin A 26
1.6.4 SSIP Immunotoxin 27
1.6.5 SS1-LR, a second-generation recombinant immunotoxin 27
1.6.6 Deimmunised *Pseudomonas* exotoxin A (dETA) -rIT Comparison with Native *Pseudomonas* exotoxin A (ETA) 29
1.7 Study Rationale 30
1.8 Study aims and objectives 30
1.8.1 Aim 30
1.8.2 Objectives 31
2 CHAPTER 2 33
MATERIALS AND METHODS 33
2.1 *In silico* cloning of antibody toxin formats 33
2.2 Molecular cloning 35
2.2.1 Plasmid transformation into competent bacterial cells. 35
2.2.2 Plasmid extraction method (Nucleobond® xtra midi) 36
2.2.3 Plasmid restriction digest 37
2.2.4 Agarose gel electrophoresis 37
2.2.5 Gel extraction of the digested product 39
2.2.6 Ligation of the DNA fragments 39
2.2.7 Restriction mapping and sequencing analysis 40
2.3 Periplasmic protein expression under osmotic stress 41
2.4 Protein extraction by sonication 41
2.5 Protein purification using immobilised Metal Affinity Chromatography 42
2.5.1 IMAC-I 42
2.5.2 IMAC-II 43
2.6 Protein Characterisation 44
2.6.1 SDS-PAGE 44
2.6.2 Concentration of full-length fusion protein 45
2.6.3 Western blotting 45

2.6.4 Quantification of purified proteins..... 46

2.7 Functionality assessment of the full-length protein 46

2.7.1 Culturing of Cervical Cancer Cell Lines 46

2.7.2 Binding analysis of fixed cell using confocal microscopy 47

2.7.3 Cytotoxicity Assay..... 48

3 CHAPTER 3..... 50

RESULTS..... 50

3.1 In silico design of anti-TROP2(scFv) and anti-MSLN (scFv) into bacteria expression vectors..... 50

3.1.1 *In silico* design of plasmids coding for ETA..... 51

3.1.2 In silico design of plasmids coding for dETA..... 53

3.2 Molecular cloning of anti-TROP2(scFv) and anti-MSLN (scFv) into pMT-ETA or dETA 54

3.2.1 Ligation of anti-TROP2(scFv)-ETA/dETA, anti-MSLN (scFv)-ETA/dETA56

3.3 Restriction mapping of cloned products 57

3.4 Protein expression and solubility analysis by SDS-PAGE 60

3.5 Protein purification and Characterisation 61

3.6 Protein quantification using densitometry..... 64

3.7 Binding assessment using confocal microscopy 65

3.8 Cytotoxicity studies 68

4 CHAPTER 4..... 71

DISCUSSION 71

4.1 Cervical Cancer: The Urgent Need for Effective Treatments..... 71

4.2 Use of the stress-induced periplasmic expression and production of rITs in *E. coli*..... 72

4.3 Production and Purification of functional rITs 74

4.4 Functional activity of anti-TROP2(scFv)- rITs on cervical cancer cell lines 78

4.4.1 Binding activity and Internalization studies 78

4.4.2 Cytotoxic activity of anti-TROP2(scFv)-ETA/dETA 79

5 CHAPTER 5..... 83

CONCLUSION AND FUTURE WORK 83

REFERENCES 85

6 APPENDIX 124

6.1 Materials..... 124

6.2 Consumable..... 124

6.2.1 Equipment 124

6.2.2 Molecular Cloning Reagents..... 126

6.2.3 Bacterial strains 128

6.3 Protein expression 129

6.4 Protein purification 130

6.5 Functionality assay 131

CHAPTER 1

LITERATURE REVIEW

1.1 Cervical Cancer

1.1.1 Disparities in Cervical Cancer Incidences and Mortality

Globally, cervical cancer ranks as the fourth most common cancer among women, with an estimated 604,127 new cases and 341,831 deaths in 2022 [1],[2]. Notably, 80% of women who died from cervical cancer that year were from developing countries. These alarming statistics emphasize the seriousness of this disease and highlight the urgent need for widespread awareness, early detection, and enhanced prevention strategies. As a preventable cancer, its impact is particularly severe in resource-constrained areas, where access to essential screening, vaccination, and treatment services is limited [3].

Cervical cancer presents a particularly severe burden in sub-Saharan Africa, where age-standardized incidence and mortality rates rank among the highest globally, as illustrated in **Figure 1.1** [4]. This disparity arises from several interrelated factors, including systemic healthcare obstacles, social issues, and limited access to preventive services [5]. A primary factor contributing to the high incidence of cervical cancer in this region is the limited availability and uptake of the human papillomavirus (HPV) vaccine, which protects against infection by the high-risk human papillomavirus (HR-HPV) strains that cause many cervical cancers. Vaccination programs in sub-Saharan Africa frequently encounter logistical challenges, such as insufficient healthcare infrastructure, low public awareness, and a lack of local vaccine manufacturing facilities. Consequently, many women in the region are unable to benefit from the protective effects of vaccination [6].

Furthermore, there is a significant gap in cervical cancer screening programs across sub-Saharan Africa [7]. Screening methods, such as Pap smears and HPV testing, are critical for early detection when treatment is most effective. However, these services are non-existent in many parts of the region, primarily due to the lack of trained healthcare professionals, limited access to medical facilities, and financial

barriers [8]. Therefore, many women are diagnosed at advanced stages of the disease when the cancer has often metastasized, drastically reducing their chances of survival.

The socio-economic factors further exacerbate the issue. In sub-Saharan Africa, women face numerous challenges, including limited access to education, low awareness of cervical cancer, and cultural factors that may discourage seeking medical assistance. Combined with the burden of other health crises, such as infectious diseases like HIV/AIDS, which increases susceptibility to HPV infections, these challenges complicate the implementation of effective preventive measures [9], [10]. Central America and Southeast Asia, which are also low- and middle-income regions, show high cervical cancer mortality rates, as illustrated in **Figure 1.1.** Similar to sub-Saharan Africa, these regions face difficulties in establishing effective vaccination programs, screening services, and treatment strategies [8]. Consequently, increased mortality and incidence rates are observed [11].

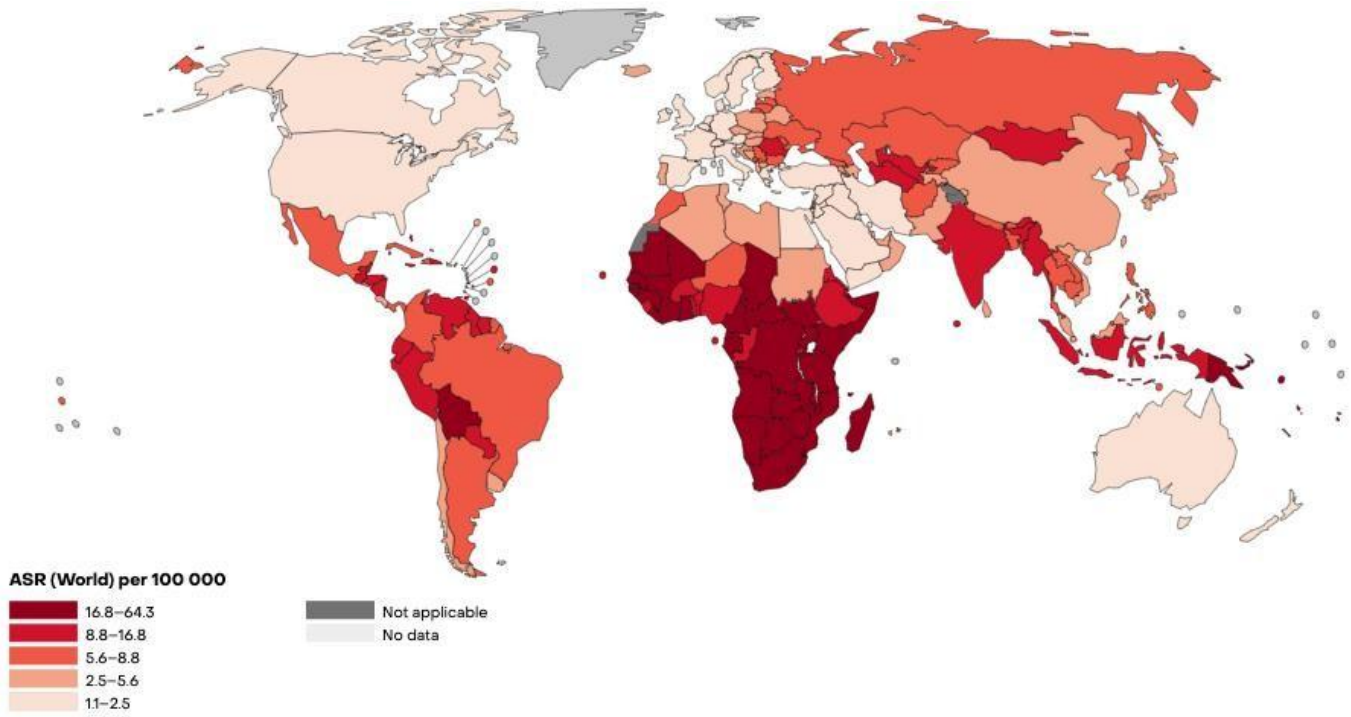

Figure 1.1: Cervical cancer estimated cumulative risk (%), mortality rate of females aged between 0 – 74 years old in 2022. Data from WHO, Global Cancer Observatory [2].

Addressing cervical cancer in its later stages, particularly once it has metastasized, remains a significant challenge. While treatment options are available for early-stage cervical cancer, the scarcity of affordable and effective treatments for metastatic cervical cancer is a growing concern. As more women receive late diagnoses due to limited access to screening, the demand for advanced therapies that can address metastasis becomes even more urgent. Current treatments, such as chemotherapy, radiation, and surgery, are often inaccessible for many women in resource-limited settings because of their high costs, limited availability, and the shortage of trained medical personnel to administer them. Furthermore, these treatments are frequently less effective in managing cervical cancer metastasis, significantly diminishing the chances of survival for patients with advanced-stage disease. The limited effectiveness of current therapies in preventing and treating metastatic spread underscores the pressing need for accessible, targeted treatments that can enhance outcomes and reduce mortality in underserved populations[12].

The COVID-19 pandemic further worsened efforts to address the global cervical cancer burden. As healthcare systems became overwhelmed, essential screening, vaccination, and treatment services were disrupted, exacerbating existing inequities in cervical cancer prevention and care [13]. The pandemic also put additional strain on already fragile healthcare systems in low- to medium-income countries (LMIC), delaying the implementation of life-saving interventions. This resulted in a backlog of undiagnosed cases and postponed treatments, especially in regions like sub-Saharan Africa, where access to healthcare was already limited [13].

Moreover, the pandemic highlighted the pressing need for local scientists to conduct more targeted research addressing the specific needs of affected populations, particularly in regions like Africa that are already grappling with limited healthcare infrastructure and insufficient medical personnel. The delay in the rollout of COVID-19 vaccines in Africa, due to the lack of local manufacturing capacity and constrained resources, serves as a stark reminder of the broader systemic challenges that must be overcome. [10], [11]. In response to these challenges, increased government intervention to provide necessary funds and resources is crucial to address these gaps [14]. Investments in healthcare infrastructure, research, and training are critical to improving cervical cancer prevention. Additionally, the development and dissemination of affordable treatment options for late-stage cervical cancer particularly those

targeting metastasis, will be vital to improving survival rates and reducing the global mortality burden. Ensuring that all women, regardless of their geographic or economic circumstances, have access to the full spectrum of cervical cancer care [15].

1.1.2 The Impact of Cervical Cancer in South Africa

Cervical cancer is the second most common cancer in South Africa and, tragically, the leading cause of cancer-related deaths among women, with an estimated 5,000 deaths annually [15], [16]. The burden of this disease is disproportionately high due to unequal healthcare resource distribution between the public and private sectors [17]. While the well-developed private sector provides high-quality care to the wealthy and insured population, the public sector struggles with inadequate resources. This disparity limits access to preventive screenings, early detection, and timely treatment for women in disadvantaged communities, leading to a high rate of late-stage diagnoses and mortality [18].

South Africa is the global epicenter of the HIV/AIDS epidemic, with an estimated 8 million people living with HIV as of 2022 [19]. People living with HIV have weakened immune systems, making them more vulnerable to HR-HPV infections that can lead to the development of cervical cancer [20]. The HPV vaccine was introduced on the global market in 2006, but was only made available to South Africa in 2014, albeit the cost of it was still significantly high [21]. The HPV vaccine is currently priced at around ZAR 700-1000 per dose when procured through the private sector [3], [21], making it out of reach for many in the country's poor and vulnerable populations. However, the Global Vaccine Alliance (GAVI) has helped provide funding and support to improve access to the HPV vaccine in LMICs. [21], [22]. South Africa does not receive direct financial support from GAVI for vaccine programs, it collaborates with GAVI in several areas, such as technical support and vaccine procurement. South Africa's middle-income status means it primarily funds its immunization programs independently but may benefit from global vaccine initiatives and partnerships facilitated by GAVI. This has included negotiating lower prices with vaccine manufacturers and working with national governments to integrate the HPV vaccine into their routine immunization programs.

Despite these efforts, the cost of the vaccine remains a significant barrier, especially for the country's poor and vulnerable populations who are disproportionately affected by HIV and cervical cancer. Strengthening the capacity of the public healthcare system, investing in training and deploying more healthcare professionals, and implementing targeted interventions to reach marginalized communities can help reduce disparities in cervical cancer outcomes.

1.1.3 Types of Cervical Cancer

Cervical cancer is a complex and multifaceted disease that affects the cervix, the lower part of the uterus that connects to the vagina [23]. This is a type of cancer that originates from the epithelial cells that line the cervix. The disease is classified into two main subtypes: adenocarcinoma, which develops from the glandular cells in the endocervix, the inner part of the cervix, and squamous cell carcinoma, which originates from the flat, thin squamous cells in the ectocervix, the outer part of the cervix [24]. The transformation zone, where the endocervix and ectocervix meet, is a particularly vulnerable region where cancerous transformations often initiate [25], [26]. This vulnerability is attributed to the higher levels of proliferation markers, susceptibility to dysplastic differentiation, and increased invasion capabilities observed in this region. This disease tends to stay within the pelvic region before potentially spreading to distant organs [27]. This process can take years to decades, providing a critical window for early detection and treatment through regular screening and HPV tests to prevent the progression of the disease [9].

1.1.4 Aetiology of Cervical Cancer

Cervical cancer is strongly associated with persistent infection by high-risk human papillomavirus (HR-HPV). [28]. Approximately 99% of cervical carcinomas are primarily associated with infection by one of the 12 HR-HPV types: HPV-16, 18, 31, 33, 35, 39, 45, 51, 52, 56, 58, and 59 [29]. However, other factors can also contribute to the development of cervical cancer, including lifestyle factors (like smoking) and reproductive factors (such as long-term use of oral contraceptives), which account for the remaining 1% of cervical cancer cases [30], [31]. HPV is a highly prevalent viral infection that affects a significant portion of the sexually active population. While most

HPV infections are temporary and resolve within a couple of years, a substantial portion, estimated to be between 10-20%, can persist without symptoms [32]. This persistent HPV infection is the primary driver of disease progression and the eventual cause of invasive cancer [33].

HPV is a non-enveloped, icosahedral, double-stranded DNA virus measuring 52-55 nm in diameter, with a genome approximately 8,000 base pairs long, as shown in **Figure 1.2** [32]. The circular DNA of all papillomaviruses is divided into three unequal segments: the early proteins, the late proteins, and the long control regions. HPV gene expression is polycistronic, meaning it can initiate multiple promoters at various stages of its life cycle [34]. These promoters are vital for the transcription of viral genes within the infected host. The expression of the E6 and E7 oncoproteins, which are essential for disrupting cell cycle regulation and promoting cellular transformation, is crucial for developing cervical cancer.

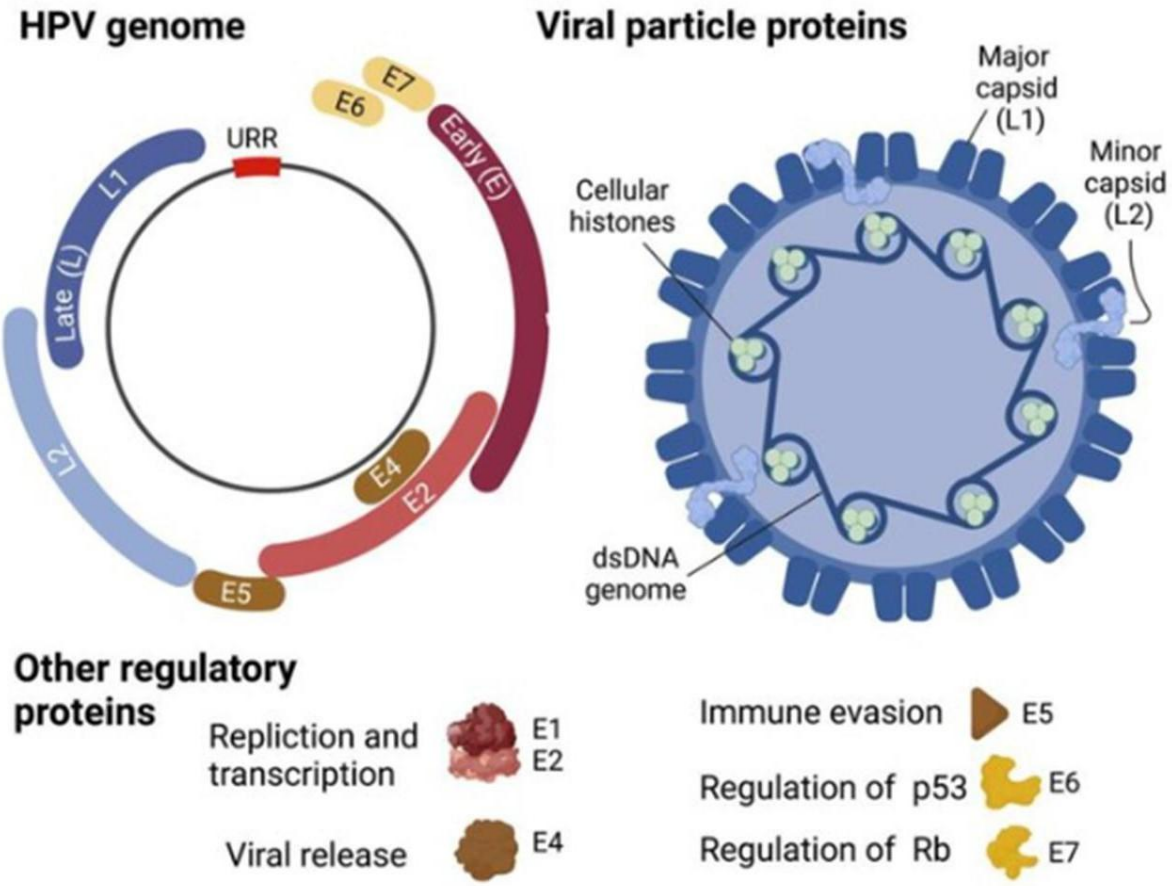

Figure 1.2: HPV genome and virion structure. Created with BioRender.com (accessed on 21 November 2024) adapted from a 2022 paper [35], [36].

Following entry into the host cell through lesions or micro-abrasions of the epithelium, the HPV genome interacts with specific receptors, such as α-6 integrin [37], to facilitate entry into the host cell. In typical infections, the viral genome does not immediately integrate into the host genome but rather exists as an episome (a circular DNA form of the viral genome), as shown in **Figure 1.3.** This progression from initial infection to integration and potential cancer development can span years or even decades. The early viral proteins, E1 and E2, play critical roles in supporting viral genome replication. E1 functions as a viral helicase, unwinding the double-stranded DNA of HPV, a necessary step for both replication and transcription [38]. E2 is a multifunctional protein that acts as a transcription factor, regulating the expression of viral genes, including E6 and E7. In cases of persistent infection, as illustrated in **Figure 1.3**, the viral genome eventually integrates into the host cell DNA. This integration often disrupts the function of the E2 gene, resulting in uncontrolled expression of E6 and E7 [39], [40].

The E6 viral protein interacts and binds to the p53 protein (a tumour suppressor gene) found in the host cells, also known as the guardian of the genome. It is found in the nucleus of cells and plays a key role in controlling cell division and cell death. Once bound, it forms a complex formation that leads to the modification of p53, and it marks it for degradation by proteasome. This allows the infected cell to evade apoptosis and divide uncontrollably. Furthermore, the E7 protein binds to the retinoblastoma protein (Rb), disrupting cell cycle regulation of the host cells and promoting cellular proliferation [41]. E6 and E7 manipulate the cell environment to facilitate viral replication and interact with several cellular proteins [39].

The L1 protein forms the major structural component of the viral capsid (the outer shell of the virus particle) and is responsible for the encapsidation of the viral genome. The L2 protein assists in the packaging of the viral DNA into the capsid and plays a role in the virus's entry into the new host cell. These late proteins are expressed in the upper layers of the epithelium, where the virus completes its replication cycle. Newly formed virions are released from the epithelium as infected cells slough off, allowing the virus to metastasize to the next host's cells [42]. Highly immunogenic virions are synthesized at the upper layers of the epithelia as they are a limited immune system surveillance [43].

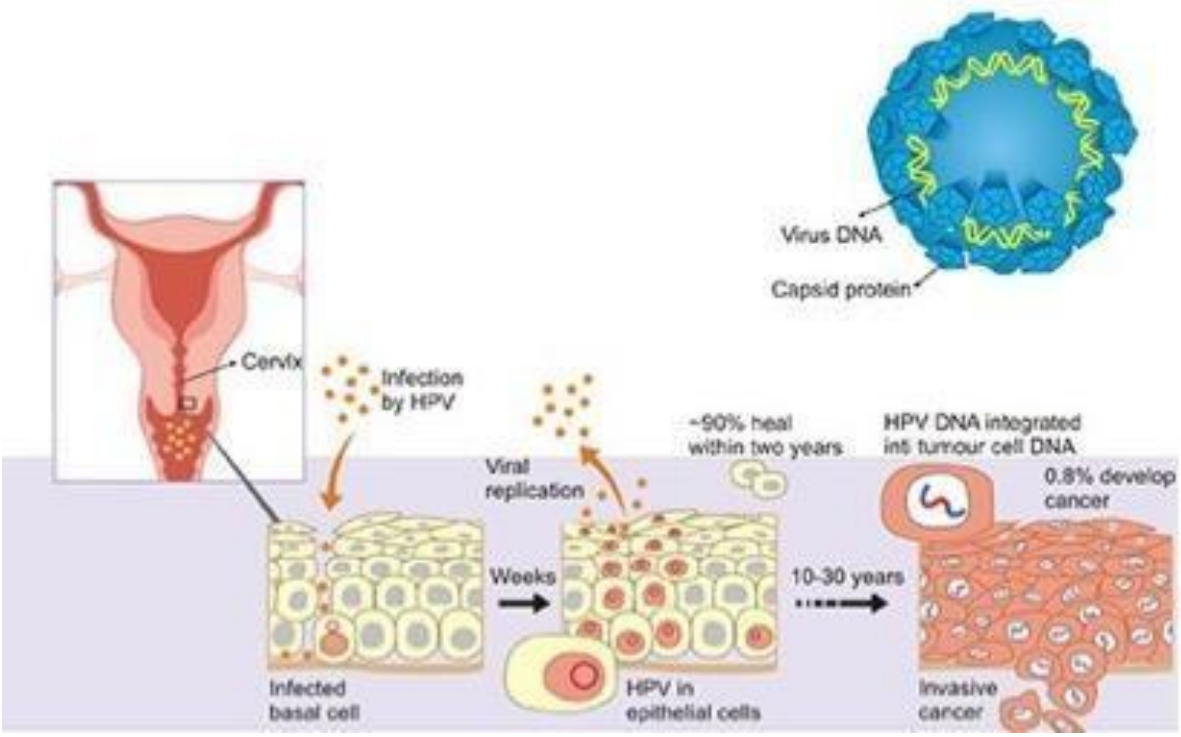

Figure 1.3: Schematic diagram demonstrating the progression of cervical cancer. Highlighting changes in both the structure of HPV DNA and cervical tissue. Derived from the Nobel Committee for Physiology or Medicine 2008 accessed November 2024 [44].

1.2 Management of Cervical Cancer

1.2.1 Vaccination

The HPV vaccine has been instrumental in preventing cervical cancer by targeting the underlying viral cause as part of active immunotherapy approaches [45]. Currently, there are three FDA-approved immunotherapeutic vaccines to prevent HPV infection [46]. Namely, the bivalent (CERVARIX®), quadrivalent (GARDASIL®), and nonvalent (GARDASIL®9) HPV vaccine types have demonstrated high efficacy in preventing HPV infection and precancerous cervical lesions [47]. The current HPV vaccines use virus-like particles made from HPV surface components. These particles resemble the real virus but lack its DNA, so they cannot cause infection. Yet, they still strongly stimulate the immune system to produce antibodies that are effective against the actual virus [48].

The GARDASIL vaccine is produced using a yeast system, which is typically a more cost-effective manufacturing method than the insect cell-based production utilized for the CERVARIX vaccine. This difference in production methods contributes to the cost discrepancies [49].

While HPV-related cellular changes and cancers take years to develop, recent clinical trials and population-based data have demonstrated that vaccines significantly reduce the risk of precancers and cancers of the cervix, vagina, and vulva in vaccinated women [49]. Vaccination is recommended for girls and boys starting at ages 9 to 14, as the vaccines are most effective when administered before exposure to HPV [36]. Although HPV vaccines do not prevent other sexually transmitted diseases or treat existing HPV-related conditions, their introduction has resulted in a significant decrease in HPV infection and related precancerous cervical lesions among vaccinated populations. However, vaccination rates remain suboptimal in many countries, likely due to high costs and other barriers that limit access [50], [51].

1.2.2 Diagnosis

Regular screening methods, such as Pap smears (to test cervical cancer) and HPV testing (to test for the presence of the virus), are effective in identifying pre-cancerous changes and early-stage cervical cancers before they progress [52], [53]. Cervical cancer often remains asymptomatic in its initial stages, with symptoms typically arising only as the disease advances. These may include abnormal vaginal bleeding, unusual discharge, and pelvic pain. The Pap test involves collecting cells from the cervix and examining them under a microscope [53], allowing for detection of abnormal changes that indicate precancerous or cancerous conditions [54]. The HPV DNA test uses a sample of cells from the cervix to check for signs of infection with high-risk HPVs. Molecular diagnostic instruments that can be employed include a polymerase chain reaction (PCR) machine and rapid tests like Cepheid's GeneXpert HPV, which integrates sample preparation, amplification, and detection in a single system. When used alongside Pap testing, it can identify the presence of high-risk HPV [55].

If abnormal results are found, diagnostic procedures such as colposcopy and biopsy are employed to closely examine the cervix [55]. Colposcopy uses a device known as a colposcope to magnify and illuminate the cervix and vagina, allowing the healthcare

provider to thoroughly inspect the cervical tissue. A biopsy involves taking a small sample of cervical tissue for microscopic examination. Various biopsy techniques exist, including punch biopsy, endocervical curettage, loop electrosurgical excision, and cone biopsy [56]. If cervical cancer is confirmed through diagnosis, imaging tests such as MRI, CT, or PET scans may be utilized to evaluate the stage of the disease and inform treatment decisions [57], [58]. If symptoms like spitting blood become evident, the cancer may have progressed to a more advanced stage, complicating treatment and decreasing the likelihood of successful management [59].

1.3 Treatments

1.3.1 Current Standard Treatment Options

Treatment for cervical cancer often focuses on addressing the underlying HPV-driven changes that lead to the disease. Therapeutic approaches, including surgery, radiation therapy, chemotherapy, and immunotherapy, are based on the stage and extent of the cancer's progression [60]. Treatment strategies may involve a combination of surgery, radiation, and chemotherapy.

1.3.1.1 Surgery

Surgery is the predominant technique for managing early-stage cancers, involving the physical removal of malignant tissues [61]. Various surgical procedures are employed, such as total hysterectomy, radical hysterectomy, loop electrosurgical excision (LEEP), conization, trachelectomy, and cryosurgery [62]. The choice of surgical intervention is largely dependent on the disease stage and extent of spread. Women of childbearing age may opt for conservative, fertility-preserving surgical approaches, including LEEP, conization, and trachelectomy [63]. At a more advanced stage, conservative approaches may no longer be viable [64]. Nonetheless, in low and middle-income countries, access to surgical intervention is limited due to the availability of surgeons skilled in performing the necessary radical surgical procedures as well as the lack of health facilities.

1.3.1.2 Radiotherapy

Radiotherapy is a type of cervical cancer treatment that uses high-energy (electromagnetic radiation) with deep penetration abilities to directly kill tumours by disrupting the DNA of rapidly dividing cancer cells [65]. This type of treatment can be highly effective for targeting localised and some advanced stages of cervical cancer. The three main types of radiation therapy currently employed include external beam radiation therapy (EBRT), which delivers radiation from an external machine to the targeted area; intensity-modulated radiotherapy (IMRT), which uses advanced technology to modulate the intensity of radiation beams for precise targeting while sparing surrounding healthy tissues; and brachytherapy, a technique that places radioactive sources inside or near the tumour for concentrated, localized treatment [12].

Radiation therapy is frequently combined with chemotherapy, a strategy referred to as chemoradiation, to enhance its effectiveness by sensitizing cancer cells to radiation [66]. Despite its advantages, radiotherapy is linked to potential side effects that can significantly affect patients' quality of life. These may include immediate effects such as skin toxicity, fatigue, and localized pain, along with long-term complications like damage to nearby organs (e.g., bowel and bladder), sexual dysfunction, and chronic bowel or urinary issues [67]. Therefore, while radiotherapy remains a crucial tool in cervical cancer management, careful planning and supportive care are vital to minimize its adverse effects and ensure optimal outcomes for patients [66].

1.3.1.3 Chemotherapy

Chemotherapy is an integral component of the standard cervical cancer treatment regimen[66]. It is commonly used as an adjuvant therapy following surgery when poor prognostic tumour features increase the risk of recurrence in combination with radiotherapy and as a standalone treatment for locally advanced disease [68]. Although chemotherapy is widely utilised, it can result in significant side effects since it kills both cancer cells and healthy cells [69]. This often results in nausea, hair loss, fatigue, and an increased risk of infection due to immune system suppression.

1.3.2 Immunotherapy

Immunotherapy is emerging as a promising strategy for improving cervical cancer treatment by modifying and recruiting the host immune system to target cancer cells more effectively [70]. Immunotherapy is a form of treatment that manipulates the body's immune system to selectively recognise and attack cancer cells without damaging healthy cells [71]. Unlike traditional chemotherapy, which uses powerful drugs to kill rapidly dividing cells, including healthy ones, immunotherapy enhances the body's immune system to recognise and attack cancer cells while sparing most healthy cells [72].

Several immunotherapeutic modalities have been explored for cervical cancer, each employing distinct mechanisms to modulate the immune system, such as:

i. Immune checkpoint inhibitors (ICIs) block regulatory pathways that suppress immune responses, thus reinvigorating T cells to mount an effective antitumor response [73].
ii. Chimeric antigen receptor (CAR) T-cell therapy consists of engineering T cells derived from patients to recognize and target tumor-specific antigens [74].
iii. Cancer vaccines stimulate immunity against oncogenic proteins recognised such as HPV E6 and E7[46].
iv. Monoclonal antibodies (mAbs) [75], synthetic proteins designed to selectively bind to tumour-associated antigens (TAAs), either directly eliminating malignant cells or marking them for immune destruction [71], [76].

Immunotherapeutic approaches can be broadly classified into active and passive strategies.

Active immunotherapy aims to stimulate the patient’s immune system to mount a sustained antitumor response. These include cancer vaccines [77] and Immune checkpoint inhibitors. In a phase 3 study, the immune checkpoint inhibitor pembrolizumab (Keytruda), combined with chemotherapy, significantly improved progression-free survival in patients with TNBC tumours expressing PD-L1, compared to chemotherapy alone [78]. Pembrolizumab is a monoclonal antibody that targets the PD-1 receptor, preventing its binding to PD-L1 and PD-L2 on tumour cells, allowing T cells to remain active against these tumours [79]. This form of immune checkpoint

inhibition is now approved for combination therapy in advanced TNBC patients with high PD-L1 expression [80].

Whereas passive immunotherapy involves administering ex vivo-generated immunotherapy components, such as monoclonal antibodies, to directly target and eliminate cancer cells [74]. In this study, passive immunotherapy was explored to target cervical cancer cells. It offers a more selective approach to treating cervical cancer by targeting specific characteristics of cancer cells. This type of strategy demonstrates promise in cervical cancer treatment, exemplified by the development of antibody-drug conjugates (ADCs) such as Tisotumab vedotin (TV). TV, an FDA-approved ADC, comprises an antibody targeting tissue factor conjugated to the cytotoxic agent monomethyl auristatin E (MMAE), which disrupts the microtubule network upon internalisation, leading to cell death [75]. Additionally, Bevacizumab (Avastin®), a vascular endothelial growth factor (VEGF)-targeting mAb, has been integrated into cervical cancer treatment regimens, demonstrating efficacy in inhibiting tumour angiogenesis [81].

1.4 Antibody-Based Cancer Targeted Therapy

Targeted therapies are transforming cancer treatment by selectively attacking cancer cells while sparing normal tissues [72]. These therapies offer a more specific alternative to traditional cancer treatments, focusing on increasingly personalised and precise approaches. Targeted therapy as a “magic bullet” date back to Paul Ehrlich's visionary work over a century ago, in which he conceptualised antibodies capable of selectively targeting diseased cells while sparing healthy tissues [82]. Since then, extensive research has deepened our understanding of tumour immunology, leading to the development of therapies with less harsh side effects.

A significant milestone in this field was the beginning of monoclonal antibodies (mAbs) in the 1970s, pioneered by Georges Köhler and César Milstein with their innovative mouse hybridoma technique [83]. This breakthrough allowed for the selection of specific B cells that produce antibodies, laying the groundwork for highly specific and targeted cancer therapies. However, the initial mouse-derived mAbs were highly immunogenic in patients, which led to the development of humanized or chimeric to

fully human antibodies to reduce side effects while maintaining efficacy and specificity [75]. The human antibody framework is better tolerated by the human immune system.

Circulating in the blood as key components of the immune system, antibodies identify and neutralize foreign substances [84]. Their primary function is to target antigens and trigger an immune response, recruiting molecules and cells to attack the identified antigen. This principle is leveraged in targeted therapy, which aims to identify and target tumour-associated antigens that are abundant on malignant cells but scarce in normal tissues. These tumour-associated antigens or biomarkers enable the selective targeting of cancer cells. Researchers carefully select target antigens based on expression levels, accessibility, and tumour specificity, a process that requires the utmost precision. Engineered antibodies can then effectively recognize and eradicate cancerous cells through various mechanisms [85].Tumour-associated antigens (TAAs) are targeted immunotherapies because they exhibit abnormal expression on cancer cells but limited expression in normal tissues, allowing for selective targeting of tumours [86]. This helps the immune system differentiate between healthy and cancerous cells, minimizing damage to healthy tissue.

Given this, this study has precisely selected trophoblast cell surface antigen 2 (TROP2) and mesothelin (MSLN) as antigen targets, given their overexpression in cervical cancer and potential for targeted immunotherapeutic strategies.

1.4.1 Tumour Associated Antigens for Cervical Cancer Immunotherapy

1.4.1.1 Mesothelin (MSLN)

Mesothelin (MSLN) is an attractive target for immunotherapy due to its limited expression in normal tissues and high expression in several cancers, including mesothelioma, ovarian, and cervical cancer. It plays a role in tumour growth, adhesion, and metastasis, making it an attractive candidate for targeted therapies [87]. MSLN is a glycosylphosphatidylinositol-linked cell surface glycoprotein [88]. This protein plays a crucial role in the process of epithelial-mesenchymal transition (EMT), a fundamental cellular mechanism that enables cancer cells to acquire a more migratory and invasive phenotype, ultimately facilitating metastatic spread [89]. In cervical cancer, MSLN

expression varies depending on the histological type, with higher expression observed in cervical adenocarcinomas compared to squamous cell carcinomas [90].

Moreover, the overexpression of MSLN activates the Akt, ERK1/2, and JNK pathways, promoting cell survival by suppressing pro-apoptotic proteins (Bim, Bad, Bax) and upregulating anti-apoptotic ones (Bcl-xL, Bcl-2) [91], as shown in **Figure 1.4.** These pathways also increase MMP-7 expression, facilitating migration and invasion during the epithelial-mesenchymal transition (EMT). Additionally, its interaction with CA-125 promotes tumour adhesion and spread [92],[91].

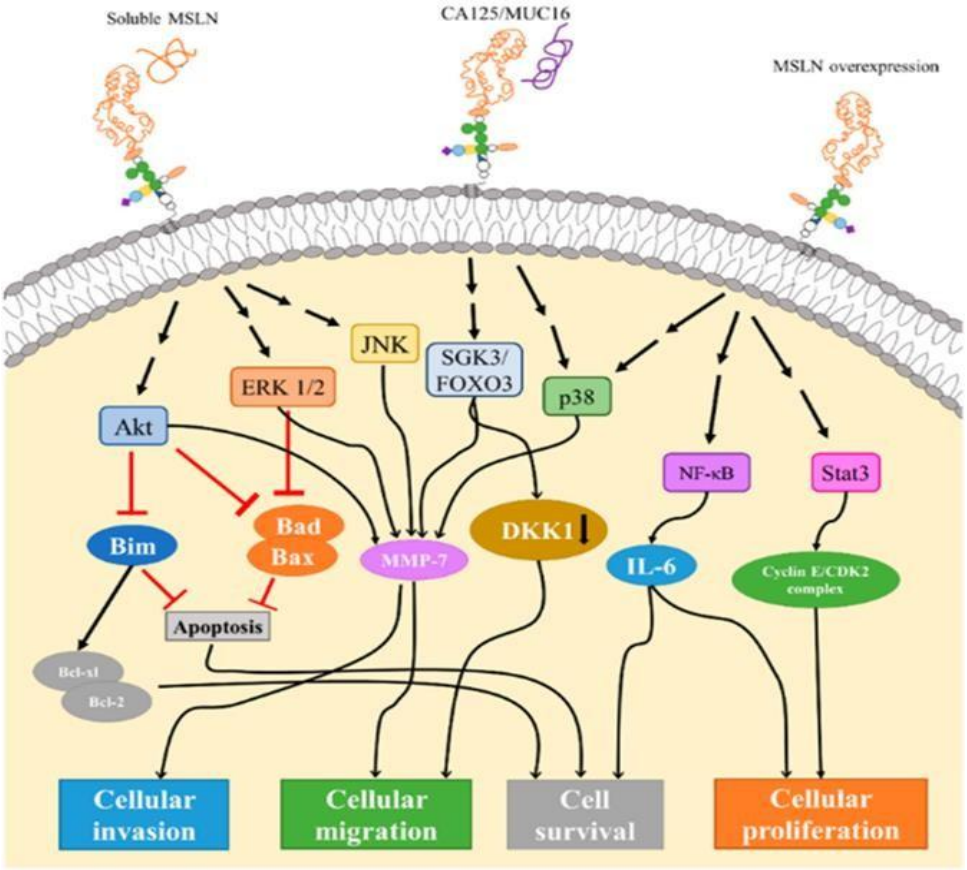

Figure 1.4: The signalling pathways that are activated by mesothelin, both in its soluble form and as a cell surface protein. This network of signalling not only supports tumour survival but also promotes EMT and tumour spread.

Clinical observations have shown that an increase in tumour burden and poor overall survival is associated with elevated MSLN expression, which may promote the migratory and invasive characteristics of cancer cells, potentially contributing to the

metastatic potential of cervical carcinomas [91]. In the discovery of MSLN, researchers noted that mutating the protein in normal tissues had no significant impact in mouse models, suggesting that MSLN does not play a critical role in normal physiological functions. This finding underscores the potential of MSLN as a selective target for immunotherapies, as targeting this antigen may mainly affect the tumour cells while sparing normal tissues [93].

1.4.1.2 Trophoblast cell surface antigen 2 (TROP2)

In recent years TROP2 has gained increasing recognition as a valuable target antigen in cancer immunotherapy. TROP2 has been extensively studied in the context of various solid cancers, including cervical cancer [94]. TROP2 is a cell-surface glycoprotein that is overexpressed in a variety of epithelial carcinomas compared to their corresponding normal tissues. The overexpression of TROP2 has been associated with increased tumour aggressiveness, metastasis, and decreased patient survival in several cancer types, highlighting its potential as a therapeutic target [95][96]. In cervical cancer, the expression of TROP2 is elevated compared to normal cervical tissue. The aberrant expression of TROP2 in cervical cancer cells has been linked to its ability to promote cell proliferation, invasion, and survival [97]. Furthermore, the nuclear translocation of the intracellular domain of TROP2 has been shown to drive self-renewal and hyperplasia in prostate cancer, suggesting a potential mechanism by which TROP2 may contribute to the neoplastic behaviour of cervical cancer cells [98].

Given the clinical evidence linking TROP2 overexpression and poor prognosis in various cancers, there has been a growing interest in exploring TROP2-targeted therapies. One of the new therapeutics targeting TROP2 antigen, is the humanized anti-TROP2 monoclonal antibody, hRS7[99]. hRS7 has demonstrated promising anti-tumour activity in preclinical studies of triple-negative breast cancer [100]. Similarly, the development of TROP2-targeting tetrakis-ranpirnase, a potent anti-tumour agent, has shown efficacy against triple-negative breast cancer models [101]. Furthermore, TRODELVY® (Sacituzumab govitecan), a TROP2-directed antibody-drug conjugate, has received FDA approval for treating certain breast and bladder cancers and is currently being investigated in clinical trials for cervical cancer [102]. The emergence

of TROP2 as a cancer antigen, with its selective expression in tumour cells and immune-privileged site in normal tissues, has further highlighted its potential as a target for immunotherapy.

1.4.2 Monoclonal Antibodies

Monoclonal antibodies (mAbs) are proteins designed to mimic the body's natural antibodies to target specific cells, including cancer cells [103]. Several techniques exist for producing mAbs, each with its own approach to generating these highly specific antibodies [104]. The most common techniques are, hybridoma technology [105] which involves engineering and producing highly specific mAbs in murine hosts, phage display technology [105][106], which involves displaying antibody fragments on the surface of bacteriophages and allowing for selection of mAbs with the desired binding properties and recombinant DNA technology [107], whereby you insert genes encoding the antibody variable regions into host cells such as bacteria, yeast or mammalian cells to produce mAbs through genetic engineering [108]. The term "monoclonal" indicates that these antibodies have identical protein sequences and, therefore, the same antigen recognition site, affinity, biological interactions, and biological effects [109]. These mAbs are designed to induce cancer cell death through various mechanisms, including direct immune-related toxicity and disruption of pathophysiological pathways in malignant cells, leading to antibody-dependent cellular cytotoxicity [109].

These immunoglobulins (Ig) are complex proteins produced by the immune system, specifically by B-cells, in response to foreign substances known as antigens. Antigens may include molecules found on the surfaces of pathogens, such as bacteria, viruses, or cancer cells [110]. Each antibody demonstrates high specificity for a particular antigen and binds to it in a lock-and-key manner [102]. Furthermore, antibodies can modulate receptor function, deliver cytotoxic payloads, or recruit additional immune cells to the tours because of their structural design.

The basic structure of an antibody comprises two heavy chains and two light chains [109]. The heavy chains of immunoglobulins are connected by disulfide bonds, and each heavy chain interacts with one of the light chains, resulting in the characteristic Y-shaped structure of antibodies. This Y-shaped configuration consists of two identical

heavy chains and two identical light chains, forming a stable and functional molecule. The structure allows for the formation of antigen-binding sites at the tips of the "Y," enabling the antibody to recognize and bind specifically to its target antigen. The flexibility of this structure also facilitates various immune responses, as it can adapt to different antigens while maintaining the integrity of the antibody's overall function.[111].

Antibodies' remarkable versatility stems from the vast diversity of their antigen-binding sites, which are generated through complex genetic mechanisms [112]. There are five main types of immunoglobulins, also known as isotypes: IgA, IgD, IgE, IgG, and IgM [110]. Each isotype differs in structure and function, contributing to the diversity and effectiveness of the immune response. IgG is the preferred subclass for the development of monoclonal antibodies [113]. This preference is due to the favourable characteristics for therapeutic applications, such as a long serum half-life [114], the ability to recruit effector cells and activate the complement system, and ease of production [115].

IgG antibodies are composed of a variable region that binds to a specific antigen and a constant region that interacts with other components of the immune system. The variable regions contain three hypervariable regions, known as complementarity-determining regions (CDRs): CDR1, CDR2, and CDR3 [116]. These regions are highly variable and play a crucial role in determining antigen-binding specificity. Among them, CDR3 exhibits the highest variability and is primarily responsible for the diversity of antibody-antigen interactions [117]. During antibody development CDRs must be carefully engineered and optimized during antibody development to enhance specificity and affinity.

Antibody engineering has progressed rapidly due to the demand for more effective and targeted therapies. The incorporation of bioinformatics tools into this field has been crucial, providing essential insights into antibody structure and function for developing novel therapeutics. By analysing structural details and binding dynamics, researchers can identify stable complexes with high target affinity. This approach is further enhanced by publicly available antibody structures and sequences in the Protein Data Bank (PDB), Patent databases which include 3D structural data from X-ray crystallography and cryo-EM studies [118].

Historically, antibody engineering has focused on improving therapeutic compatibility with the human immune system [119]. Early efforts focused on humanizing monoclonal antibodies, as the initial mouse-derived monoclonal antibodies had limited therapeutic use due to their inability to efficiently activate human effector functions and their immunogenicity, which triggered human anti-mouse antibody responses in patients. To overcome these challenges, genetic engineering techniques were developed. These advancements began with the creation of chimeric antibodies, which combined human constant regions with mouse variable domains. This was followed by CDR grafting, where mouse CDRs were transferred onto human variable regions. These developments eventually led to the production of full human antibodies with significantly reduced immunogenicity [116], [120].

Solid tumours present physical barriers that can reduce antibody penetration, thereby limiting therapeutic efficacy [121]. To overcome this challenge, smaller antibody (as illustrated in **Figure 1:5**) fragments can be employed to increase efficacy and enable deeper tissue penetration. This approach also helps minimize off-target toxicities, which have been reported in some patients treated [122]. The structure of the whole antibody and its mechanism of targeting and cellular entry may contribute to these side effects [123]. Hence, small antibody fragments offer several advantages, including enhanced penetration of solid tumours, reduced immunogenicity, ease of production, and lower production costs [124], [125]. MAbs are being armed with potent cytotoxic molecules through two primary strategies: antibody-drug conjugates (ADCs) and immunotoxins (ITs) [126],[127].

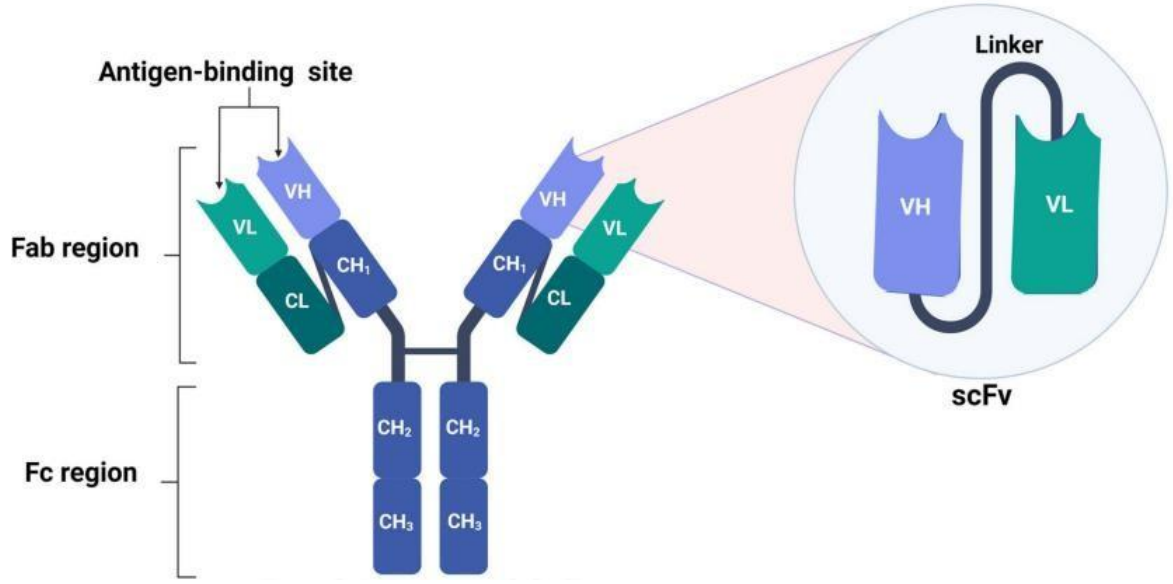

Figure 1.5 Structure of a complete antibody and an scFv antibody fragment. The different regions are highlighted, showing the makeup of the antibody's Fab region (with VL and VH domains) and Fc region. Additionally, the scFv is depicted with a flexible linker joining the VL and VH domains [128].

1.5 Antibody Drug-Conjugates (ADCs)

Antibody-drug conjugates (ADCs) are immunotherapies designed to deliver cytotoxic drugs specifically to malignant cells by linking a monoclonal antibody to a drug via either a cleavable or non-cleavable linker [129]. However, the large size of antibodies can hinder their ability to effectively penetrate solid tumours [117]. Smaller antibody fragments may offer improved tumour penetration and accessibility [127]. This precise targeting minimizes damage to healthy tissue, making highly toxic drugs safer when delivered directly to tumour cells.

The use of ADCs in low-income countries faces significant challenges related to their complex synthesis, high costs, and the need for specialized infrastructure [130]. Despite their potential, the intricacies of ADC manufacturing, involving antibody generation, linker synthesis, and drug conjugation, lead to a costly process [131]. The variability in drug-to-antibody ratios often results in inconsistent therapeutic effects, emphasizing the need for homogeneity to optimize how the drug moves through and affects the body [132]. These limitations highlight the need for alternative targeted

therapies, such as immunotoxins, which may overcome some of the obstacles associated with ADCs [133].

1.6 Development of Immunotoxins for Anticancer Therapy

Immunotoxins are targeted anti-cancer therapies designed to kill cancer cells by delivering a cytotoxic protein from either bacteria or plants. They consist of two main components: a monoclonal antibody and a toxin [134]. Commonly used protein toxins in immunotoxins include diphtheria toxin, *Pseudomonas* exotoxin A (a bacterial toxin), and ricin (a plant toxin). These toxins exert their cytotoxic effects by inhibiting protein synthesis, inducing DNA damage, or disrupting cell signalling pathways, ultimately leading to cell death [135]. Over time, various immunotoxins have been developed, with each generation incorporating structural modifications aimed at reducing adverse effects and immunogenicity while enhancing therapeutic efficacy [136].

The first generation of immunotoxins was developed by chemically conjugating the entire toxin to a murine monoclonal antibody [137]. However, this design presented significant clinical challenges. The conjugation process was complex, resulting in low yields of active protein, and the final conjugation product was heterogenous with a non-uniform ligand-to-toxin ratio. Consequently, the toxin could be attached at multiple, uncontrolled sites [138]. Additionally, the use of the full toxin moiety introduced a cell-binding domain that enabled the toxin to enter normal cells, leading to severe off-target effects and significant adverse side effects during clinical trials [137]. Further complications arose from the murine antibodies, which accumulated in the liver, causing severe hepatotoxicity and heightened immunogenic responses. These first-generation immunotoxins were also characterized by low stability and heterogeneity due to the chemical conjugation methods. Moreover, production was expensive and technically challenging. Advances in understanding toxin structure and function paved the way for the development of the second generation of immunotoxin, which aimed to address these limitations [139].

In second-generation immunotoxins, non-essential regions of the toxin were removed to minimize adverse effects while retaining the catalytic domain responsible for cytotoxic activity. This truncation reduced the overall size of the molecule when conjugated to the antibody. Although the second generation demonstrated improved

specificity, as observed in phase 1 trials, several challenges persisted. The heterogeneity of the conjugates and the large molecular size of the antibody hindered tumour penetration, leading to side effects such as like vascular leak syndrome (VLS) [135]. To overcome these challenges, the third generation of immunotoxins was developed using recombinant DNA technology [140]. This approach enabled the precise engineering of immunotoxins with defined molecular structures, improved stability, and reduced immunogenicity, representing a significant advancement in immunotoxin design. The third-generation recombinant immunotoxins (rITs) were designed to improve specificity, efficacy, stability, and safety [139]. Key innovations included reducing the size of the antibody fragment, retaining only its binding region, and genetically fusing it to the catalytic domain of the toxin. These rITs were easier, faster, and inexpensive to produce, with low non-specific toxicity, and the compositions were homogeneous [141]. This resolved many of the limitations faced by earlier generations, enabling a more efficient and scalable approach to immunotoxin production [142].

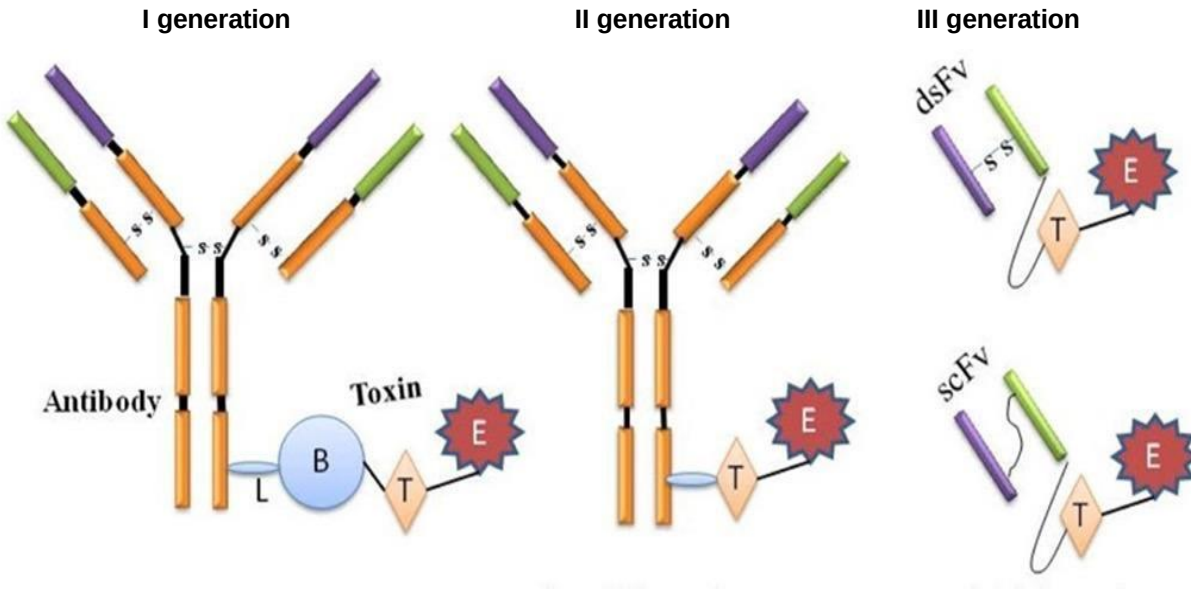

Figure 1.6: The progression of immunotoxin development over three generations. The first generation involved chemically conjugating monoclonal antibodies to full-length *Pseudomonas* exotoxin A toxins. The second generation used truncated toxins, missing their native binding domain, conjugated to the antibody. The

third generation genetically fuses the antibody's binding domain directly to the toxin's catalytic or enzymatic domain [143].

1.6.1 *Pseudomonas* Exotoxin A (ETA/PE)

When developing recombinant immunotoxins, several factors should be considered, including the ability of the catalytic domain to separate predictably from the binding ligand only after internalisation into the target cell. This feature is seen in bacterial toxins such as the *Pseudomonas* exotoxin A (ETA) the most toxic virulent factor secreted by the gram-negative bacterium *Pseudomonas aeruginosa*. Liu *et al.* discovered the ETA toxin while isolating pathogenic *Pseudomonas* species using antisera against species-specific extracellular antigens [144],[145]. PE was shown to inhibit protein synthesis in mammalian cells. This mechanism has since been harnessed and manipulated to target and eliminate cancer cells [146]. ETA enzymatically inhibits protein synthesis by ADP-ribosylation of elongation factor-2 (EF-2), herewith halting protein synthesis a [140][141][142][143] and inducing cell death. A mechanism associated with its role as a pathogenic factor.

ETA has been extensively studied and characterised, identifying the functions of its structure domain [137][138][139]. As illustrated in Figure 1.4, ETA can be divided into three major domains: the receptor binding domain, the translocation domain, and the ADP-ribosylation domain. It is composed of 638 amino acids and has mono-ADP ribosyl transferase activity [147].

The domain I found in the N-terminal domain is a cell recognition site, binding to cellular receptors, enabling attachment, and entry into target cells. Domain II facilitates translocation, allowing the toxin to cross cellular membranes and reach the cytoplasm. It also has an essential amino acid motif RHRQPRF, which is exposed on the exterior protein surface for cleavage by the protease furin. Domain 1 b's function is unknown but assumed to be important in the secretion of the toxin and is part of domain III, the catalytic domain, which contains ADP-ribosyl transferase activity, which inactivates EF-2 within the cell [148]. It also contains the REDLK amino acid motif, located on the carboxylic end of the toxin recognition sequence for aiding the translocation of ETA into the cytosol from an endocytic compartment and retaining the toxin in the endoplasmic reticulum. The coordinated action of these structural domains enables

the toxin's entry, internalization, and cytotoxic activity, making it highly effective at killing cells [149].

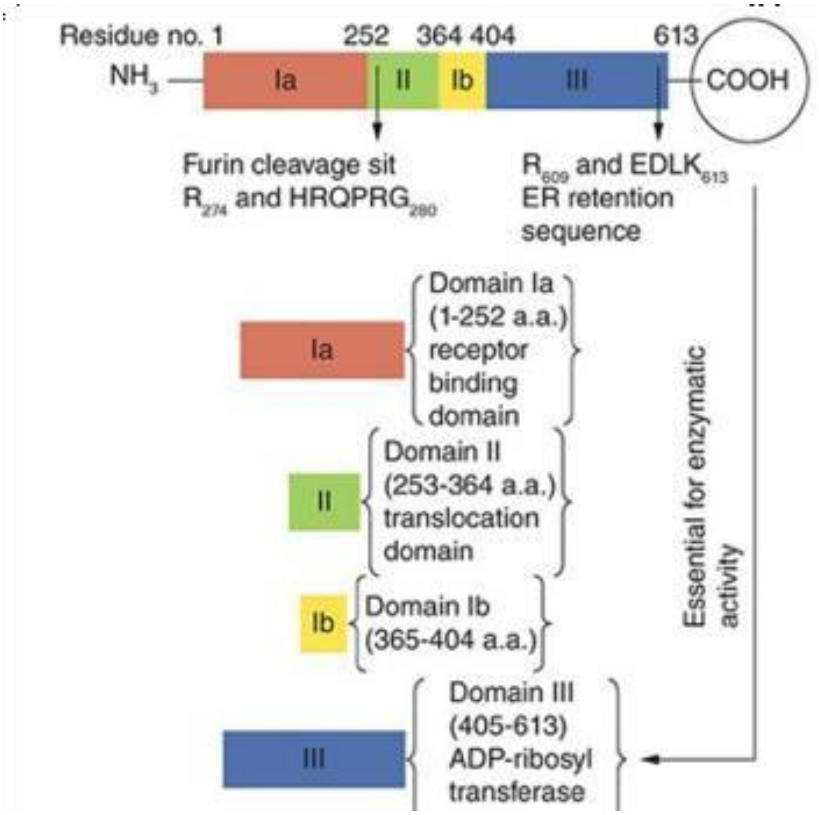

Figure 1.7: ETA Structural and functional domains of the *Pseudomonas* exotoxin A. Domain 1a is the receptor binding domain, Domain II is the translocation domain and has the Furin cleavage sites, and Domain IB and III holds the catalytic domain of the toxin. Accessed 07 November 2024 from a 2023 paper [150].

In this study, the truncated version of ETA is used that lacks the domain I and the majority of domain II and is referred to as ETA. This version was shown to increase specificity and strong cell-killing abilities once fused to an antibody.

1.6.2 The mechanism of action of the *Pseudomonas* exotoxin A (ETA)

The mechanism of action of an antibody fused to the ETA toxin aligns well with the goal of precision medicine in oncology [151]. Upon binding to a specific target on a cancer cell, the rIT is internalized via receptor-mediated endocytosis, forming an endocytic vesicle, **Figure 1.8** [152]. Inside the endosome, the toxin domain is

separated from the antibody fragment by the Furin cleavage, exposing the translocation domain to transport the catalytic domain [153]. The antibody-antigen complexes are directed toward lysosomal for degradation. While the toxin domain unfolds and becomes fully activated. It is then trafficked to the Golgi region and subsequently to the endoplasmic reticulum, where the amino acids in the REDLK peptide sequence at the C-terminus of ETA bind to the KDEL receptor (intracellular sorting receptors).

The toxin binds to EF-2, a key protein involved in peptide chain elongation during translation [154]. EF-2 undergoes a unique modification at histidine (715aa), forming a diphthamide tip. This tip is then targeted by ADP-ribosylating enzymes, including domain III of *Pseudomonas* exotoxin. Domain III utilizes intracellular NAD+ to cleave nicotinamide from ADP-ribose, creating an oxocarbenium intermediate. This intermediate is then linked to the diphthamide residue of eEF-2, forming an ADP-ribosylated complex. This modification impairs tRNA and mRNA through the ribosome, halting protein synthesis and disrupting peptide chain elongation [154], [155]. The inhibition of protein synthesis triggers apoptosis through signalling, involving pro-apoptotic and anti-apoptotic proteins. The inhibition relies on the pro-apoptotic protein Bim, the depletion of the pro-survival protein Mcl-1, and activation of the pro-apoptotic protein Bak [156]. This process initiates a complex apoptotic signalling cascade involving multiple key proteins as shown in **Figure 1.8** [157].

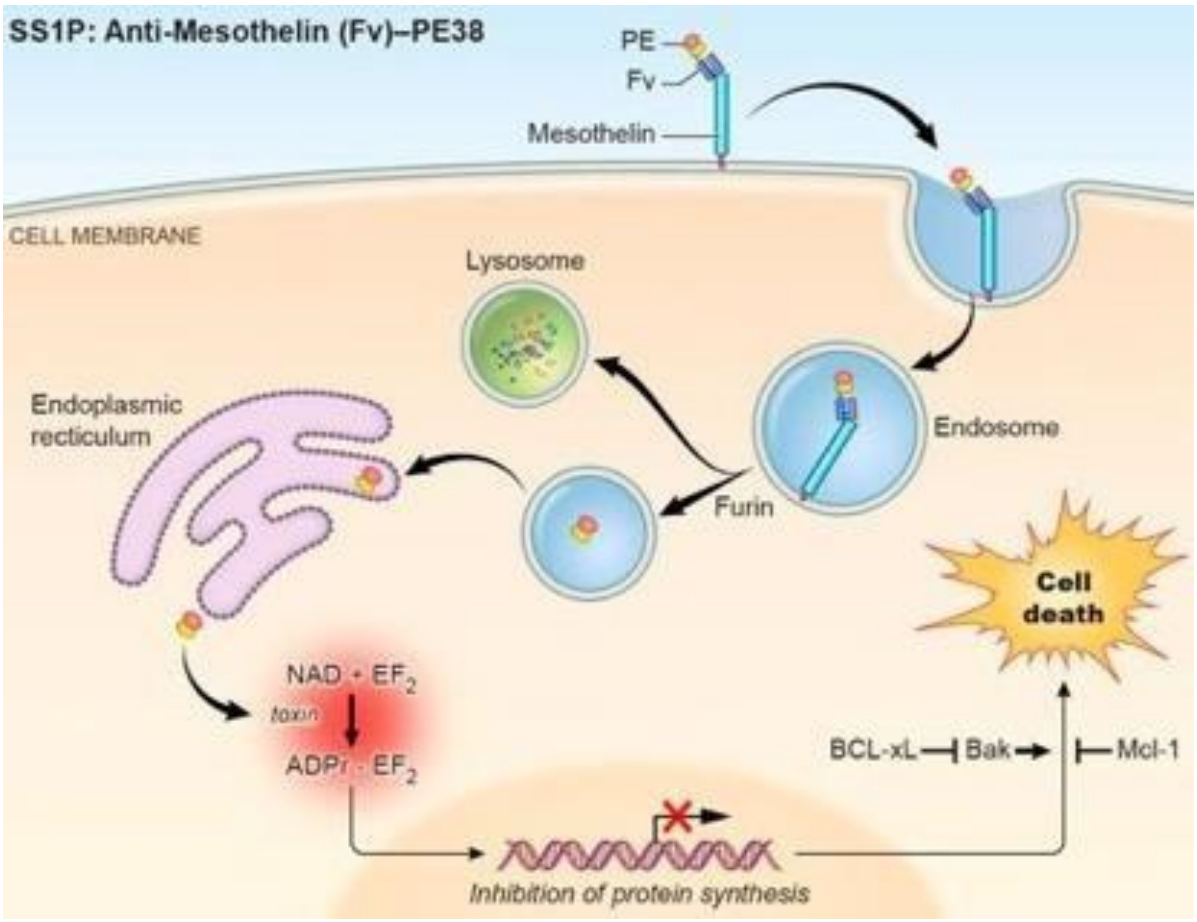

Figure 1.8: *Pseudomonas* exotoxin A (PE) mechanism of action: 1) Anti-Mesothelin-PE38 binds to the target antigen, and it is internalized into endocytic compartments within the cell. **2)** Within these compartments, the Furin protease cleaves the antibody fragment from the toxin-catalytic domain of the rIT. **3)** The toxin is trafficked and secreted in cytosol, inhibiting protein synthesis. **4)** Inducing cell death [158].

1.6.3 Advances in Recombinant Immunotoxins with *Pseudomonas* Exotoxin A

Early developments in rITs involved fusing a cell-surface antigen-targeting antibody to truncated fragments of ETA, such as the 38-kDa version PE38 [159]. This ETA version contains a deletion of the of domain I from native ETA. One example is the anti-CD22(Fv) fused to PE38, known as Moxetumomab pasudotox (Lumoxiti), which showed great promise in clinical trials, particularly in treating hematologic malignancies like drug-resistant hairy cell leukemia. These malignant cells are easily

accessible, allowing patients to undergo multiple treatment cycles before developing neutralizing antibodies [160].

However, the transition of the PE38-based rIT into solid tumor trials revealed a major limitation, such as the rapid development of neutralizing antibodies, which severely reduced the number of treatment cycles [161]. To address this the researchers shifted their focus to look for tumour cell surface antigens highly expressed on cancerous cells and not on normal cells. In search of the antigen, researchers discovered MSLN, an antigen expressed on lung, breast, gastric, and ovarian cancer. This led to the development of SS1P immunotoxin [162].

1.6.4 SSIP Immunotoxin

SS1P is a PE38-based recombinant immunotoxin targeting MSLN (anti-mesothelin (dsFv)-PE38) [163]. It was evaluated in a phase 1 clinical trial involving patients with mesothelin-expressing solid tumours, including mesothelioma, ovarian cancer, and pancreatic cancer [164]. As a single agent, it showed a favourable safety profile; however, its efficacy was still limited, as 90% of patients developed neutralizing antibodies against the rIT following one cycle of therapy [162]. It also exhibited off-target toxicity, particularly capillary leak syndrome (CLS), which hindered SS1P from achieving its full therapeutic potential [163]. To address this, the treatment was combined with a lymphocyte-depleting regimen, allowing patients to receive doses [159]. The lymphocyte-depleting regimens (pentostatin and cyclophosphamide) selectively reduce T- and B-cell populations, thereby delaying the formation of neutralizing antibodies against the immunotoxin [165], [166]. Among treated patients, only a few developed neutralizing antibodies after multiple cycles, indicating successful mitigation of immunogenicity [165]. Thus, this improved outcomes for patients with mesothelioma and potentially other solid tumors expressing MSLN.

1.6.5 SS1-LR, a second-generation recombinant immunotoxin

To address the limitations associated with SS1P, particularly its immunogenicity, researchers further developed SS1-LR using protein engineering technology [167]. SS1-LR was created by removing the protease-sensitive regions of PE38, resulting in

a molecule designed to withstand degradation in the endo-lysosomal compartment of target cells. This generated a lysosomal degradation-resistant variant (LR) of a PE24-based rIT that lacks most of domains Ib and II of ETA fused to mesothelin [168]. This variant exhibited lower immunogenicity and off-target toxicity in mice; however, it demonstrated reduced cytotoxic activity compared to SS1P on cell lines [169]. To enhance SS1-LR's activity, the researchers added a Gly–Gly–Ser peptide linker to improve the accessibility of the furin cleavage site, creating SS1-LR/GGS. Furin increases the cytotoxic efficacy of immunotoxins through its specific cleavage mechanism. They tested a panel of furin site mutants and selected the most potent variant - SS1-LR/GGS/8M. In vitro experiments showed that the new molecule, SS1-LR/GGS, exhibited cytotoxic activity comparable to SS1P on several mesothelin-expressing cell lines. Additional improvements were made by introducing eight-point mutations in the catalytic domain of ETA to reduce immunogenicity, resulting in SS1-LR/GGS/8M. This new variant retained similar cytotoxic activity to SS1P on mesothelioma and lung cancer cell lines and showed superior activity on primary cells from patients with mesothelioma [162], [166].

When tested in mice, SS1-LR/GGS/8M was administered at a dose of 10 mg/kg for three doses and achieved superior tumour growth inhibition compared to the maximum tolerated dose of 0.4 mg/kg for three doses of SS1P, which can cause serious side effects at higher doses [170]. Additionally, SS1-LR/GGS/8M demonstrated reduced immunogenicity and off-target side effects, such as a lower likelihood of inducing capillary leak syndrome in a rat model and decreased reactivity with antibodies in the serum of patients previously treated with SS1P [171],[167].

The development of SS1-LR/GGS/8M represents a significant improvement over the SS1P [170]. These results led to the development of a recombinant immunotoxin with mutations that depleted human B-cell epitopes on the *Pseudomonas* exotoxin A component, enhancing its safety for the human immune system.

Mapping human B-cell epitopes allows for the design of immunotoxins that minimize immune responses. Using alanine scanning mutagenesis, the researchers constructed a dETA variant with seven-point mutations in domain III (R467A, R490A, R427A, R458A, D463A, R505A, and R538A), which ablated human B-cell epitope [167]. To enhance the antitumor efficacy, they included a furin cleavage site [172].

This mechanism ensures that the active form of the toxin is released inside the cell, minimizing the off-target effect [173]. The resulting toxin was LR-LO10. The resulting toxin LR-LO10 was reported to display significantly reduced reactivity to sera from patients treated with PE38. LR-LO10 also demonstrated the highest cytotoxic and anti-tumour activity among all mutants prepared

In other studies, researchers identified and silenced the T-cell epitopes in the immunotoxin, resulting in a deimmunised (dETA) variant named LMB-T18 [174]. Reports indicate that the modified toxin, LMB-T18, demonstrated anti-tumour efficacy [175].

Later studies revealed that the R458A mutation, which removed the H3 B-cell epitope on L010 reduced its toxin activity. To address this issue, researchers introduced an R456A mutation in place of R458A, resulting in a new deimmunized rIT, the RG7787 variant [174],[170].

1.6.6 Deimmunised *Pseudomonas* exotoxin A (dETA) -rIT Comparison with Native *Pseudomonas* exotoxin A (ETA)

The RG7787 (dETA) consists of a humanized anti-MSLN Fab fragment fused to PE24 of *Pseudomonas* exotoxin A [176]. It has the seven-point mutations that silenced the B-cell epitopes and T-cell epitopes, a LR, GSS spacer with a R456A mutation. These modifications enhance safety and reduce nonspecific toxicity. Additionally, RG7787 allows for higher dosing with minimal adverse effects, allowing patients to undergo multiple treatment cycles without the need for immunosuppressive agents [177].

However, comparing RG7787 to SSIP wild type, it was reported to have a lower cytotoxic effect. To address this limitation and further enhance the activity of RG7787 while maintaining its reduced immunogenicity, our laboratory, the Medical Biotechnology and Immunotherapy Research Unit (MB&I) at the University of Cape Town collaborated with the Department of Computational Biophysics at the German Research School for Simulation Sciences, led by Professor Paolo Carloni [178]. We utilized advanced supercomputing molecular dynamics simulations to identify new hotspot mutations, R456T and R456C, which could potentially restore the cytotoxicity

activity of RG7787 to the level of the wild type of ETA [178]. These new mutations were introduced alongside the existing modifications on RG7787 to develop a more potent and less immunogenic immunotoxin-based therapy for cancer treatment. The new version of the rIT was made of a single chain variable fragment of either anti-MSLN or anti-TROP2 genetically fused to the deimmunised version of ETA with a R456T mutation that I will refer to as dETA- based rIT in the study.

1.7 Study Rationale

Cervical cancer remains a significant public health challenge, particularly in low- and middle-income countries, where treatment options are limited and the traditional treatments such as radiotherapy often exhibit undesirable side effects due to the lack of specificity. Recombinant immunotoxins offer promising alternatives by selectively targeting and eliminating cervical cancer cells while minimizing side effects. In this research, we explore the potential of using a deimmunized version of the recombinant immunotoxin RG7787 for cervical cancer treatment. By building on past improvements, this study aims to demonstrate a possible restoration of the enzymatic activity of RG7787 to that of the wild type (ETA) by introducing a point mutation with restorative potential. Simulations of potential mutations identified R456T and R456C as the most promising candidates for favourable outcomes. In this study, the R456T point mutation was evaluated. The deimmunised *Pseudomonas* exotoxin A with R456T henceforth referred to as dETA.

1.8 Study aims and objectives

1.8.1 Aim

This study aims to develop and evaluate the functionality of novel recombinant immunotoxins derived from antibody formats, specifically anti-TROP2/MSLN (scFv) fused to *Pseudomonas* exotoxin A (ETA) and its deimmunized variant (dETA), targeting TROP2 or MSLN biomarkers in cervical cancers. These novel therapeutics will provide preliminary insights into the potential application of this rIT in Cervical cancer treatment.

1.8.2 Objectives

i. To utilise *in silico methods, to* design and synthesize anti-TROP2 (scFv) and anti-MSLN (scFv).

ii. To clone the anti-TROP2 (scFv) and anti-MSLN (scFv) fragments into the pMT-ETA and pMT-dETA backbones using DNA recombinant engineering techniques.

iii. To express the recombinant plasmids, pMT-anti-TROP2/MSLN (scFv)-ETA/dETA in the periplasmic space of Escherichia coli (*E. coli*) strain (BL21DE3), using osmotic stress expression.

iv. To perform protein purification using Immobilised Metal Affinity Chromatography (IMAC) and characterise the full-length protein.

v. To perform functional analysis using confocal microscopy to observe the specificity binding/ internalisation of the rIT produced.

vi. To analyse the specific killing ability of the ETA compared to the dETA on cervical cancer cell lines.

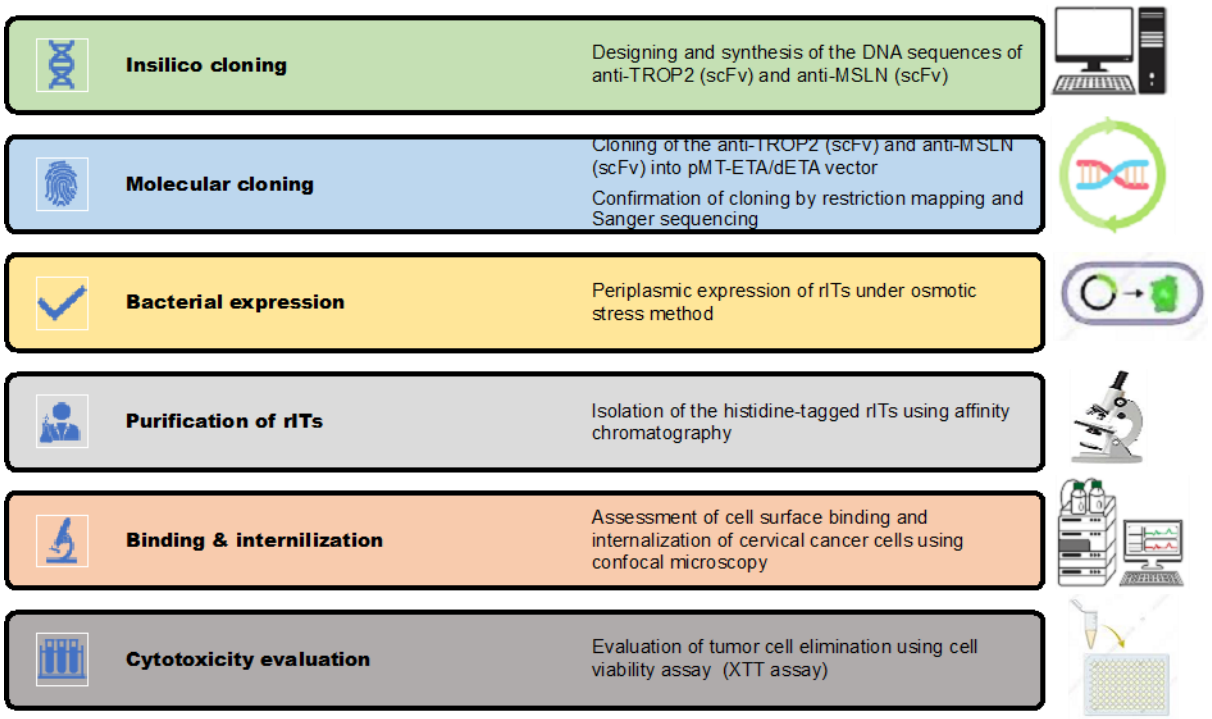

Figure 1.9: Study workflow. In silico technology is first employed to design antibody formats using publicly available antibody sequences, which are then incorporated into expression plasmids that already contain the toxin gene. This process is followed by

molecular cloning, bacterial protein expression, and purification using Immobilized Metal Affinity Chromatography (IMAC). The purified recombinant immunotoxins (rITs) are subsequently conjugated to fluorophores for binding analysis via confocal microscopy and tested for therapeutic efficacy using XTT assays.

CHAPTER 2

MATERIALS AND METHODS

This chapter details the experimental procedures and techniques employed in this research study to generate functional rITs targeting overexpressed biomarkers in cervical cancer. Chapter 1 provided the rationale and background for this study, highlighting an urgent need for targeted therapy to address the crisis of cervical cancer among African women, taking into account the accessibility of resources and the cost-effective production of recombinant therapeutics.

All the materials and equipment listed in this chapter were utilized in accordance with the Medical Biotechnology and Immunotherapy (MB&I) Research Unit methodologies and optimized standard operating procedures (SOPs). Reagents were prepared following manufacturer guidance. Additionally, where necessary, previous MB&I publications and the student's thesis were referenced as relevant to the subject. The buffers and equipment used are detailed in **Appendix 7.1.**

2.1 *In silico* cloning of antibody toxin formats

The Human trophoblastic cell surface antigen 2 (TROP2) antibody sequence used in this study was derived from the antibody phage display library developed by Hong Lin *et al*. (patent ID: US 9,670,287 B2) [179]. The mesothelin (MSLN) antibody sequence was sourced from patent databases (patent ID: US 6,809,184 B1) [180]. The *Pseudomonas* exotoxin A (ETA) bacterial protein toxin and its deimmunized version (dETA) in the pMT-H22(scFv)-ETA and pMT-H22(scFv)-dETA expression vectors were designed and produced previously by our group at the MB&I Research Unit, University of Cape Town.

The sequences obtained were analysed using the IgBLAST software tool (https://www.ncbi.nlm.nih.gov/igblast/) to identify the variable heavy chain (VH) and variable light chain (VL) domains of the antibodies. The variable domains were then joined using a flexible (Gly4Ser)3 linker sequence (5'-GGTGGCGTGGATCC-3'). The anti-TROP2-(scFv) and anti-MSLN-(scFv) DNA sequences were codon-optimized for bacterial expression using the IDT codon optimisation tool

(https://eu.idtdna.com/CodonOpt). The anti-TROP2-(scFv) and anti-MSLN-(scFv) DNA sequences were flanked with *SfiI* and *NotI* restriction sites. SnapGene® software (v.8.0.8, GSL Biotech LLC, USA) was used to annotate the plasmid maps, confirm the correct alignment of sequences, and verify the proper theoretical translation of the open reading frame (ORF) using the simulation tool within the application. The components of the plasmid expression are listed in **Table 2:1** below. The optimized sequences were sent for synthesis at GeneScript (New Jersey, USA).

Table 2.1: pMT expression vector critical features and their function

Feature	Function
Bom	Basis of mobility region (from pBR322), essential for conjugal mobility of conjugative plasmids
Enterokinase site (EKS)	A specific amino acid sequence recognised by the enzyme enterokinase which cleaves proteins at this site, used to remove the His- tag.
ETA /dETA toxin	Pseudomonas Exotoxin A, produced by *Pseudomonas aeruginosa* /deimmunised version of the ETA
fl-ori	Origin of replication for the filamentous phage, which allows a plasmid to replicate when it is in a host bacterium.
10x His-tag	10 histidine residues to facilitate purification and detection of proteins of interest.
Kanamycin resistance (KanR)	Provides bacteria with resistance to the antibiotic kanamycin, allowing the selection of bacteria that have been successfully transformed with a plasmid containing this gene.
Lac operator	lac operon system used to control gene expression in response to lactose or IPTG
Lac I	This is the gene encoding the lac repressor protein. Lac I, binds to the lac operator to inhibit transcription of the genes downstream. It can be induced to release from the operator by lactose or IPTG, allowing gene expression.

Lac I promoter	It controls the transcription of the lac I gene, regulating the production of the lac repressor protein.
pelB signal sequence	It directs the secretion of recombinant proteins into the periplasmic space of *E. coli*, facilitating protein folding and post-translational modifications.
Ribosome binding site (RBS)	Initiating translation and thus protein synthesis.
Rop	Regulating the number of plasmid copies within a bacterial cell.
T7 promoter	Drives high level of gene expression by using T7 RNA Polymerase
T7 terminator	This sequence signals the termination of transcription by T7 RNA polymerase. It ensures that transcription stops at a defined point, producing a stable and complete mRNA transcript.
ScFv	Antigen binding domain. Containing the light chain and heavy chain immunoglobulin chains (variable regions) Me /TROP2.
SfiI /Not restriction sites	Selective cleavage of plasmid allowing the insertion of the scFv sequences of interest.

2.2 Molecular cloning

2.2.1 Transformation of Chemically Competent Bacterial Cells.

DH5-α *E coli* competent cells were transformed according to New England BioLabs transformation protocol (New England BioLabs (NEB), USA). Sixty µL aliquots of competent cells were thawed on ice, 100 ng plasmid DNA was added, and the mixture was incubated on ice for 30 minutes. The mixture was then subjected to heat shock for 30 sec at 42ºC in order to allow for the exogenous plasmid DNA to enter the membrane through pores that resulted from the heat shock. Afterward, the cells were incubated on ice for 5 min, and after incubation, 950 µL of pre-warmed (37°C) Super Optimal Broth with Catabolite Repression (SOC) media was added. The transformation suspension was incubated for 60 min at 37°C in a shaking incubator for 250 rpm. Subsequently, bacterial cells were pelleted at 5000 RPM for 10 minutes in a microcentrifuge. About 950 µL supernatant was discarded, and cells were gently

resuspended with the remaining media. Subsequently, a total of 100 µL of the transformation mixture was spread out on pre-warmed LB agar plates containing ampicillin or kanamycin according to the vectors' antibiotic resistance. Agar plates were then incubated overnight, allowing colonies to grow at 37°C.

The following day, individual bacterial colonies were selected and inoculated into 50 mL LB broth supplemented with either ampicillin (100 ng/µL) for pUC57 plasmids or kanamycin (50 mg/mL) for pMT plasmids. These cultures were incubated overnight at 37°C on a shaker (180 RPM). Glycerol stocks were made of all cultures by mixing an aliquot with 50% glycerol in a 1:1 ratio. Glycerol stocks were stored at -80°C. To extract plasmid DNA from bacterial cells.

2.2.2 Plasmid Extraction and Purification method (Nucleobond® xtra midi)

Plasmid extraction from 50 mL overnight cultures was performed using the Nucleobond® extraction kit (Catalogue number: 740410.50, Macherey-Nagel, Germany) following the manufacturer's instructions. The overnight bacteria cultures containing the plasmid of interest were pelleted by centrifugation at 4000 xg speed for 15 minutes at 4°C using an Allegra X-22R centrifuge (Beckman Coulter). The supernatant was discarded, and the pellet was resuspended in buffer (Buffer S1) from the kit containing RNase.

The lysis buffer (Buffer S2) was added, and the mixture was gently inverted to homogenize the suspension. The lysate was incubated for 3 minutes at room temperature, followed by the addition of the neutralization buffer (Buffer S3). The mixture was again gently inverted until an off-white flocculate formed. The lysate was placed on ice for 5 minutes to precipitate the SDS and denature chromosomal DNA, enabling the separation of plasmid DNA from genomic DNA, which is a critical step for the selective isolation of the plasmid of interest. The mixture was centrifuged for 10 minutes to separate the supernatant containing the plasmid DNA from cellular debris and denatured DNA. The clarified lysate was then carefully applied to the equilibrated Nucleobond® column (Buffer N2) through a column filter. The flow-through was discarded, and the column was washed twice with the wash buffer (Buffer N3).

Plasmid DNA was eluted using 5 ml of elution buffer (Buffer N5), with a pH range of 7 to 9. Molecular-grade isopropanol was added to precipitate the eluted plasmid DNA, and the mixture was centrifuged at 4000 xg for 30 minutes. The supernatant was discarded, and 2 ml of 70% ethanol was added to the pellet, followed by centrifugation at 5000 xg for 10 minutes at room temperature. The supernatant was discarded again, and the pellet was dried using the SpeedVac Vacuum (Thermo Fisher Scientific, USA). Finally, the plasmid DNA pellet was reconstituted in sterile,deionized distilled H_2O (ddH_2O) at 50°C.

2.2.3 Restriction Enzyme Digestion

Restriction digestion of the Open Reading Frame (ORF) was performed using *SfiI* and *NotI* high-fidelity restriction enzymes (Catalogue numbers R0123S and R0189S, respectively, New England Biolabs, USA) according to the manufacturer's instructions. V The process produced two compatible sticky ends of the DNA fragments in preparation for ligation.

Restriction enzyme digestion was performed on the ETA and dETA expression plasmid and the pUC57 plasmids containing the scFv according to the manufacturer's instructions. Depending on the chosen enzyme (*SfiI* and *NotI*) present on the restriction sites. Restriction enzyme (RE) digestions were carried out in accordance with the manufacturer's instructions. Generally, the reactions contained 2 µg DNA template, 1 x CutSmart buffer, 1 U restriction enzyme, and nuclease-free water up to 20 µL (**Table 2.3**). The digest with *SfiI* (2000 units/mL) was carried out for 4 hours at 50°C, while digestion with *NotI* (2000 units/mL) was performed for a minimum of 5 hours to 16 hours maximum, depending on the user preference at 37°C. The digest reactions were heat-inactivated at 65°C for 10 minutes and were analysed using agarose gel electrophoresis (**section 2.2.4**).

2.2.4 Agarose Gel Electrophoresis

Plasmid DNA and restriction enzyme digestion were confirmed by agarose gel electrophoresis using 1.2 % (w/v) agarose gels. The gel was prepared with 1x TAE buffer [0.1 M Tris, 0.05 M EDTA (pH 8.0)] containing SYBR™ Safe (Catalogue

number: S33102, Invitrogen, South Africa) (DNA gel stain) at a 1:10000 dilution to enable visualisation of the DNA fragments. The stain binds specifically to the DNA double helix, allowing it to be seen under UV light. When excited with UV or blue light (with a blue light excitation maximum at 509 nm), any SYBR Safe® that is bound to DNA fluoresces with a bright green colour. Due to the light sensitivity of the stain, the gel was poured into the casting apparatus and allowed it to solidify in the dark. Two DNA ladders, the Quick-Load 100 bp DNA ladder and the 1 kb DNA, were used to track the size of the digested plasmid DNA.

To visualize the migration of the DNA samples during electrophoresis and to ensure the DNA samples are loaded successfully into the wells, ten µL of each digestion product was mixed with 10 µL of 6X Purple Gel Loading Dye at a 1:1 ratio upon loading on the agarose gel. A Bio-Rad system (a flat sub-cell GT wide-mini buffer tank) was used for the electrophoresis at 120 V for 45 min, and DNA was visualized with a Molecular Imager® Gel Doc™ XR+ Imaging System (Bio-Rad, South Africa) at 509 nm, and the resulting images were analysed using Image Lab v6.1.0. software. After the AGE was complete, the DNA fragments of interest were carefully excised from the gel for further processing.

Table 2.2: Agarose gel and buffer recipes

Buffer	**Recipe**
10x TAE	0.4 M Tris Base 0.5 M EDTA (pH 8) 1.14 % (v/v) glacial acetic acid ddH2O – topped up to 1 L
1XTAE	100 mL of 10x TAE buffer ddH2O – topped up to 1 L
1,2% Agarose gel Solution	1.2 g Agarose gel electrophoresis powder (AGE) 100 mL 1x TAE buffer (Boiled to dissolve the AGE powder) 10 µL SYBR™ Safe (Added after cooling)

Table 2.3: Restriction digestion reaction mixture of pU57 and pMT-(scFv)-dETA/ETA

Component	Quantity
Plasmid DNA	2 µg
Cut Smart Buffer®	5 µl
Restriction enzyme (*SfiI* *NotI*)	1 µl
Nuclease free water	Top up to 50 µl

2.2.5 Gel extraction of the digested product

Following the manufacturer's protocol, the excised DNA fragments were purified using a QIAquick Gel Extraction Kit (Qiagen, Germany). In the final step of the procedure, the DNA fragments were eluted from the QIAquick® column after a 5-minute incubation with molecular-grade nuclease-free water at 50°C. The concentration and purity of the purified DNA fragments were then assessed. Given the inherent fragility of the recovered DNA, it was used for ligation immediately.

2.2.6 Ligation of the DNA fragments

Ligation of the backbone to the inserts was done using the T4 DNA ligase enzyme (Catalogue number: M0202S, New England Biolabs®, USA), which forms a covalent phosphodiester bond, and the reaction was incubated overnight at 16°C, following the manufacturer's instructions. The reaction parameters are detailed in **Table 2.4**. The vector-to-insert ratios 1:1, 1:3, and 1:5 (vector: insert) were prepared for the ligation reaction. Controls included a vector-only reaction and a vector with a ligase to evaluate the efficacy of the ligation process.

The amount ratios used to vector to insert required for a successful ligation depending on the fragment sizes (bp) was calculated on NEBioCalculator® version 1.15.5 (NEBioCalculator). Following a overnight incubation at 16°C, the ligation reaction was terminated by heat inactivation of the ligase enzyme at 65°C for 10 minutes. Using the heat shock method, the ligated product was then transformed into 50 µL of competent DH5α E. coli. The transormed *E. coli* was plated onto agar plates supplemented with kanamycin (50 mg/mL) to distinguish recombinant plasmids from partially digested plasmids. The plates were incubated overnight at 37ºC.

Colonies were selected based on the ratio of colony-forming units (CFUs). At least three clones were picked to identify a correctly ligated construct. Selected colonies were incubated overnight at 37°C in 5 mL of LB media supplemented with kanamycin (50 mg/mL) while shaking, on 180 RPM. Following the manufacturer's instructions, plasmids were isolated from the cultures using the Zyppy™ Miniprep kit (Zymo Research, USA). The DNA concentration of the isolated plasmids was measured using the Denovix™ spectrophotometer (Thermofisher Scientific, USA).

Table 2.4: Ligation reaction setup

Component	**Quantity**		
T4 DNA Ligase buffer	2 µl		
Vector DNA (Backbone)	50 ng		
Vector: Insert DNA	1:1	1:3	1:5
T4 DNA Ligase	1 µl		
Nuclease free Water	Top to 20 µl		

2.2.7 Restriction mapping and sequencing analysis

Restriction mapping was used to confirm the successful cloning of recombinant plasmids. Plasmid DNA was reconstituted in a final volume of 20 µL. Samples were prepared from the stock for restriction analysis. Confirmed clones were subsequently used for downstream experiments.Specific restriction enzymes digested the plasmids to map their structures and verify the presence of the desired clones. Unique cutters, including *XbaI*, *MaubI*, *SacI*, *PvuII,* and *NotI,* were employed. The selected restriction enzymes and the expected fragment sizes were simulated using SnapGene® software v.8.0.8 (GSL Biotech LLC, USA). This method ensured accurate confirmation of the integrity of the recombinant constructs and the presence of the desired inserts.

The DNA was sent for Sanger sequencing analysis at Inqaba Biotec in South Africa. Primers were designed and obtained from Inqaba Biotechnical Industries in Pretoria, South Africa. Sequencing data were analyzed using SnapGene software and aligned to the designed ORF as reference sequences.

2.3 Periplasmic protein expression under osmotic stress

The confirmed DNA sequences were transformed into the chemically competent *E. coli* BL21(DE3) expression bacterial cell line (New England Biolabs, USA) using the transformation protocol outlined in **Subsection 2.21**.

The transformed Colonies were selected and inoculated into 50mL of starter culture terrific broth (TB) medium (Conda Laboratories, Spain) supplemented with 50 mg/mL kanamycin for protein expression. The cultures were incubated overnight at 37°C in a shaking incubator at 200 rpm.

The recombinant immunotoxins were expressed using the osmotic stress expression method as described by Barth *et al.* [181]. The next day, 20 mL of the starter culture was used to inoculate 500 mL of terrific broth supplemented with 50 mg/mL kanamycin prepared with glycerol. The total culture volume expressed per construct was 2Lgrown at 26°Cshaking at 180 RPM until the optical density (OD_{600nm}) reached approximately 1.6 to 2.0. The OD_{600nm} was monitored hourly using a Bio Photometer Plus Spectrophotometer (Eppendorf, Germany).

Compatible solutes (4 % (w/v) NaCl, 0.5 M sorbitol, and 40 mM Glycine-Betain) were added to induce osmotic stress on the cells. After 30 minutes of stress induction, protein expression was initiated by adding 1 mM isopropyl-B-d-thiogalactopyranoside (IPTG). The cultures were incubated for 16 hours at 26°C with shaking at 180 RPM. The bacterial cells were harvested by centrifugation at 4000 RCF for 30 minutes at 4°C. The resulting pellet was weighed and stored at -80°C until ready for protein purification.

2.4 Protein extraction by sonication

To extract the expressed protein, the frozen pellet was thawed on ice and then re-suspended in cell lysis buffer (containing 100 mM Tris HCl, 300 mM NaCl, 5 mM DTT, EDTA-free protease inhibitor cocktail (Roche), and 10% v/v glycerol). Protein extraction from the periplasmic space was achieved through sonication, conducted for 1 minute and 30 seconds, with the sonicator (Qsonica, USA) operating at 40% amplitude. This setting was selected based on initial optimization experiments to ensure efficient disruption of cell membranes while minimizing protein denaturation. Sonication was performed in cycles of 15 seconds of sonication followed by 15

seconds off to prevent overheating. The high-frequency sound waves generated during sonication effectively disrupted cell membranes, releasing the protein of interest into the buffer solution. This method facilitated the extraction of target proteins from the periplasmic space, enabling subsequent purification steps. Following sonication, the bacterial lysate was clarified by ultracentrifugation at 24,000 x g for 30 minutes at 4°C. This step separated the soluble protein fraction from cellular debris (insoluble fraction), preparing the sample for downstream processing and purification of the expressed protein.

2.5 Protein purification using immobilised Metal Affinity Chromatography

Protein purification of the bacterial lysate post-sonication was achieved by Immobilized Metal Affinity Chromatography (IMAC) using the ÄKTA Avant system (GE Healthcare). IMAC is based on the principle of selectively binding histidine-rich proteins or proteins tagged with a poly-histidine (His-tag) sequence to solid support containing chelated metal ions, e.g., nickel, cobalt, or zinc. The histidine residues on the protein form coordinate covalent bonds with the metal ions on the resin, allowing for specific and reversible binding of the target protein while non-His-tagged proteins are washed away.

2.5.1 IMAC-I

The clarified cell lysate was first filtered through a 0.45 µM syringe filter (HVLP04700, Merck, USA) before undergoing a two-step purification process.

IMACI aimed to remove substantial quantities of contaminating protein quickly. A 10x poly-histidine tag on the recombinant immunotoxins enabled high-affinity interaction with a Ni^{2+} Sepharose affinity resin within a 5 ml His trap high-performance column (GE Healthcare, USA).

Buffers were prepared using ultrapure water, adjusted to pH 8.0, degassed, and filtered with a 0.45µm polyvinylidene difluoride (PVDF) membrane. The column was initially washed with 5 column volumes (CV) of deionised H_2O to remove residual ethanol. The column was then equilibrated with 5 CVs of with an equilibration buffer (100 mM Tris, 1M NaCl pH 8.0). The clarified cell lysate was applied to the 5mL His

Trap HP column at a 4 ml/min and washed 5mL/min flow rate during the first IMAC purification step. The target protein was then eluted using a buffer containing a high concentration of imidazole (250mM) at 2mL/min, which displaces His-tagged proteins from the resin, enabling the collection of full-length proteins. The parameters for IMAC II, including the buffer compositions, are detailed in **Table 2.7**.

Table 2.5: First IMAC purification

Purification System	**AKTA-AVANT**
Purification Matrix	Ni^{2+}- Chelating Sepharose
Purification column	HiTrap Chelating HP, 5 ml
Loading/Washing Buffer	100 mM Tris-base, 1 M NaCl (pH 8.0)
Elution Buffer	100 mM Tris-base, 1M NaCl, 250 mM Imidazole (pH 8.0)
Flow rate (Load)	4 ml/min
Flow rate (Elution)	2 ml/min

2.5.2 IMAC-II

IMAC-II was designed to enhance the selective isolation of the rIT, effectively eliminating the contamination from other impurities or native proteins. To achieve higher purity, the eluted protein underwent a second IMAC step using a 1 mL His Trap HP column at a reduced flow rate of 0.5 mL/min to maximise binding efficiency. Before applying the sample, buffer exchange was performed to remove imidazole from the IMAC I eluted fractions. This was done using a 10kDa Amicon® Ultra-15 Centrifugal filter unit (Catalogue number: UFC9010, Sigma-Aldrich, USA) centrifugation at 3,500 RCF. The buffer exchange was carried out by replacing the sample with three volumes of fresh buffer to ensure the effective removal of imidazole.

After loading the sample using a loading buffer with 10mM Imidazole, it was extensively washed with 15CV of the wash buffer containing concentrations of imidazole 30 mM. The final elution was performed with a buffer containing 250 mM imidazole at 1 mL/min. The parameters for IMAC II, including the buffer compositions, are detailed in **Table 2.8**.

Fractions collected during the elution steps were analysed by 10% sodium dodecyl sulfate-polyacrylamide gel electrophoresis (SDS-PAGE) to verify protein purity and integrity.

Table 2.6: Second IMAC purification

Purification System	**AKTA-AVANT**
Purification Matrix	Ni^{2+}- Chelating Sepharose
Purification column	HiTrap HP, 1 ml
Loading Buffer	20 mM Tris-HCl, 500 mM NaCl, 10 mM Imidazole pH 8.0
Wash Buffer	20 mM Tris-base, 500 mM NaCl, 30 mM Imidazole pH 8.0
Elution Buffer	20 mM Tris-base, 500 mM NaCl, 250 mM Imidazole, pH 8.0
Flow rate (Load)	0.5 ml/min
Flow rate (Elution)	1 ml/min

2.6 Protein Characterisation

2.6.1 SDS-PAGE

Following IMAC purification, the structural characterization of the full-length protein was first assessed using SDS-PAGE. Briefly, the 4x Laemmli sample buffer was mixed with protein samples in a 1:4 ratio (v/v) and heated for 10 minutes at 95°C. Denatured protein samples (20 µl) were loaded into a polyacrylamide gel prepared as described in **Table 2.7,** alongside 3 µl of a prestained protein molecular weight marker (Bio-Rad Laboratories, USA) for size reference. The proteins were separated by electrophoresis at 120V for 2 hours in a mini-protean II chamber using 1x running buffer. After separation, the gel was stained with Aqua stain (Bulldog Bio, UK) for 10-20 minutes to visualize the protein bands, which allowed for the evaluation of the protein's purity and confirmation of the expected molecular weight bands.

Table 2.7: 10% SDS PAGE composition

Buffer	Component
Stacking Gel	4 % Acrylamide /Bis-acrylamide 0.1 % SDS 190 mM Tris-Cl (pH 6.8) 0.1 %Ammonium persulphate 0.1 % TEMED
Resolving Gel	10 % Acrylamide/Bis-acrylamide 375 mM Tris-Cl (pH 8.8) 0.1 % SDS 0.1 %Ammonium persulphate 0.1 % TEMED
Running buffer	25 mM Tris-HCl (pH 8.3) 192 mM Glycine 0.1 % SDS

2.6.2 Concentration of full-length fusion protein

The analyzed fractions containing the full-length fusion proteins (FPs) 72kDa were pooled and concentrated using Amicon Ultra-15 centrifugal filters (Merck, USA) with a 30 kDa cut-off. A 30kDa amicon filter can effectively remove smaller impurities and contaminants while retaining the protein of interest. 72 kDa (FP) is twice as large than the 30kDa cut off , making it less likely to pass through the filter. At the same time, buffer exchange was carried out to replace the elution buffer with imidazole with 1xPBS (pH 7.4) for long-term protein storage.

2.6.3 Western blotting

Western blotting (WB), also referred to as protein immunoblotting, was utilized to detect poly-histidine-tagged proteins. Following separation by SDS-PAGE, a polyvinylidene difluoride (PVDF) membrane, recognized for its high protein-binding capacity, was activated by incubating it in methanol for one minute, followed by three washes with distilled water. The proteins were subsequently transferred from the SDS-PAGE gel to the activated PVDF membrane using the Bio-Rad Trans-Blot® Turbo™ system (Bio-Rad, South Africa) at 20V for 40 minutes. After the transfer, the membrane

was blocked for one hour with fat-free milk to prevent non-specific antibody binding. Subsequently, the membrane was incubated overnight at 4°C with gentle agitation in fat-free milk containing anti-His-tag HRP-conjugated primary antibodies at a 1:5000 dilution. The following day, the membrane was washed three times for 5 minutes each with Tris-buffered saline containing 0.1% Tween-20 (1xTBS-T) to remove unbound antibodies. Finally, the membrane was stained with a 1-step TMB blotting solution (Thermo Fisher Scientific, USA) to visualize the protein bands.

2.6.4 Quantification of purified proteins

The enriched protein samples were first quantified using the DeNovix™ spectrophotometer. While this provided an estimate of the overall protein content, the samples contained contaminants. Thus, to determine the precise concentration of the full-length fusion protein, serial dilutions of bovine serum albumin (BSA) (Merck, USA) at 16, 8, 4, 2, 1, and 0.5 µg, were prepared and resolved on a 10% SDS-PAGE gel. alongside purified fusion protein samples.

The gel image was captured using the Gel Doc XR+ imager and analysed using ImageJ software (v1.52). The intensities of the BSA standards and the band corresponding to the target protein were measured. The BSA standards were used to generate a standard curve, which was plotted in Microsoft Excel. The densitometric values of the target protein bands were compared against the standard curve to calculate the precise concentration of the recombinant immunotoxin.

2.7 Functionality assessment of the full-length protein

2.7.1 Culturing of Cervical Cancer Cell Lines

The human cervical cancer cell lines used in this study were CaSki (ATCC: CRL-1550™), HeLa (ATCC: CCL-2™), and Me180 (ATCC: HTB-33™), with HEK293T (ATCC: CRL-3216™) serving as a negative control. These cell lines were cultured in Roswell Park Memorial Institute (RPMI) 1640 medium (Catalog number: 52400-025, Gibco, USA), supplemented with 10% (v/v) Fetal Bovine Serum (FBS) (Catalog number: A3840001, Gibco, USA) and 1% Penicillin-Streptomycin (PenStrep) (Catalog number: 15140122, Gibco, USA). Cultures were maintained under standard tissue culture conditions (37°C, 95% humidity with 5% CO_2) in the incubator (NuAire, UK).

Cells were passaged twice a week by adding 1X trypsin-EDTA (Catalogue number: T4174, Sigma-Aldrich, USA) to detach the adherent cells. To passage cells, the supplemented media was first removed, and the cell culture flask was rinsed twice with 1X PBS to remove residual media. Trypsin-EDTA® solution was then added and incubated for 3-5 minutes at 37°C to detach the cells from the flask. The trypsin-EDTA® solution was inactivated with the addition of FBS-supplemented media, resuspended the cells in the media, and passaged the cells, retaining 5% of the cells in the fresh media. The rIT functionality was examined when the cells were growing optimally.

2.7.2 Binding analysis of fixed cell using confocal microscopy

Confocal microscopy was used to assess the interaction between the rIT and Cervical cancer cells. Binding analysis required the attachment of the rIT to the anti-His-Tag Alexa- Fluor™ a fluorescent chemical compound that can re-emit light upon excitation The recombinant immunotoxin conjugated to anti-his-Alexa-Fluor™ 488 (catalogue number: MA1-21315-A488 ThermoFisher) or anti-his-Alexa- 647Fluor™(Catalogue number: MA1-21315-A647, ThermoFisher USA), for qualitative validation of surface binding and internalization. The anti-His-Alexa-488 fluorophore has an excitation wavelength of 488nm and emits light between 499 and 520 nm, producing green fluorescence. In contrast, anti-His-Alexa 647 has an excitation peak at 650 nm and an emission peak at 671 nm, emitting a bright, far-red fluorescent dye. This enables the visualisation of cell surface binding and internalisation to the antigen expressed on the tumour cell line.

For binding studies, cells were washed with 1x PBS to remove the supplemented media and then lifted using Trypsin-EDTA®. Following the manufacturer's instructions, the cells were counted with the T20 automated cell counter (Bio-Rad, USA). To perform fixed cell binding studies, 1 x 10^5 cells were seeded onto a coverslip in a 6-well plate (Catalogue number: 30006, SPL Life Sciences, KR). The seeded cells were incubated overnight at 37°C, 95% humidity, and 5% CO_2, using 1 ml of supplemented media per well. The next day, rITs were conjugated to the anti-his-Alexa Fluor™ 488/647 as detailed in **Table 2.10**. This reaction mixture was incubated for 1 hour in the dark at 37°C using a thermomixer heating block. During this incubation, the cells were washed three times with 1x PBS. Hoechst nuclear stain (Thermo Fisher

Scientific, South Africa) was diluted in supplemented media at a 1:5000 ratio, and 200 µl was applied to the cells for 30 minutes at 37°C. The cells were then washed three times with 1x PBS. A solution of 25 µM of the conjugated protein was added to 200 µL of non-supplemented media and incubated for 30 minutes at 37°C. The cells were subsequently washed twice with 1x PBS and fixed using 4% paraformaldehyde (PFA) (Catalogue number: J19943.K2, ThermoFisher, South Africa) for 20 minutes at room temperature. The fixed cells were washed twice with 1x PBS and mounted on coverslips using a Mowiol solution (Catalogue number: 475904, Merck, South Africa) (at least 50 µl), mixed with small amounts of anti-fade per slide. The slides were viewed and imaged using the Zeiss LSM880 confocal with Airyscan (Carl Zeiss AG, Germany) at the Confocal & Light Microscope Imaging Facility at the University of Cape Town, South Africa. Confocal images were analyzed using Fiji software (v. 2.9.0/1.53t).

Table 2.8: The components for the conjugation of the anti-His-Alexa-Fluor-488 to rIT

Component	Concentration
DL-Dithiothreitol (DTT)	1 mM
anti-his tag alexa-488/647	10 µM
Anti-TROP2(scFv)-ETA /dETA	25 µM
1x PBS (Final volume)	Top up to 50 µl

2.7.3 Cytotoxicity Assay

To assess the cytotoxic effect of ETA or dETA on antigen-positive tumor cells, the XTT Cell Proliferation Kit II (Catalogue number: X12223, Roche, Switzerland) was utilized. The XTT (2,3-Bis(2-methoxy-4-nitro-5-sulfophenyl)-2H-tetrazolium-5-carboxanilide) cell proliferation assay is a colorimetric method used to evaluate cell viability, proliferation, and cytotoxicity based on metabolic activity; cells reduce the tetrazolium salt XTT (2,3-bis(2-methoxy-4-nitro-5-sulfophenyl)-5-carboxamide-2H-tetrazolium, monosodium salt) to orange-colored formazan compounds. This water-soluble formazan dye absorbs light at 450 nm, allowing for the quantification of cell viability and metabolic activity [182]. Cell lines were seeded into 96-well plates (Catalogue number: 30006, SPL Life Sciences) at a density of 5 x 10^3 cells per well and allowed to adhere overnight at 37°C, 5% CO_2, and 95% humidity. The following day, cells were

treated with varying concentrations of recombinant immunotoxin treatments and incubated for 72 hours. Each treatment was run in triplicate ensure technical consistency.

As controls, cells treated with Zeocin (100 µl/mL) (Catalogue number: R25005, Gibco, USA) served as a positive control to achieve 100% cell killing, while the untreated cells served as a negative control (100% cell viability). Following treatment exposure, XTT reagents were added to each well and incubated for 4 hours. The absorbance readings were taken using a spectrophotometer (iMarkTM Microplate Absorbance Reader, Bio-Rad, USA). XTT reagent (Catalogue number: 11465015001, Roche, Switzerland) quantifies metabolic/cellular viability by reducing XTT, which absorbs light at 450nm (measurement filter) and 650 nm (reference filter). The 50% inhibitory concentration (IC50) of each rIT was calculated by normalising data to untreated control and zeocin controlsl on the respective cancer cell lines using GraphPad Prism v10.0 software (GraphPad Software, USA). Statistical significance was determined by a p-value of <0.05 (calculated using GraphPad Prism) and data were expressed as mean ± standard error of mean (SEM) unless otherwise indicated, Student t test was used for all statistical comparisons..

CHAPTER 3

RESULTS

TROP2 and MSLN are overexpressed antigens that play critical roles in the progression and aggressiveness of cervical cancer. TROP2, a transmembrane glycoprotein, is strongly associated with tumour proliferation, invasion, and poor prognosis in cervical cancer, as well as other malignancies. Similarly, MSLN is highly expressed in cervical adenocarcinomas and other cancers, making both antigens promising therapeutic targets. Consequently, rITs targeting TROP2 and MSLN offer significant potential for more effective and targeted cervical cancer therapies compared to conventional, non-specific treatments. This thesis evaluates the therapeutic potential of four rITs: anti-TROP2(scFv)-ETA/dETA and anti-MSLN (scFv)-ETA/dETA.

3.1 In silico design of anti-TROP2(scFv) and anti-MSLN(scFv) bacterial expression vectors

The development of next-generation rITs required the selection of an optimal single-chain variable fragment (scFv) sequence that specifically targeted cervical cancer tumor antigens, which were identified as TROP2 and MSLN. The sequences of the variable region genes of the heavy chain (VH) and light chain (VL) for αTROP2 and αMSLN were obtained from patents US 9,670,287 B2 and US 6,809,184 B1, respectively. To design TROP2(scFv) and MSLN(scFv), a flexible linker [(Gly)4Ser]3] was included to join or fuse the VH and VL sequences. This linker was selected because of its flexibility, allowing the two constituent proteins to achieve their respective native folds. The TROP2(scFv) and MSLN(scFv) ORFs were synthesised from GenScript cloned into pUC57 using SfiI and NotI restriction sites shown in **Figure 3.1A**. TROP2(scFv) and MSLN(scFv) ORFs were codon optimized to remove rare and repetitive codons to enhance stability and reduce nuclease degradation.

Following optimisation, SnapGene® software used for the in-silico design of the anti-TROP2(scFv)—ETA/dETA and anti-MSLN (scFv)-ETA/dETA vector maps, where the optimised TROP2 and MSLN scFv sequences were inserted into the pMT-ETA (wild

type) and pMT-dETA (RG7787 (R456T)-R490A backbone vector (Figure 3.1 and Figure 3.2) respectively using the *SfiI* and *NotI* restriction sites.

3.1.1 *In silico* design of plasmids coding for ETA

The *in-silico* design of the plasmids adhered to a structured cloning strategy described in **section 2.1**. The pMT-H22(scFv)-ETA plasmid (used as the backbone) (**Figure 3.1 b**) was successfully engineered to include flanking *SfiI* and *NotI* restriction sites, which were strategically chosen for subsequent molecular cloning via restriction digestion. This design allowed for the removal of the H22(scFv) fragment, and the insertion of the new target antibody fragments X (TROP2 and MSLN) contained in pU57-X plasmid (**Figure 3.1 a**), where "X" represents either anti-TROP2 or anti- MSLN scFv. These gene of interest also flanked by the same SfiI and NotI restriction sites. This ensured ease of cloning into the backbone with compatible ends generating pMT-X-ETA F**igure 3.1 C.** Unique cutter restriction sites (XbaI, SacI, and MaubI) were identified within the sequence to aid in future manipulations. In total, two new recombinant plasmids encoding ETA targeting TROP2 and MSLN (pMT-anti-TROP2(scFv)-ETA and pMT-anti-MSLN (scFv)-ETA) were successfully designed *in silico***.**

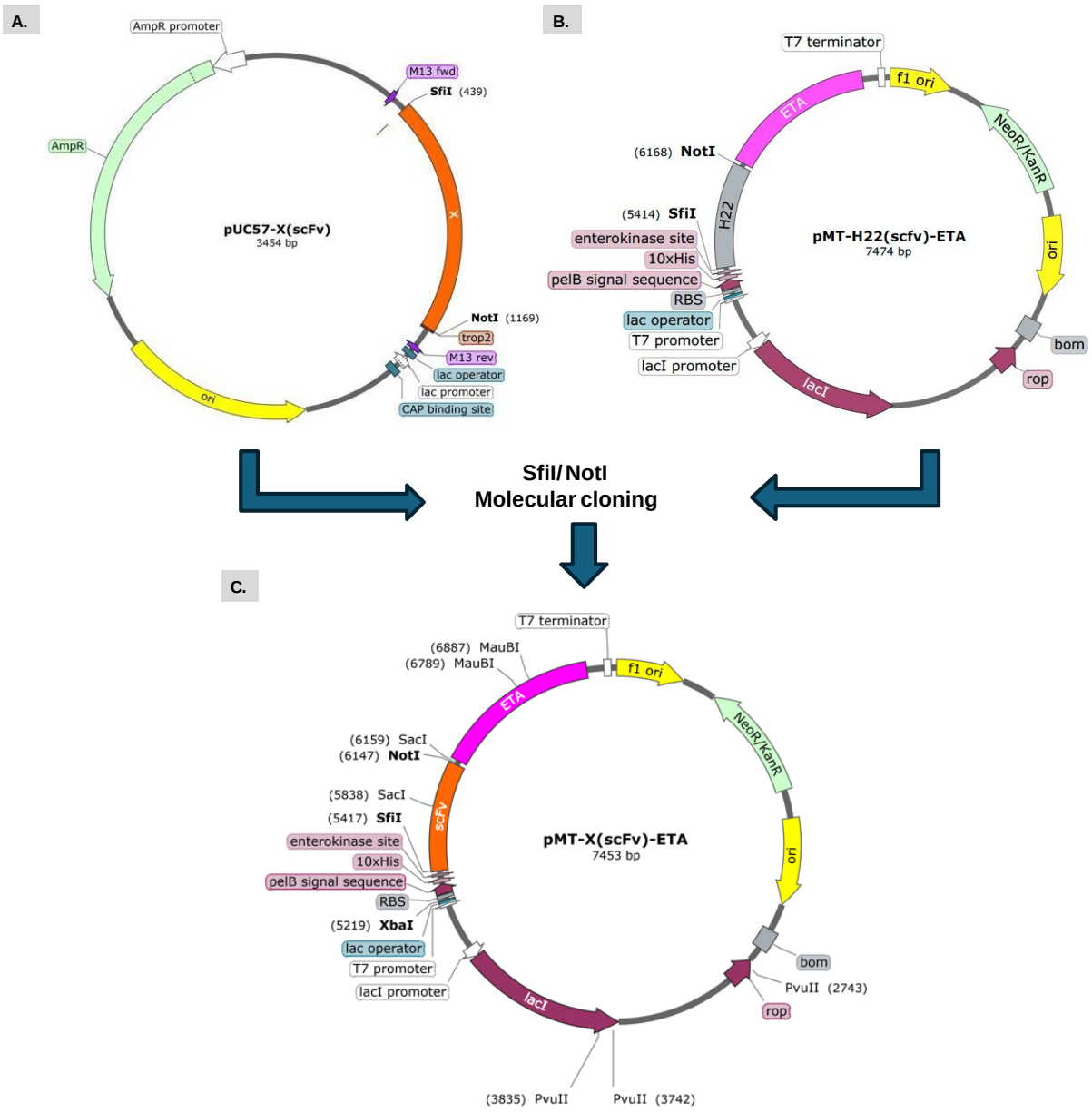

Figure 3.1: Plasmid maps showing the molecular cloning process and key features of the pMT-ETA and pUC57- vector. A.) pUC57 commercial vector containing the gene of interest ("X," represents either TROP2/MSLN) to be designed for excision and cloning into an expression vector. **B.)** pMT-H22(scFv)-ETA expression vector containing the toxin gene. **C.)** pMT-X-ETA expression vector, representing the final product (pMT-anti-TROP2(scFv)-ETA and pMT-anti-MSLN (scFv)-ETA) after the insertion of the gene of interest into the expression vector.

3.1.2 In silico design of plasmids coding for dETA

Building upon the cloning strategy described in section 3.1.1, the *in-silico* design of plasmids coding for a deimmunized variant of ETA (dETA) was successfully performed. The pMT-H22(scFv)-dETA plasmid (expression vector backbone), **Figure 3.2 b** was engineered to include flanking *SfiI* and *NotI* restriction sites for molecular cloning via restriction digestion. The new dETA toxin of (RG7787) contains mutations that include a R456T point mutation. The H22(scFv) was successfully replaced with the anti-TROP2 or anti-MSLN scFv from the pU57-X plasmid (**Figure 3.2 c**). These genes of interest were also flanked by compatible *SfiI* and *NotI* restriction sites, ensuring efficient cloning into the backbone to generate pMT-X-dETA (**Figure 3.2c**). In total, two new recombinant plasmids encoding dETA targeting TROP2 and MSLN (pMT-anti-TROP2(scFv)-dETA and pMT-anti-MSLN (scFv)-dETA) were successfully designed *in silico.*

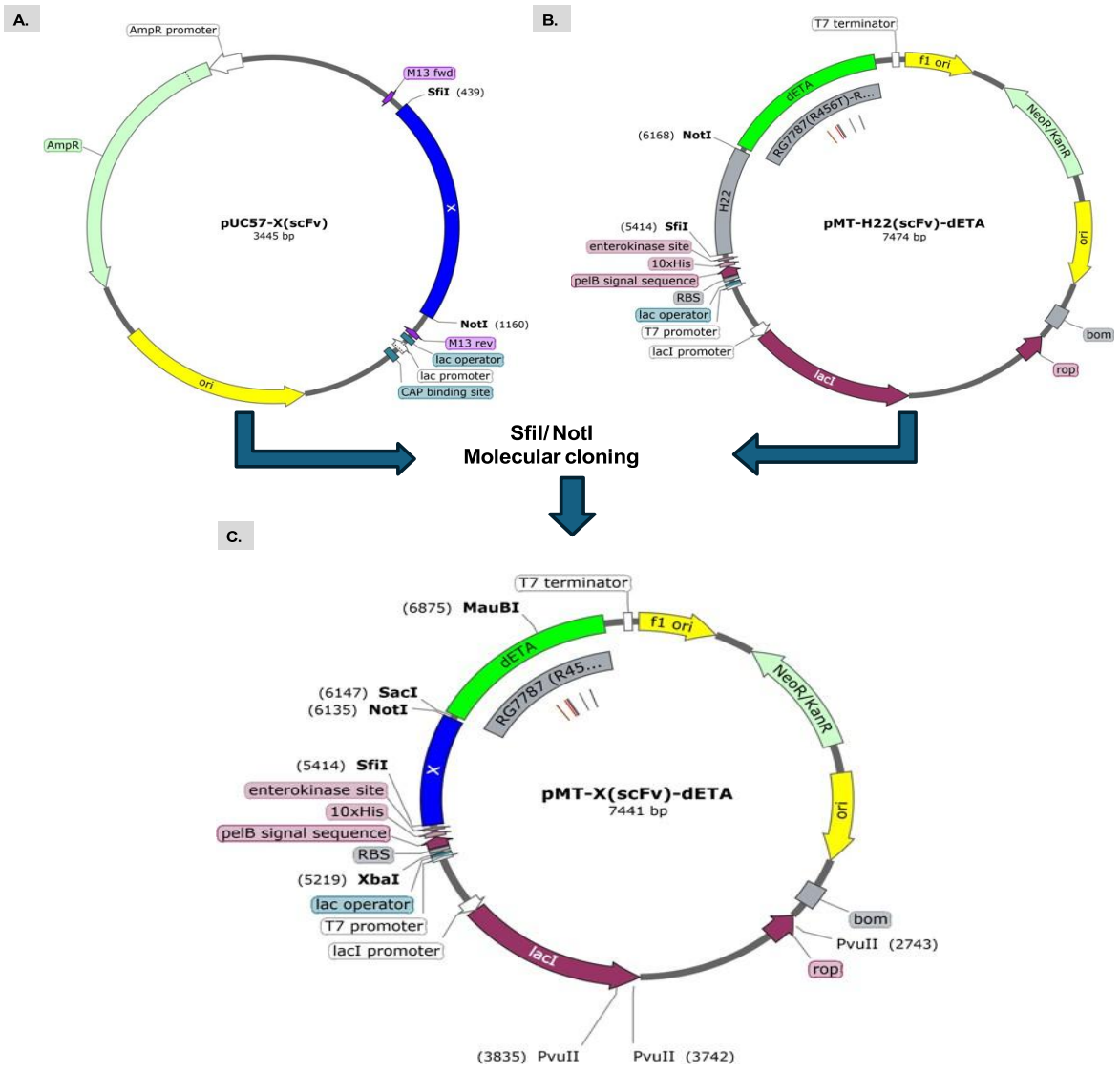

Figure 3.2: Plasmid maps showing the molecular cloning process and key features of the pMT-dETA and pUC57- vector. A.) pUC57 commercial vector containing the gene of interest ("X," represents either TROP2/MSLN) to be designed for excision and cloning into expression vector. **B.)** pMT-H22(scFv)-dETA expression vector containing the toxin gene. **C.)** pMT-X-dETA expression vector, representing the final product (pMT-anti-TROP2(scFv)-dETA and pMT-anti-MSLN (scFv)-dETA) after the insertion of the gene of interest into the expression vector.

3.2 Molecular cloning of anti-TROP2(scFv) and anti-MSLN (scFv) into pMT-ETA or dETA

The TROP2(scFv) and MSLN(scFv) ORFs were synthesized by GenScript. The TROP2(scFv) and MSLN(scFv) from GenScript were supplied cloned into pUC57 vector at the *SfiI* and *NotI* sites. The pUC57-anti-MSLN (scFv), pUC57-anti-TROP2(scFv), pMT-H22(scFv)-ETA, and pMT-H22(scFv)-dETA plasmids were transformed into competent DH5-α *E. coli* cells, as described in **subsection 2.2.1** for bulk plasmid preparation. After 16 hours of culturing at 37°C, the plasmids were extracted, purified, quantified, and assessed for purity. **Table 3.1** summarizes the nucleic acid concentrations and purity ratios (A260/A280) obtained after bulk preparation with purity ratios ranging between 1.8 to 1.85, confirming successful purification. The recorded DNA concentrations were sufficient for further studies.

After plasmid quantification, the plasmids were digested using *Sfi*I and *NotI* restriction endonucleases detailed in **subsections 2.2.1-2.2.3** generating stick ends, which subsequently facilitated the ligation of the TROP2/MSLN (scFv) insert into the pMT-ETA/dETA backbone, from the pUC57, plasmid DNA was digested with *SfiI* and *NotI* restriction enzymes. DNA fragments were resolved on 1.2% agarose gel electrophoresis. The expected size of the insert is 1 476 base pairs, and the expected size of the plasmid backbone is 730 bp for anti-MSLN (scFv) (**Figure 3.3 A**), 721 bp for anti-TROP2(scFv) (**Figure 3.3 B**) and 2724 bp (pUC57 backbone). As can be seen from **Figures 3.3A** and **B**, bands of the expected sizes were present on the gel after digestion with *SfiI* and *NotI*. Furthermore, the control sample, which was digested with *SfiI* or *NotI*, showed only one band on the gel.

The *SfiI* and *NotI* restriction enzymes were also used to remove the H22(scFv) fragment from both the pMT-H22(scFv)-ETA and pMT-H22(scFv)-dETA plasmids. The expected fragment sizes of 754 bp [H22(scFv)] and 6720 bp (pMT-ETA and pMT-dETA) were obtained (**Figure 3.3 C**). The pMT-ETA/dETA expression vector were precisely engineered to incorporate all essential features necessary for subsequent experiments **Table 2.1**. This design facilitated the efficient expression of functional anti-TROP2(scFv)-ETA/dETA and anti-MSLN (scFv)-ETA/dETA recombinant immunotoxins, specifically crafted to facilitate selective production of cells harbouring the plasmid and purification of the protein of interest.

Table 3.1: Quantification of plasmid DNA concentrations following a midi prep.

Construct	**260/280**	**Final Concentration**
pUC57-TROP2 (scFv)	1.80	2897 ng/µl
puC57-MSLN (scFv)	1.83	3134 ng/µl
pMT-H22(scFv)-ETA	1.85	5118 ng/µl
pMT-H22(scFv)-dETA	1.84	4523 ng/µl

After plasmid quantification, the plasmids were digested using *Sfi*I and *NotI* restriction endonucleases detailed in **subsections 2.2.1-2.2.3** generating stick ends, which subsequently facilitated the ligation of the TROP2/MSLN (scFv) insert into the pMT-ETA/dETA backbone. DNA fragments were resolved on 1.2% agarose gel electrophoresis. The pUC57-anti-MSLN(scFv) and pUC57-anti-TROP2(scFv) plasmids were successfully double digested with *SfiI* and *NotI,* restriction enzymes, and the expected fragment sizes of 730 bp for anti-MSLN (scFv) (**Figure 3.3 A**), 721 bp for anti-TROP2(scFv) (**Figure 3.3 B**) and 2724 bp (pUC57 backbone). The *SfiI* and *NotI* restriction enzymes were also used to remove the H22(scFv) fragment from both the pMT-H22(scFv)-ETA and pMT-H22(scFv)-dETA plasmids. The expected fragment sizes of 754 bp [H22(scFv)] and 6720 bp (pMT-ETA and pMT-dETA) were obtained (**Figure 3.3 C**).

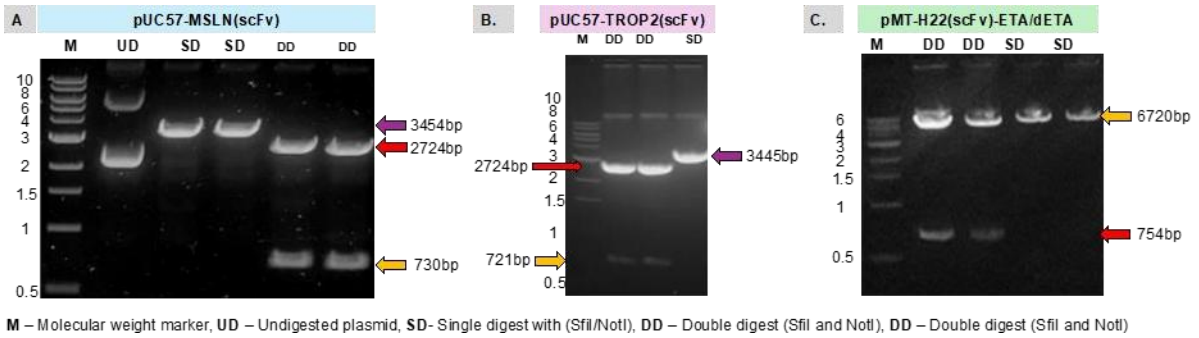

M – Molecular weight marker, **UD** – Undigested plasmid, **SD**- Single digest with (SfiI/NotI), **DD** – Double digest (SfiI and NotI), **DD** – Double digest (SfiI and NotI)

Figure 3.3: Cloning of the anti-MSLN (scFv) and anti-TROP2 (scFv) genes into pMT-ETA and dETA plasmids. Plasmid map schematics and 1.2% (w/v) Agarose Gel for the restriction enzyme digestion. A.) pUC57-anti-MSLN (scFv) schematic plasmid. **B.)** pUC57-anti-MSLN (scFv) agarose gel, **Lane 1:** Undigested, **lanes 2-3:** Single digest with *Not*I and *Sfi*I, respectively, **lanes 4-5:** Double-digest with *Not*I and *Sfi*I. **C.)** pUC57-anti-TROP2(scFv) schematic plasmid. **D.)** pUC57-anti-TROP2(scFv) agarose gel, **Lane 1-2:** Double-digestion with *Not*I and *Sfi*I, **Lane 3:** Single digest *Sfi*I. **E.)** pMT-H22(scFv)-ETA schematic. **F.)** pMT-H22(scFv)-dETA schematic **G.)** pMT-H22(scFv)-ETA and pMT-H22(scFv)-dETA agarose gel, **lane 1:** pMT-H22(scFv)-ETA digested with *Not*I and *Sfi*I, **lane 2:** pMT-H22(scFv)-dETA digested with *Not*I and *Sfi*I, **lane 3:** pMT-H22(scFv)-ETA and pMT-H22(scFv)-dETA digested with *Not*I, **Lane M:** 1kb DNA ladder (New England BioLabs®, USA). The plasmid maps were generated using SnapGene (GSL Biotech LLC, Chicago, IL, USA) bioinformatics software.

3.2.1 Ligation of anti-TROP2(scFv)-ETA/dETA, anti-MSLN (scFv)-ETA/dETA

The anti-MSLN(scFv) and anti-TROP2(scFv) fragments were excised from the agarose gels, gel purified and subsequently cloned into either pMT-ETA or pMT-dETA backbones in varying ratios using the T4 DNA ligase enzyme described in **subsection 2.2.5-2.2.6** by ligation to create four plasmids pMT-anti-MSLN(scFv)-ETA, pMT-anti-TROP2(scFv)-ETA, pMT-anti-MSLN (scFv)-dETA and pMT-anti-TROP2(scFv)-dETA. The plasmids were transformed into competent cells (DH5α cells) and plated on agar plates supplemented with 50 mg/mL kanamycin, facilitating the isolation of successful transfectants, and positive colony growth was observed after incubation. No growth was observed in the control plate that lacked insert and ligase for (anti-MSLN (scFv) or anti-TROP2(scFv)). However, colonies on vector only with ligase indicated auto ligation of the backbone as illustrated in **Table 3.2.** Different colony density across the

plates was observed, corresponding to different insert-to-vector ratios. The plate with a higher insert-to-vector ratio exhibited greater transformation efficiency. Although the 1:5 ratio displayed high colony growth, making individual colony selection difficult, colonies from the 1:3 (vector: insert) ratio were chosen instead **(Table 3.2**). Across all constructs, the 1:3 ratio demonstrated a significant increase in transformation efficiency compared to the 1:0 (with ligase) control plate, thus increasing the likelihood of selecting properly cloned plasmids. Consequently, restriction mapping digest was employed to ensure the plasmid contains the correct insert in the correct orientation.

Table 3.2: *E. coli* colonies transformed with pMT-MSLN-ETA/dETA and pMT-TROP2-ETA/dETA.

Ligation ratio	**Transformation Efficiency (CFU)**			
	pMT-MSLN		**pMT-TROP2**	
Vector: Insert	**ETA**	**dETA**	**ETA**	**dETA**
0:0	**0**	**0**	**0**	**0**
1:0	0	0	0	0
1:0 (with ligase)	10	3.9×10^1	8	5
1:3	2×10^2	1.1×10^4	1.5×10^2	2.2×10^2
1:5	4.1×10^2	2.2×10^4	6.1×10^3	5.1×10^3

3.3 Restriction mapping of cloned products

The correctly ligated recombinant plasmids pMT-anti-MSLN (scFv)-ETA/dETA and pMT-anti-TROP2 (scFv)-ETA/dETA were confirmed through restriction mapping. The plasmid map schematics and restriction mapping banding patterns (**Figure 3.4 a, b, & d**) were predicted using Snap Gene® (GSL Biotech LLC, Chicago, IL, USA) bioinformatics software. Enzymes that produced a unique banding pattern were utilized. The expected band patterns were generated with Snap Gene® software. After

digesting the plasmids for one hour at 37°C, the products were separated by 1.2% Agarose gel (**Figure 3.4 b & d**). These results further confirmed the successful cloning and transformation of pMT-anti-MSLN (scFv)-ETA, pMT-anti-MSLN (scFv)-dETA, (scFv)-ETA, and pMT-anti-TROP2 (scFv)-dETA. Consequently, two colonies per construct were selected for sequencing due to their profiles closely matching those predicted for a successful clone based on the *in-silico* mapping simulation. Following sequencing confirmation, both plasmids were deemed successfully cloned and suitable for downstream experimentation.

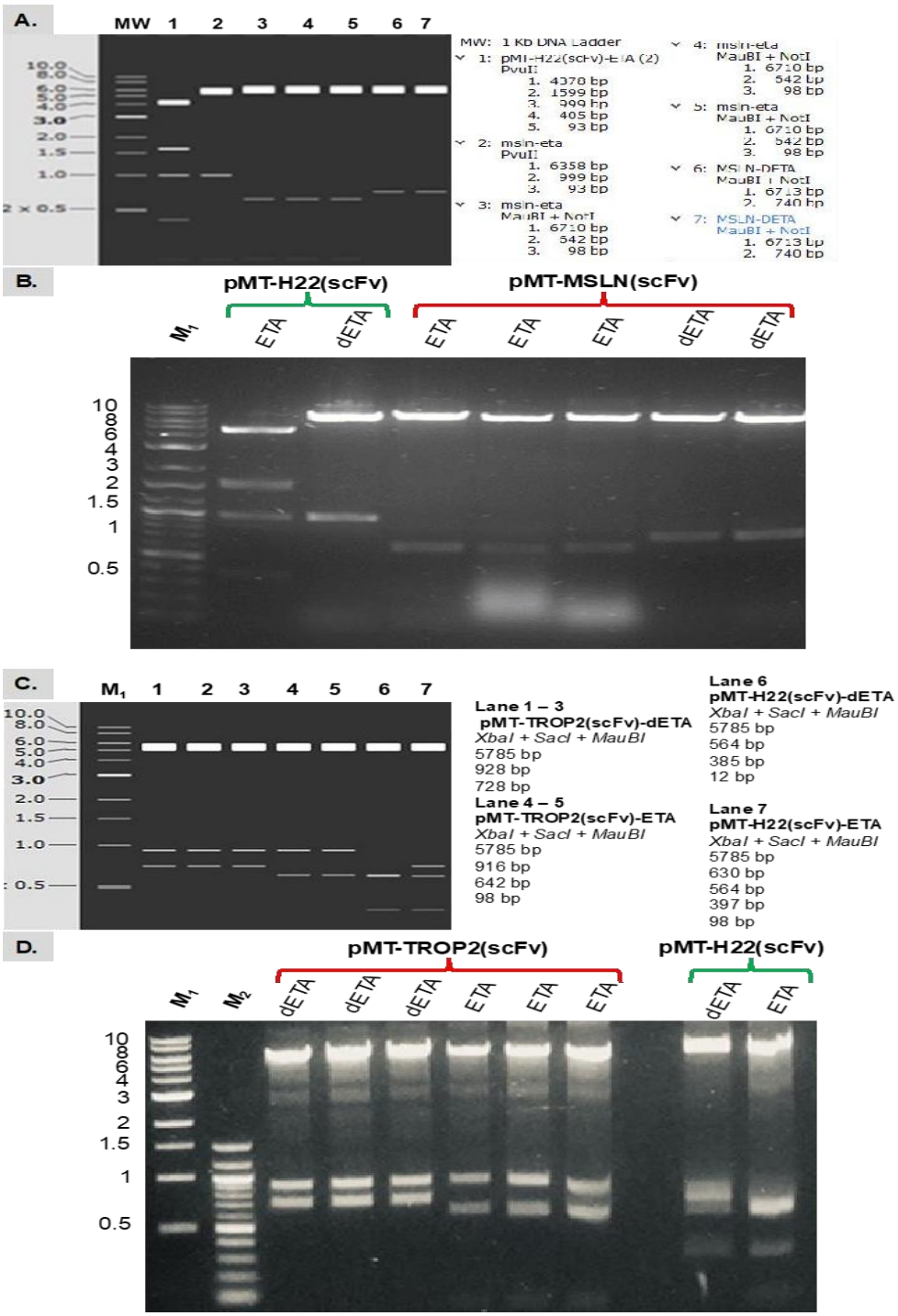

Figure 3.4: Verification of selected colonies to contain the pMT-anti-MSLN (scFv)-ETA/dETA and pMT-anti-TROP2(scFv)-ETA/dETA plasmids by restriction endonuclease mapping. (A.) *In silico* restriction digest analysis of the pMT-anti-MSLN(scFv)-dETA/ETA using *PvuII* ,*MaubI* and *NotI*, simulated with SnapGene software. **(B.)** 1.2% agarose gel of pMT-anti-MSLN(scFv)-ETA /dETA restriction digest analysis of the recombinant plasmids using *PvuII* ,*MaubI* and *NotI* from colonies transformed with ligated DNA**. (C.)** pMT-anti-TROP2(scFv)-dETA/ETA simulated with

SnapGene software. **(D.)** 1.2% agarose gel of pMT-anti-TROP2(scFv)-ETA /dETA restriction analysis of the recombinant plasmids using *XbaI, SacI*, and *MauBI* from colonies transformed with ligated. **M1** and **M2** represent 1kb DNA ladder and 100 bp DNA ladder (Catalogue number: N0467S and N3232L, respectively, New England Biolabs®, USA) molecular weight markers. The plasmids restriction mapping simulation were generated using SnapGene (GSL Biotech LLC, Chicago, IL, USA) bioinformatics software.

3.4 Protein expression and solubility analysis by SDS-PAGE

Following confirmation of the recombinant plasmids (pMT-anti-MSLN (scFv)-ETA, pMT-anti-MSLN (scFv)-dETA, pMTanti-TROP2(scFv)-ETA, and pMTanti-TROP2(scFv)-dETA), which were verified through restriction mapping and Sanger sequencing, these plasmids were transformed into BL21 *E. coli.* The transformed BL21 *E. coli* containing the recombinant plasmids of interest were cultured to perform periplasmic protein expression under osmotic stress, as detailed in **section 2.3.** The proteins anti-MSLN(scFv)-ETA/dETA and anti-TROP2(scFv)-ETA/dETA were expressed in *E. coli* BL21(DE3), and for confirmation of expression, proteins were analysed using SDS-PAGE (**Figure 3.5)**. The harvested cells were lysed by sonication and ultra-centrifuged, with the protein samples separated into insoluble and soluble (clear lysate) fractions for each protein. **Figure 3.5** presents SDS-PAGE gels showing the protein profiles of the four rIT at different stages of protein extraction. This illustrates the successful expression of the target protein at approximately 72 kDa, with traces of protein present in inclusion bodies and a satisfactory amount of soluble fraction, indicating that the target protein was successfully solubilized. These results were consistent across all the expressed proteins analysed.

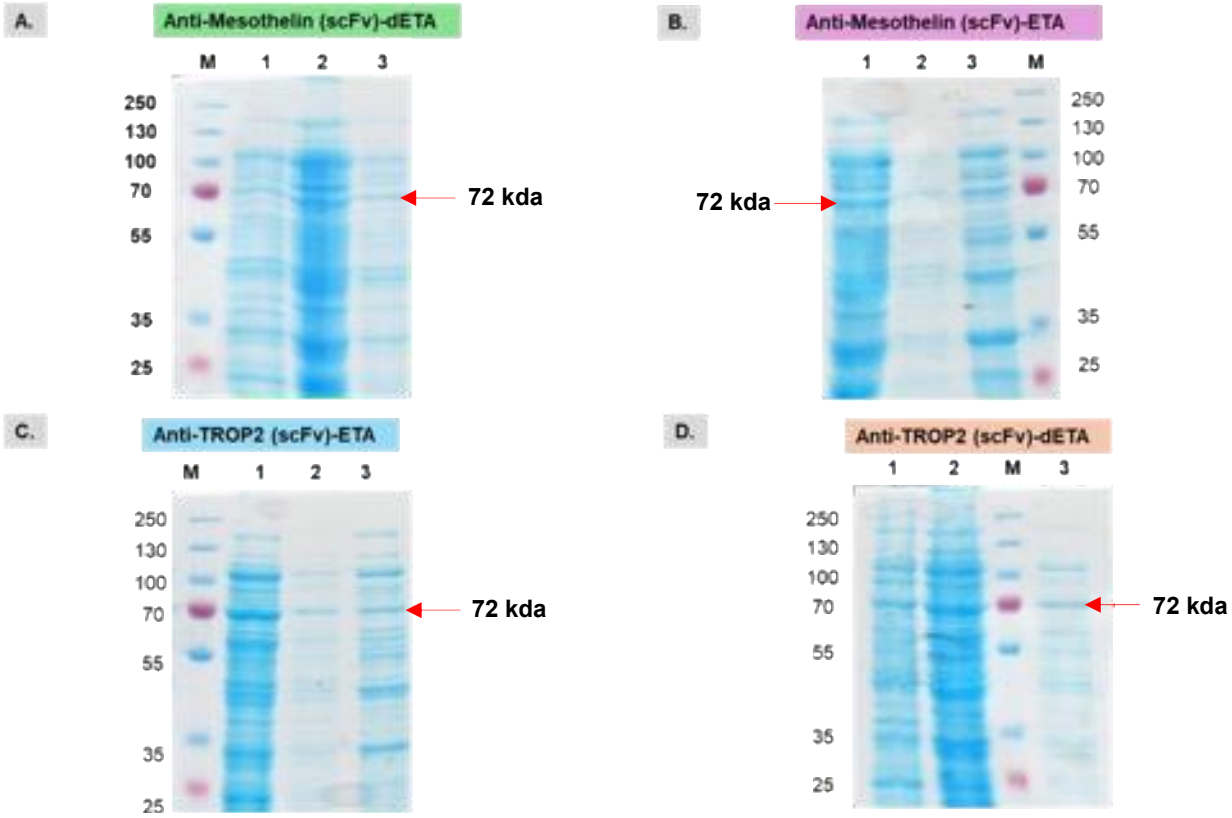

Figure 3.5: SDS-PAGE analysis of the anti-MSLN (scFv)-ETA/dETA and anti-TROP2(scFv)-ETA/dETA expression and extraction. (A) anti-MSLN(scFv)-dETA: **Lane 1** shows the induced fraction, **Lane 2** shows the insoluble fraction, and **Lane 3** shows the soluble (clear lysate) fraction. **(B)** anti-MSLN(scFv)-ETA: **Lane 1** shows the soluble fraction, **Lane 2** shows the insoluble fraction, and **Lane 3** shows the induced fraction. **(C)** anti-TROP2(scFv)-ETA: **Lane 1** shows the induced fraction, **Lane 2** shows the insoluble fraction, and **Lane 3** shows the soluble fraction. **(D)** anti-TROP2(scFv)-dETA: **Lane 1** shows the insoluble fraction and **Lane 2** shows the induced fraction. **Lane M**: Wide Range Blue-Red Two-Color Protein Ladder, Prestained (NBS Biologicals, UK)

3.5 Protein purification and Characterisation

The rITs were purified using a two-step IMAC method following the protocol described **in Section 2.5** with the ÄKTA Avant system (GE Healthcare). The first IMAC purification employed high flow rates (4 mL/min) and a high concentration of 1 M NaCl in the buffers. This purification step aimed to remove a bulk of impurities and contaminants while capturing the rITs, which were eluted at 250 mM imidazole.

Analysis of fractions with a 10% SDS gel indicated that we successfully purified anti-MSLN (scFv)-ETA, anti-MSLN (scFv)-dETA, anti-TROP2 (scFv)-ETA, and anti-TROP2 (scFv)-dETA. The online molecular weight calculator (https://www.bioinformatics.org/sms/prot_mw.htmL) was utilized to compute the molecular weights of the rITs. All the rITs had an approximate molecular weight of 72 kDa. Figure 3.6.(i) shows the eluted fractions with a prominent 72 kDa band, confirming the successful expression and initial purification of all the proteins, although faint additional bands indicate the presence of minor contaminants.

To thoroughly purify the rIT, the second IMAC (IMAC II) purification step was employed. IMAC II was designed to achieve the selective isolation of rIT from contaminating proteins. This step utilized strongly reduced flow rates and followed the protocol described in **section 2.5.2**, which allowed for more robust binding to the column. The buffers used in this purification step included small concentrat/ions of imidazole to enhance stringency. This addition helps to selectively bind to the Ni^{2+} matrix (His trap ff IMAC column), as imidazole competes with histidine residues on rIT, resulting in high-affinity binding of the His-tagged protein, while other impurities are washed out, as shown in **Figure 3.6ii** with fewer impurities of rIT. After the IMAC II step, fractions containing the target protein (72kDa) and minimal contaminants were pooled and concentrated using a 30 kDa Amicon® filter column.

However, significant degradation of anti-MSLN (scFv)-ETA (**Figure 3.6.d (i)**) was observed after the second purification step as confirmed by western blot analysis.

A comparison of the SDS-PAGE gel and western blot showed bands corresponding to histidine-tagged proteins, however major degraded products were evident in both anti-MSLN (scFv)-dETA and anti-MSLN (scFv)-ETA (**Figure 3.6 & b**). As a result, further work on these two proteins was discontinued.

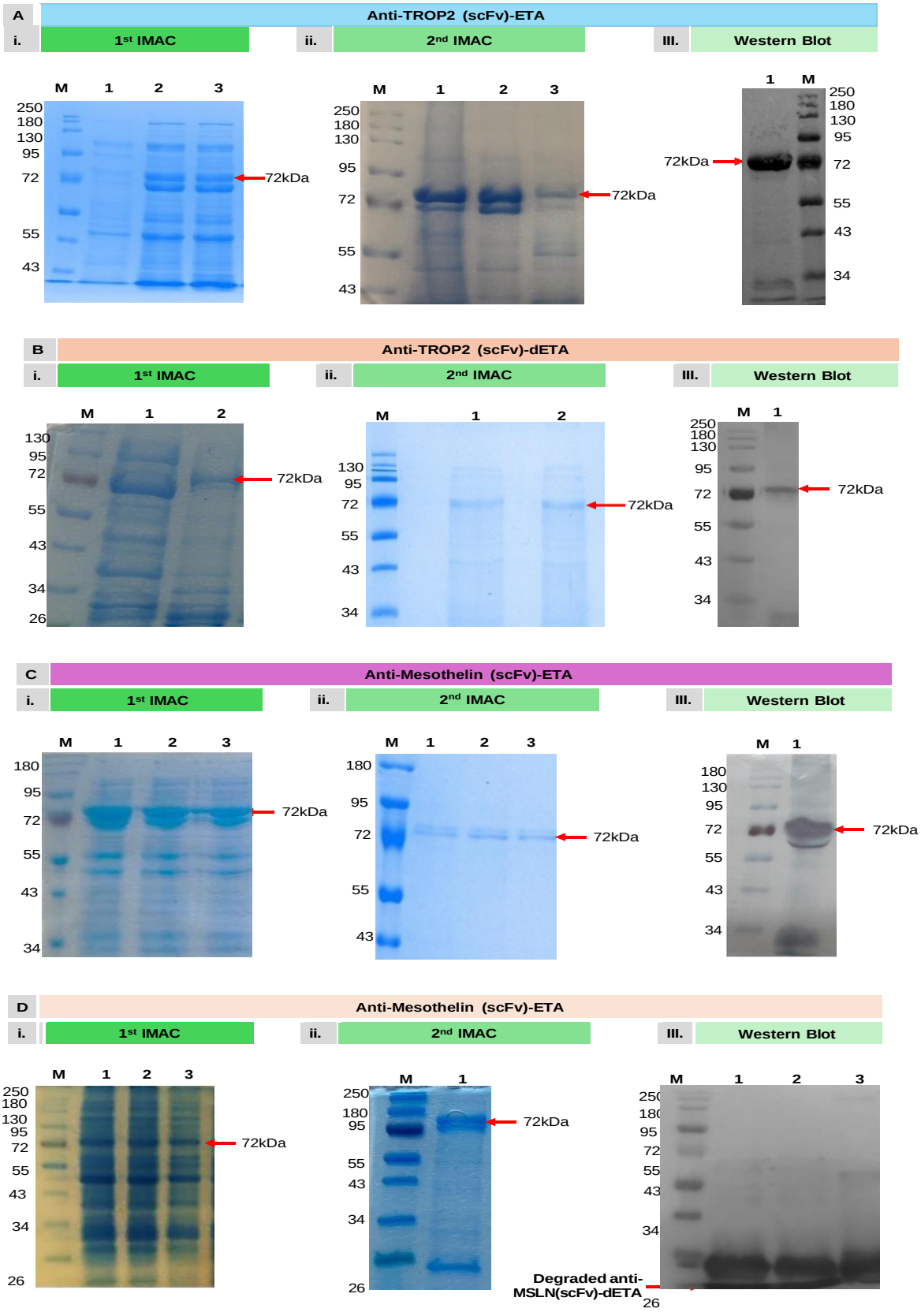
A
Anti-TROP2 (scFv)-ETA
i. 1st IMAC
ii. 2nd IMAC
III. Western Blot
M 1 2 3
250 180 130 95 72 55 43
72kDa
M 1 2 3
250 180 130 95 72 55 43
72kDa
1 M
250 180 130 95 72 55 43 34
72kDa
B
Anti-TROP2 (scFv)-dETA
i. 1st IMAC
ii. 2nd IMAC
III. Western Blot
M 1 2
130 95 72 55 43 34 26
72kDa
M 1 2
130 95 72 55 43 34
72kDa
M 1
250 180 130 95 72 55 43 34
72kDa
C
Anti-Mesothelin (scFv)-ETA
i. 1st IMAC
ii. 2nd IMAC
III. Western Blot
M 1 2 3
180 95 72 55 43 34
72kDa
M 1 2 3
180 95 72 55 43
72kDa
M 1
180 130 95 72 55 43 34
72kDa
D
Anti-Mesothelin (scFv)-ETA
i. 1st IMAC
ii. 2nd IMAC
III. Western Blot
M 1 2 3
250 180 130 95 72 55 43 34 26
72kDa
M 1
250 180 95 55 43 34 26
72kDa
M 1 2 3
250 180 95 72 55 43 34 26
Degraded anti-MSLN(scFv)-dETA

Figure 3.6: 10% SDS-PAGE and Western blot analysis of purified anti-TROP2(scFv)-ETA, anti-TROP2-(scFv)-dETA, anti-MSLN-ETA, and anti-MSLN-dETA following 2 step IMAC purification. A.) SDS-PAGE gel screening analysis of anti-TROP2(scFv)-ETA protein fractions from IMAC I **(i),** IMAC II **(ii),** and Western blot confirmation **(iii). B.)** SDS-PAGE gel analysis of TROP2-dETA protein fractions from IMAC I **(i),** IMAC II **(ii),** and Western blot confirmation **(iii). C.)** SDS-PAGE gel screening of ANTI-MSLN-ETA protein fractions from IMAC I **(i),** IMAC II **(ii),** and Western blot confirmation **(iii), D.)** SDS-PAGE gel screening of ANTI-MSLN-dETA protein fractions from IMAC I **(i),** IMAC II **(ii)**, and Western blot confirmation **(iii)** All SDS-PAGE gels were run at 120V for 2 hours, stained with Aquastain solution, and imaged using the Gel Doc XR+ system. A broad-range colour pre-stained protein standard was used to determine molecular weight. Each well was loaded with 10 µl of protein, selected from fraction peaks, to assess purity following each IMAC purification step.

3.6 Protein quantification using densitometry

Protein quantification of the bacterially expressed rITs was performed using densitometry analysis on SDS-PAGE gels. Densitometry analysis was conducted on the SDS-PAGE gel to estimate the concentrations of BSA dilutions ranging from 0.5 µg to 16 µg, enabling the estimation of rIT concentration in the purified fractions (**Figure 3.7**).

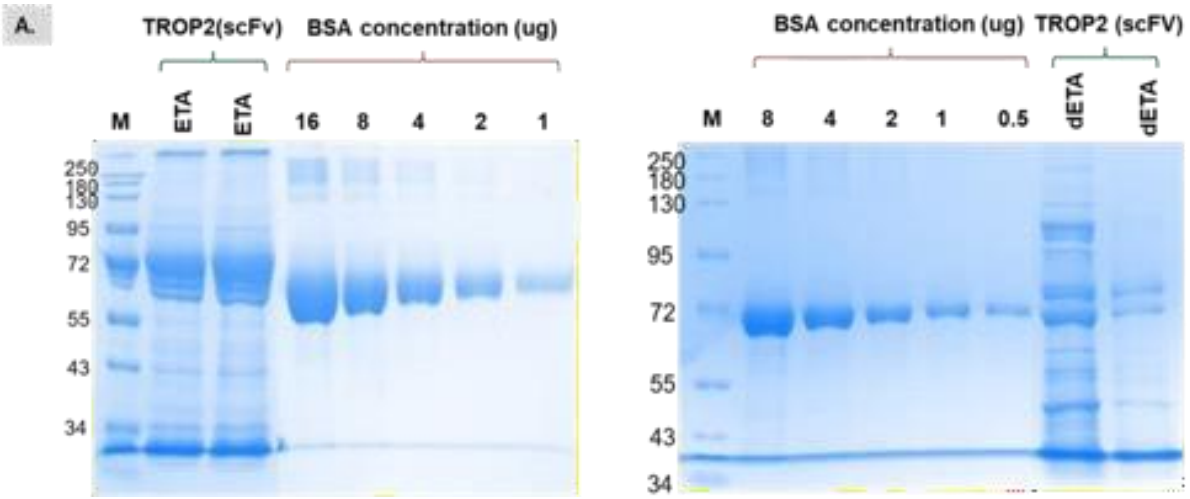

Figure 3.7: Estimation of TROP2(scFv)-dETA and ETA using densitometry. A.) 10% SDS-PAGE gel for pMT-anti-TROP2(scFv)-ETA **B.)** pMT-anti-TROP2(scFv)-

dETA with the BSA standard protein with a two-fold serial dilution was loaded from 16 – 0.5 ug. The gel image was imaged using Gel Doc XR+ (GelDoc™ XR System) and analysed using ImageJ software v.1.53e (https://imagej.net/), the band intensities of BSA standards versus the protein samples were compared and quantified

.The total protein yield was determined based on the densitometry analysis and subsequent calculations, as detailed in **Table 3.4**. The purified protein for anti-TROP2(scFv)-ETA and anti-TROP2(scFv)-dETA demonstrated sufficient purity and concentration, making it suitable for downstream functionality tests, including antigen binding, internalization, and cytotoxicity assays.

Table 3.3: Protein quantification and yields of bacterially expressed recombinant immunotoxins

Protein sample	Total amount expressed (L)	Total pellet (g)	rIT in sample (%)	Densitometry concentration (ug/ul)	Protein yield (mg/L)	Absolute protein yield (mg)
Anti-TROP2-(scFv)-ETA	2	37	33	4.234	0.831	1.6615
Anti-TROP2-(scFv)-dETA	2	42	44.96	6.3	1.87	3.735

3.7 Binding assessment using confocal microscopy

The primary aim of this study is to investigate the functional activities of rITs on TROP2-overexpressing cervical cancer cells. The antigen-binding and internalization properties of rITs, including anti-TROP2(scFv)-ETA/dETA, were assessed by labeling the recombinant proteins with anti-histidine Alexa Fluor 488 or anti-histidine Alexa Fluor 647 dyes and using confocal microscopy imaging to examine fluorescence around the cell surfaces (as described in **Subsection 2.7.2)**.

As documented, anti-TROP2 (scFv)-positive cell lines displayed both cell surface binding and internalization of the rITs, indicated by the green fluorescence signal from anti-Alexa Fluor 488, as shown in **Figures 3.8 A & B,** or in red using anti-Alexa Fluor

647 in **Figure 3.8 C**. Surface binding was demonstrated by the fluorescence localized along the cell membrane, confirming the rITs' specific binding to anti-TROP2 (scFv) expressed on the cell surface (**Figure 3.8**). Internalization was noted, as fluorescence signals were detected within the cytoplasm, indicating active internalization of the rITs. The dotted intracellular distribution seen in the cytoplasm suggests that the rITs may have been trafficked to intracellular compartments, such as endosomes or lysosomes [183],[184].

In contrast, the TROP2(scFv)-negative HEK293T cell line exhibited minimal to no fluorescence signals (green or red), indicating negligible binding or internalization of the rITs. This result establishes it as an effective negative control and confirms that any detected signal above the background would signify binding and internalization events. Subsequently, this supports the specificity of the rITs, anti-TROP2(scFv)-ETA/dETA for TROP2 overexpressing cells.

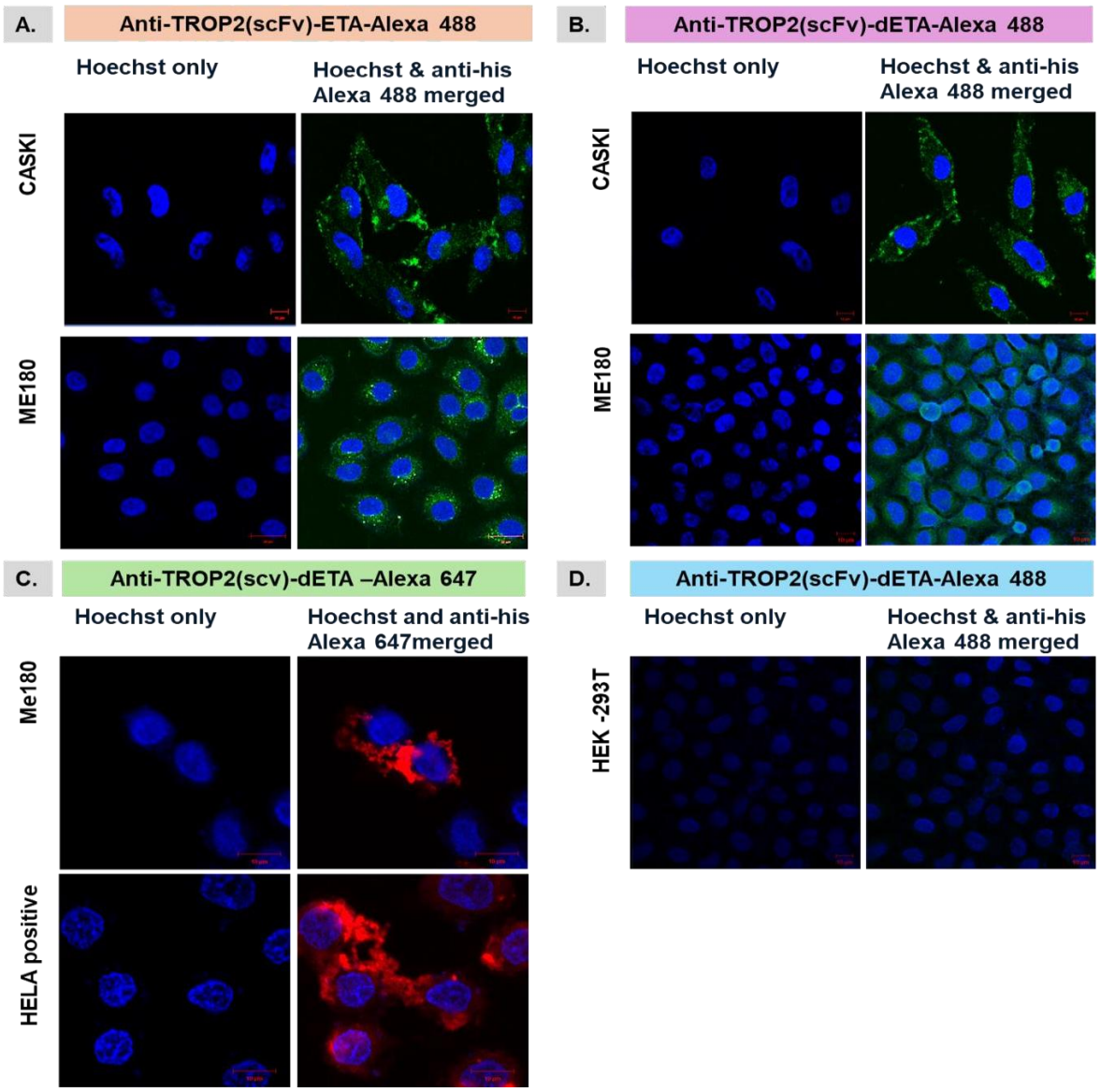

Figure 3.8: Fixed cell imaging using a confocal microscope, visualising anti-TROP2(scFv)-Immunotoxin Binding and Uptake by anti-TROP2(scFv)-Expressing cervical cancer cell lines. A.) CaSki and ME180 cell line, antigen-positive treatment with anti-TROP2(scFv)-ETA conjugated to anti-his-Alexa -488. **B.)** CaSki and ME180 cell line treated with TROP2(scFv)-dETA conjugated to anti-His-Alexa 488, **C.)** ME180 and HeLa cell line treated with anti-TROP2(scFv)-dETA conjugated with anti-his-Alexa 647. **D.)** HEK293T cell TROP2(scFv) negative cell line treated with anti-TROP2-(scFv)-dETA conjugated to anti-his-Alexa 488.

3.8 Cytotoxicity studies

The cell viability (XTT) assay was employed to assess the cytotoxic activity of recombinant anti-TROP2(scFv)-ETA and anti-TROP2(scFv)-dETA proteins on TROP2-overexpressing cancer cell lines (ME180 and CaSki). The results indicated that the CaSki cell line exhibited dose-dependent cytotoxicity when treated with both anti-TROP2(scFv)-ETA and anti-TROP2(scFv)-dETA. In comparison, anti-TROP2(scFv)-ETA demonstrated greater effectiveness, with an IC50 of 11.28 nM (**Figure 3.9 b),** while anti-TROP2(scFv)-dETA displayed reduced potency, with an IC_{50} of 24.67 nM (**Figure 3.9 a**). A similar dose-dependent killing pattern was observed in the ME180 cell line. Anti-TROP2(scFv)-ETA had an IC_{50} of 23.47 nM (**Figure 3.9 d)**, whereas anti-TROP2(scFv)-dETA was less effective, with an IC_{50} of 40.78 nM (**Figure 3.9 c**). Anti-TROP2(scFv)-dETA/ETA did not show significant cytotoxicity in the HEK293T cell line, confirming its specificity for TROP2-expressing cells.

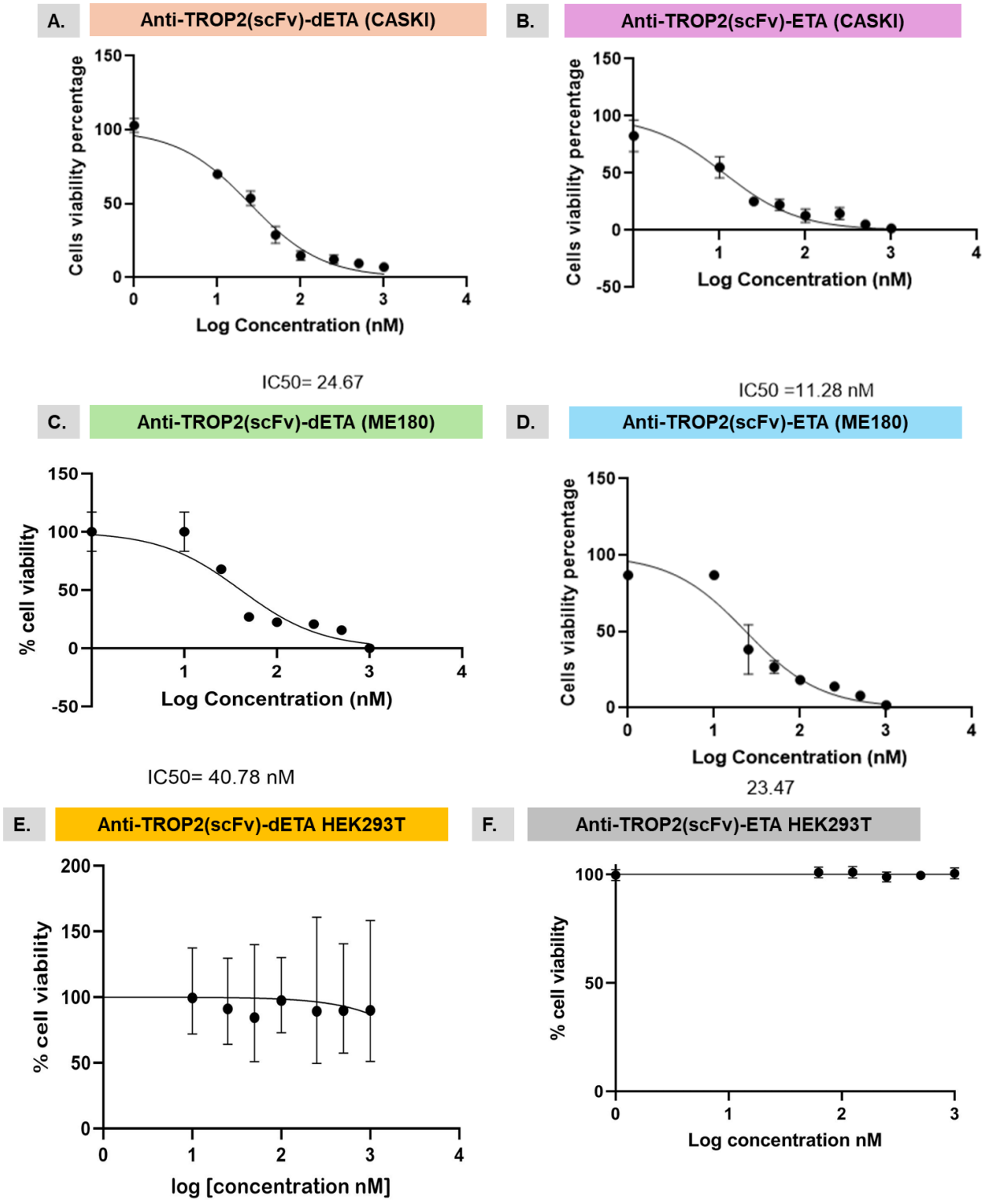

Figure 3.9: Dose-response curves showing the cytotoxic effects of anti-TROP2 (scFv)-ETA and anti-TROP2 (scFv)-dETA on cervical cancer cell line. Cell viability was assessed using the XTT assay after a 68-hour treatment of TROP2(scFv) positive cell lines (ME180 and CaSki) and a negative control cell line (HEK293T). Cells were incubated with recombinant immunotoxins (rIT) at varying concentrations ranging from 1000 nM to 1 nM. Dose-response curve and IC50 value of rIT were evaluated. **(A)**

Anti-TROP2(scFv)-dETA in CaSki cells. **(B.)** anti-TROP2(scFv)-ETA in CaSki cells. **(C.)** anti-TROP2(scFv)-ETA in ME180 cells **(D.)** anti-TROP2(scFv)-dETA in ME180 cells **(E.)** anti-TROP2(scFv)-dETA, **and (F.)** anti-TROP2(scFv)-ETA on HEK293T cells. Each data point represents the mean cell viability percentage ± standard deviation from triplet measurements. GraphPad Prism was used to calculate the IC50 and the sigmoid curve.

CHAPTER 4

DISCUSSION

4.1 Cervical Cancer: The Urgent Need for Effective Treatments

Cervical cancer remains one of the most common cancers affecting women globally, particularly in low- and middle-income countries (LMICs), where access to prevention programs, including human papillomavirus (HPV) vaccination and cervical screening are suboptimal. [185]. Despite advancements in early detection and treatment, cervical cancer continues to present a significant public health challenge, particularly due to its high mortality rates at advanced stages, especially following metastatic progression. [186]. Early-stage cervical cancer is typically managed through surgery, radiation, and chemoradiation; however, these conventional approaches have limited efficacy and are often associated with significant complications [63], [187].

Once the disease metastasizes to distant organs, it becomes more aggressive, which leads to increased mortality and poor prognostic outcomes. Metastatic cervical cancer poses a significant clinical challenge, with limited treatment options resulting in a poor prognosis. Patients with advanced-stage cervical cancer endure considerable physical and emotional burdens, underscoring the urgent need for innovative and more effective therapeutic strategies [188].

Developing novel targeted cancer therapies, such as recombinant immunotoxins (rITs), holds significant promise in addressing this unmet need. Recombinant immunotoxins offer a highly specific mechanism of action, enabling more effective tumour control than traditional treatments. The antibody component of the immunotoxin binds to cancer-specific antigens, facilitating its internalization and subsequent delivery of the toxin to the cell cytosol. Within the cytosol, the toxin exerts its effects by inhibiting protein synthesis or inducing apoptosis, thereby selectively eliminating cancer cells while minimizing off-target effects [126].

4.2 Use of the stress-induced periplasmic expression and production of rITs in *E. coli*

The *E. coli* expression system is the most widely used and cost-effective method for producing recombinant proteins. It offers advantages such as a faster growth rate under optimized conditions and the capability to achieve high cell density quickly using inexpensive media [189], making it ideal for large-scale fermentation processes. Consequently, this study utilized the *E. coli* expression system to obtain substantial quantities of rITs, enabling seamless transitions from small-scale laboratory experiments to large-scale industrial production without major protocol changes. [190].

Despite the benefits of using the *E. coli* expression system, a significant number of recombinant proteins are not effectively produced in this system. One notable drawback is the aggregation of proteins into insoluble forms known as inclusion bodies (IBs) [191]. The formation of IBs represents a considerable challenge, as these aggregates obstruct the production of soluble proteins that have proper biological functionality at both laboratory and industrial scales [192]. Furthermore, recovering functional proteins from IBs involves a labor-intensive and time-consuming process of denaturation and renaturation, often leading to low yields of active, full-length proteins [193].

To address this challenge, this study employed a periplasmic osmotic stress expression method established in 2000 by Prof. Dr. Dr. Stefan Barth, aiming to overcome difficulties associated with expressing proteins that tend to aggregate into inclusion bodies (IBs) [181]. This method involves adding salt to introduce osmotic stress alongside compatible solutes to facilitate recombinant expression in otherwise inhibitory conditions for E. coli. These compatible solutes induce a stress response that enhances the production of heat shock proteins and molecular chaperones by creating a stabilizing periplasmic microenvironment at high salt concentrations. The addition of compatible solutes to shaking cultures allows for bacterial growth under these osmotic stress conditions, as implemented in this thesis. Several studies have demonstrated that the inclusion of certain compatible solutes enhances the expression of soluble recombinant proteins in *E. coli* [194], [195], [196]. *E. coli* adapts to osmotic pressure by accumulating osmolytes, which improve protein solubility and stability by facilitating refolding and preventing aggregation. Osmolytes can inhibit aggregation, and substances such as betaine and sorbitol play a crucial role in enhancing protein

solubility and stability by aiding protein refolding and preventing aggregation [197]. Specifically, betaine is known to modulate the free energy of the denatured state, favorably shifting the equilibrium toward the native state of the recombinant protein.

This method was designed to facilitate the production of recombinant soluble proteins, such as immunotoxins, within the periplasm of *E. coli* under osmotic stress conditions [181]. Using the periplasmic space of *E. coli* for protein expression offers several advantages compared to cytoplasmic production. Protein isolation is easier because the periplasmic fraction is less contaminated with cytoplasmic proteins and endotoxins; this simplifies downstream processing and purification.

In this study, anti-TROP2(scFv)-ETA/dETA and anti-MSLN(scFv)-ETA/dETA were successfully expressed as soluble proteins with minimal visible aggregation, as illustrated in **Figure 3.5**. Although some aggregates were still observed, the expression yielded predominantly soluble full length protein, indicating favourable solubility under the conditions used.Strategies such as reducing the induction temperature, using low IPTG concentration, and inducing during the early log phase have been shown to enhance the production of soluble recombinant proteins *in E. coli* [198], [199], [200]. This occurs because the energy conservation response slows down central carbon metabolism, leading to a slower growth rate [201]. Expressing proteins imposes a metabolic burden on the host, which can result in the accumulation of target proteins in insoluble aggregates. Protein aggregation is more likely at elevated temperatures due to the strong temperature dependence of hydrophobic interactions among amino acids. Thus, lowering the induction temperature can help prevent protein aggregation [201]. Higher temperatures can also increase the likelihood of plasmid loss due to the accelerated growth rate [195].

The optical density of the expression culture is important because high cell densities may not be ideal for protein production [201]. Factors such as nutrient depletion, acetate production, reduced oxygen, and elevated carbon dioxide levels can decrease recombinant gene expression at high cell densities [202]. The duration of induction is crucial, as extended incubation may lead to protein aggregation. Many studies have standardized the induction duration at 16 hours, and we followed this approach in the present study. However, the optimal induction duration can vary depending on the specific protein being expressed, the host organism, and other factors [203]. Longer

or shorter induction times may be necessary to achieve the highest yield and solubility of the recombinant protein. Therefore, careful optimization of the induction conditions, as described above, is essential for successful recombinant protein production.

Previous research within the MB&I laboratory has demonstrated the successful expression of difficult-to-express proteins using the periplasmic osmotic stress production method in the presence of compatible solutes [204], [205], [206]. This current research further provides evidence that the stress-induced expression procedure supported by compatible solutes generates functional recombinant proteins.

4.3 Production and Purification of functional rITs

The production of pure rITs is crucial for their therapeutic efficacy and safety. rITs work by specifically targeting diseased or cancerous cells and delivering a toxic payload to induce apoptosis while sparing healthy cells [207], [208]. However, impurities can compromise the biological activity of rITs, reducing their therapeutic potency and increasing the risk of adverse immunologic responses [208]. Therefore, high-purity rITs are essential to ensure consistent pharmacological effects, minimize off-target toxicity, and meet the stringent quality standards required for clinical applications. Achieving optimal purity is particularly challenging due to the inherent difficulties associated with expressing and folding complex recombinant proteins, yet it remains a fundamental requirement for the successful development of these targeted therapies [209].

This study used a two-step immobilized metal affinity chromatography (IMAC) purification method to purify rITs [210]. The research unit MB&I, where this study was conducted, supports projects for over 20 postgraduate students; therefore, prudent resource management is needed. Each construct was subject to a limited number of purification cycles, so the buffers and columns had to be optimized to establish a proof of concept.

The optimization process required careful consideration of various parameters, including the type of chromatography, buffer components, flow rate, column size, and recovery rate. IMAC was chosen for this study due to its ability to utilize the His-tag on the recombinant protein, which binds to the metal ions immobilized on the

chromatography matrix [211]. The imidazole ring in the histidine side chain can bind to transition metal ions that are often immobilized on chromatography resin [211]. This selective binding enables proteins with a histidine tag to be captured and purified from complex mixtures. The His-tag, comprising 6 to 10 amino acids, can be easily added at either the N- or C-terminus of the protein, allowing flexibility in construct design [212]. The His-tag was selected for this study because of its straightforward incorporation into the peptide sequence of the recombinant immunotoxins (rITs) compared to other affinity tags like Arg-tag and Strep-tag [212]. Additionally, the His-tag's effectiveness at small sizes helps minimize the risk of hindering protein folding or function. The histidine tag can be efficiently eluted from the resin using imidazole, which competitively binds to the immobilized metal ions, facilitating the displacement of the tagged protein and permitting the purification of the target protein.

The first step in the IMAC purification process involved using a 5 mL His-Trap FF crude column. This column is specifically designed for purifying His-tagged proteins and is optimized for crude lysate sample [213] [207]. This size allows for a greater binding capacity, which is essential when purifying proteins from larger lysate volumes. Therefore, to improve the clarity of the lysate and facilitate the loading of a non-viscous sample onto the column, ultra-centrifugation and filtration steps were performed prior to IMAC [214]. This is critical in preventing issues such as clogging and excessive pressure on the column.

The first IMAC purification, detailed in **section 2.5.1,** was conducted at a high flow rate of 4 mL/min, using an equilibration and wash buffer that contained 1 M NaCl but no imidazole. High salt concentration effectively reduced non-specific interactions and led to a significant decrease in contaminants and impurities. High salt shields charged residues on contaminant proteins, weakening their binding to the IMAC matrix [215]. However, some native bacterial proteins were still co-purified with our protein of interest. *E. coli* proteins naturally contain histidine-rich regions or metal-binding motifs, which enable them to bind to IMAC resins, contributing to this co-elution.

A second IMAC purification of the collected eluted fractions from IMAC I, as described in **section 2.5.2,** was conducted at a reduced flow rate of 0.5 mL/min using a wash buffer that contained 500 mM NaCl and 30 mM imidazole. This adjustment successfully eliminated many contaminants, as confirmed by SDS-PAGE analysis,

which showed the presence of full-length anti-TROP2(scFv)-ETA and anti-TROP2(scFv)-dETA proteins at 72 kDa, along with a significant reduction in contaminant bands. The chosen concentration of imidazole effectively prevented the non-specific binding of proteins while allowing the His-tagged target proteins to outcompete for binding sites on the column [216]. In protein purification, the primary goal is to maximize the yield of the target protein while minimizing contamination and degradation [212]. The choice of buffer plays a crucial role in achieving this objective [215]. The slow flow rate purification method detailed in **subsection 2.5.2** was specifically designed to remove a high amount of contaminating proteins, resulting in higher quality purification. This approach gives more time for the protein to bind to the column, thus increasing binding activity and reducing protein loss [207].

In this study, the flow rate for IMACII was reduced to 0.5 mL/min, leading to a notable improvement in both the chromatographs and protein yield. However, even with these enhancements, some impurities still persisted after the second purification. Some studies recommend adding 10 mM 2-mercaptoethanol to the loading, washing, or elution buffers [217],[218]. This addition may help resolve the remaining issues regarding protein purity. They also propose that nonspecific hydrophobic interactions with the IMAC matrix could be a possible cause of nonspecific protein coelution. To address this, incorporating low levels of non-ionic detergents, such as Triton X-100 or Tween 20, into the buffers may help diminish the interactions of nonspecific proteins without interfering with the target protein's binding to the IMAC matrix [219].

Overall, these results underscore the significance of optimizing buffer conditions during IMAC to obtain high-purity target protein preparations [218]. Although the total purity of all the proteins fell considerably short of previously established benchmarks for other scFv and ETA-based rITs, these findings demonstrated an improvement in protein yield following the proof of concept, suggesting that the skills and techniques employed were notably enhanced. Given constraints in time and resources, it was not practical to continue these experiments to achieve further increases in protein purity.

In developing the periplasmic expression protocol, Barth *et al.* outlined a purification strategy that began with immobilized metal affinity chromatography (IMAC) to quickly eliminate a substantial amount of contaminants [181]. This was followed by size exclusion chromatography (SEC) to achieve further purification of the protein and

improve its stability. From SEC the researchers could obtain above obtain protein purity levels above 90% to 95% [220], [221]. However, in the present study, suitable SEC columns were not readily available, so two consecutive IMAC purifications were implemented as previously described. The optimized two-step IMAC purification method proved sufficient for the downstream application of functional anti-TROP2(scFv)-ETA/dETA.

Unlike anti-TROP2 (scFv), western blot analysis of anti-MSLN (scFv) rITs indicated degradation following the second IMAC (**Figure 3.6**). This degradation may be attributed to several factors related to protein handling and purification techniques. To mitigate degradation stringent temperature control post bacterial expression is needed. This entails maintaining the protein samples at temperature low enough to preserve their integrity during pelleting, sonication and purification. Another potential source of degradation is during sonication. Sonication can be damaging to recombinant proteins. The mechanical forces and local heating generated during sonication can lead to protein denaturation, aggregation, and loss of biological activity. While sonication is effective for releasing recombinant periplasmic soluble proteins from *E. coli*, it can negatively affect protein quality by inducing misfolding and degradation. Combining sonication with gentle extraction methods and optimizing sonication parameters can mitigate these effects and improve recovery of active, soluble proteins. Furthermore, for optimal protein stability, the buffer pH should be within a few pH units of the pI, ideally 1-2 units away. At the pI, the protein is least soluble and most likely to precipitate or aggregate. The second IMAC buffers used contain Tris, which can increase in pH at lower temperatures, potentially further destabilizing the protein [218]. Despite these challenges, the potential of our research to improve cervical cancer treatment remains promising, instilling confidence in the future of this field.

Size exclusion chromatography (SEC) is commonly employed as a final polishing step in protein purification to achieve high purity. However, SEC was not performed in this study due to limited access to SEC columns, which was influenced by the high number of students the laboratory needed to support, as well as the associated costs. Instead, a second-step IMAC purification was performed, which successfully yielded 3.735 mg of anti-TROP2-dETA and 1.6615 mg of anti-TROP2-ETA. While SEC can enhance the purity of recombinant proteins, the second IMAC step proved effective for obtaining

sufficient quantities of soluble protein for downstream applications.

4.4 Functional activity of anti-TROP2(scFv)- rITs on cervical cancer cell lines

4.4.1 Binding activity and Internalization studies

The primary aim of this study was to produce a functional recombinant immunotoxin [anti-TROP2 (scFv)] capable of selectively binding to cells expressing the target antigen, TROP2. To ensure functionality, non-degraded anti-TROP2(scFv)-ETA or anti-TROP2(scFv)-dETA was utilized, and its specificity was evaluated using confocal microscopy with TROP2-positive and TROP2-negative cell lines. Antigen-binding and internalization properties were assessed by conjugating the histidine-tagged rIT with either anti-histidine Alexa Fluor 488 or Alexa Fluor 647 dyes, as detailed in **subsection 2.7.2**. The results demonstrated that TROP2-positive cell lines exhibited clear cell surface binding and subsequent internalization of the rIT, evidenced by the green fluorescence signal from anti-His-Alexa Fluor 488 (**Figure 3.8 a & b**) and red fluorescence from anti-His-Alexa Fluor 647 (**Figure 3.8 c**). Incubation of rIT conjugates with various cancer cell lines (ME180, CaSki, and HeLa) revealed distinct fluorescence signal patterns, reflecting differences in binding and internalization dynamics [224], [225].

The fluorescence signals confirmed surface binding localized along the cell membrane, indicating a specific interaction of the rIT with TROP2 expressed on the cell surface (**Figure 3.6**). Notably, anti-TROP2(scFv)-ETA or dETA binding on CaSki cells showed increased fluorescent membrane binding intensity, as these cells are known for their high level of surface expression of TROP2 [226], which likely contributes to enhanced antibody binding. In contrast, ME180 cells demonstrated more rapid internalization of the rIT, which may be attributed to differences in membrane dynamics that facilitate quicker internalization [115], [227].

Intracellular signals within the cytoplasm further evidenced the internalisation of the rIT, suggesting active uptake and trafficking to intracellular compartments such as endosomes or lysosomes [228]. The dotted fluorescence pattern observed in the cytoplasm supports this hypothesis. HeLa cells demonstrated moderate binding to the rIT, with less strong surface interactions compared to CaSki cells but internalisation

rates comparable to ME180.

In contrast, the TROP2-negative HEK293T cell line displayed minimal to no fluorescence (green or red), signifying negligible binding or internalisation of the rIT. These findings underscore the receptor specificity of the rIT, as the observed binding and internalisation were restricted to TROP2-positive cells. In conclusion, these results validate the receptor-specific activity of anti-TROP2(scFv)-ETA and anti-TROP2(scFv)-dETA on TROP2-expressing cells. They demonstrate their potential as targeted therapeutic agents for TROP2-positive cancers, offering a promising future in cancer treatment.

While the results may have successfully demonstrated proof of concept with a limited number of cell lines, future studies should utilize a broader range of cell lines during initial screenings. This will help ensure robust findings that apply across diverse cell types. Cell lines are easy to use, cost-effective, and have established research protocols, allowing for standardized experiments and initial testing of potential interactions. However, to translate findings into clinically relevant insights, subsequent studies should prioritize using patient-derived tumours instead of just cell lines. Patient-derived xenograft models better capture the characteristics of human tumours, including their appearance and genetic makeup [229]. PDX models enable researchers to study drug responses, resistance mechanisms, tumour diversity, and metastasis. As PDX tumours grow in immunocompromised mice, they retain the molecular features of the original patient tumours, including mutations, genomic changes, and epigenetic features [230]. This allows PDX models to reflect the diversity and heterogeneity of patient tumours. PDX models also aid in evaluating both the anti-cancer effects and toxicity of new therapies, accurately assessing their potential [231]. PDX is an important preclinical cancer model that overcomes the limitations of cell lines and provides results that are more reflective of clinical outcomes.

4.4.2 Cytotoxic activity of anti-TROP2(scFv)-ETA/dETA

Recombinant immunotoxins (rITs) represent a novel class of targeted therapeutic agents designed to selectively destroy cancer cells [232]. These agents consist of an antibody fragment that recognizes specific tumours antigens fused to a toxic payload, typically derived from bacterial sources such as *Pseudomonas aeruginosa* exotoxin

(ETA) [144]. The mechanism of action of rITs begins with the binding of the immunotoxin to its target antigen on the surface of cancer cells. This interaction facilitates receptor-mediated endocytosis, which leads to the internalization of the rIT into the cytosol. Once inside the cell, the toxic component exerts its cytotoxic effects by inhibiting protein synthesis. Specifically, PE ADP-ribosylates elongation factor 2 (EF-2), which is critical in translation. This inhibition effectively halts protein synthesis, leading to cellular apoptosis or necrosis [233]. The high specificity of rITs allows for a targeted approach that minimizes damage to surrounding healthy tissues, a significant advantage over conventional chemotherapeutic agents [234].

The XTT assay, a widely used method in cancer research, was applied to evaluate the efficacy of rITs. This assay measures cell viability based on metabolic activity, offering a reliable and quantitative assessment of the cytotoxic effects of rITs on cancer cell lines [235]. In this assay, live cells exhibit active mitochondrial enzymes that can reduce the tetrazolium salt XTT to an orange-colored formazan product [235]. The intensity of this color change is directly proportional to the number of viable cells present in the culture. The absorbance of the formazan product is measured using a spectrophotometer, typically at wavelengths of 450 nm, with a reference wavelength of 660 nm to account for background absorbance [236]. This assay delivers a quantitative measure of cell viability, allowing researchers to evaluate the cytotoxic effects of rITs on cancer cell lines.

The therapeutic potential of the two rITs, anti-TROP2(scFv)-ETA and anti-TROP2(scFv)-dETA, was assessed on TROP2-positive cervical cell lines (ME180 and CaSki). Using the cell viability (XTT) assay, the R456T mutation on RG7787(dETA) was particularly assessed versus the ETA wild type.

Both anti-TROP2(scFv)-ETA and anti-TROP2(scFv)-dETA exhibited dose-dependent cytotoxicity on TROP2-overexpressing cells ME180 and CaSki. In comparison, anti-TROP2(scFv)-ETA showed significantly higher potency, with IC_{50} values of 11.28 nM in CaSki cells and 23.47 nM in ME180 cells, while anti-TROP2(scFv)-dETA had IC_{50} values of 24.67 nM and 40.78 nM, respectively. Notably, anti-TROP2(scFv)-dETA and anti-TROP2-ETA exhibited negligible cytotoxicity in the HEK293T cell line, confirming their specificity for TROP2-expressing cells, as illustrated in **Figure 3.9.**

The outcome of this study aligns with previous results from our lab, which demonstrated the potential of ETA and dETA variants targeting TAA, such as CD90, EpCAM, and LGR5 [206], [237]. It showed that wild-type ETA-based rITs were more effective than the new dETA-based rITs, exhibiting two-fold in-vitro cytotoxic activity. However, when comparing the newly generated dETA variant with R456T, we observe an improvement, showing enhanced cell-killing abilities compared to the previous RG7787. For future investigations, in vivo studies utilizing murine models would be beneficial to further evaluate and compare the immunogenicity of both RG7787 and the newly generated dETA-based rITs. Such studies would provide valuable insights into the potential differences in immune responses elicited by these two types of rITs, which is crucial for assessing their clinical potential and safety.

In a study by Hassan et al., a PE38-based recombinant immunotoxin (rIT) called SS1P was developed and tested in a phase 1 clinical trial for targeting the mesothelin receptor [238]. However, limited therapeutic effects were observed, as 90% of patients developed neutralizing antibodies against the bacterial toxin after a single treatment cycle [93]. This induction of immunogenicity in patients was the major drawback of this rIT. Subsequently, SS1-LR was developed, which involved removing protease cleavage sites, some B-cell epitopes, and the majority of domain II [239]. This new generation PE24 permitted the safe administration of 5- to 10-fold higher dosages [169], [174]. The resulting mutant, designated LR, was further engineered to eliminate human B-cell epitopes. Using alanine scanning mutagenesis, the authors constructed a PE variant with seven-point mutations in domain III that ablated human B-cell epitopes. The resulting toxin LR-LO10 showed significantly reduced reactivity to sera from patients treated with PE38 [174]. Later, the authors identified that an R458A mutation to eliminate the H3 B-cell epitope on PE38 was responsible for the decreased activity of LO10. An R456A mutation was introduced to restore enzymatic activity to replace R458A in RG7787 [176], [240].

Alewine *et al.* evaluated the mesothelin-targeted immunotoxins SS1P and its PE24 derivatives, SS1-LR and RG7787, in mesothelin-expressing triple-negative breast cancer (TNBC) and gastric cancer cell lines. Their findings demonstrated that SS1-LR generally exhibited greater cytotoxic potency compared to both SS1P and RG7787. For instance, in TNBC cell lines such as HCC70 and SUM149, statistically significant

differences were observed between SS1P and SS1-LR, with SS1-LR displaying markedly lower IC_{50} values (e.g., 0.94 ± 0.56 ng/mL vs. 4.6 ± 3.2 ng/mL in HCC70; and 1.5 ± 1.4 ng/mL vs. 15.7 ± 9.8 ng/mL in SUM149, $P < 0.05$). In contrast, no statistically significant difference was found between SS1P and RG7787 in the HCC70 cell line ($P = 0.38$), although RG7787 did demonstrate some cytotoxic activity.

In broader analyses across both TNBC and gastric cancer cell lines, SS1-LR continued to show higher potency than RG7787. For example, SS1-LR achieved IC_{50} values ranging from 5.5 pM to 37.1 pM, whereas RG7787 exhibited IC_{50} values ranging from 75.6 pM to >1200 pM. The only exception was the MKN45 gastric cancer cell line, in which RG7787's activity was comparable.

Overall, the results suggest that while RG7787 retains cytotoxic activity, its potency is generally lower than that of SS1-LR. The study highlights the challenge of maintaining high cytotoxic efficacy while reducing immunogenicity. The superior cytotoxicity observed with newer constructs, such as the dETA variant, compared to RG7787 suggests that targeted modifications may further enhance the therapeutic potential of deimmunized immunotoxins.

.

CHAPTER 5

CONCLUSION AND FUTURE WORK

Developing effective and affordable treatments for cervical cancer is an urgent global health priority, particularly in low-income regions where limited funding and resources hinder access to adequate healthcare [241]. Advancing therapeutic options will significantly improve outcomes for patients affected by this disease [16].

Recombinant immunotoxins (rITs) have emerged as promising therapeutic agents for both invasive and non-invasive cancers due to their high specificity and potency [242]. In this study, we successfully generated potent anti-TROP2-based rITs. These rITs were expressed in *E. coli,* providing a scalable and cost-efficient production system [243]. The periplasmic expression strategy ensured proper protein folding and functionality. Purification was achieved using IMAC in a two-step process, yielding protein purity. However, further refinement with size exclusion chromatography (SEC) could enhance purity levels, aligning with previous studies on ETA-based proteins [204],[181],[234],[237]. A noteworthy observation was that the anti-mesothelin(scFv) protein did not bind properly to the column and was also degraded owing to buffer conditions [211]. Future efforts should focus on fine-tuning buffer compositions to mitigate degradation and maintain protein integrity and increase binding to the column.

One of the key findings of this study includes the selective binding of anti-TROP2 (scFv)-ETA and anti-TROP2(scFv)-dETA to TROP2-positive cells with no observable binding to TROP2-negative cells. This specificity demonstrates the targeted action of the immunotoxins and provides insights into their potential mechanisms of operation. Notably, the dETA-based rITs exhibited a two-fold improvement in in vitro cytotoxicity activity compared to their ETA-based counterparts, highlighting the success of the introduced mutation in enhancing cytotoxicity relative to RG7787.

In the future, we should prioritise increasing the purity of these immunotoxins using IMAC and SEC, which could enhance their cytotoxic effects and improve their clinical applicability. To evaluate immunogenicity and therapeutic potential, high-purity dETA-based rIT should be assessed in mice models. The findings of this study demonstrate the potential of the recombinant immunotoxins herein as a locally

produced and cost-effective treatment solution for cervical cancer, offering hope for improved treatment outcomes in resource-limited settings.

REFERENCES

[1] Z. Momenimovahed, A. Mazidimoradi, P. Maroofi, L. Allahqoli, H. Salehiniya, and I. Alkatout, “Global, regional and national burden, incidence, and mortality of cervical cancer,” *Cancer Rep*, no. October 2022, pp. 1–10, 2022, doi: 10.1002/cnr2.1756.

[2] D. Stelzle *et al.*, “Estimates of the global burden of cervical cancer associated with HIV,” *Lancet Glob Health*, vol. 9, no. 2, pp. e161–e169, Feb. 2021, doi: 10.1016/S2214-109X(20)30459-9.

[3] R. Slavkovsky, E. Callen, C. Pecenka, and M. Mvundura, “Costs of human papillomavirus vaccine delivery in low- and middle-income countries: A systematic review,” *Vaccine*, vol. 42, no. 6, pp. 1200–1210, Feb. 2024, doi: 10.1016/j.vaccine.2024.01.094.

[4] D. Singh *et al.*, “Global estimates of incidence and mortality of cervical cancer in 2020: a baseline analysis of the WHO Global Cervical Cancer Elimination Initiative,” *Lancet Glob Health*, vol. 11, no. 2, pp. e197–e206, Feb. 2023, doi: 10.1016/S2214-109X(22)00501-0.

[5] E. Jedy-Agba *et al.*, “Trends in cervical cancer incidence in sub-Saharan Africa,” *Br J Cancer*, vol. 123, no. 1, pp. 148–154, Jul. 2020, doi: 10.1038/s41416-020-0831-9.

[6] C. Clendinen, Y. Zhang, R. N. Warburton, and D. W. Light, “Manufacturing costs of HPV vaccines for developing countries,” *Vaccine*, vol. 34, no. 48, pp. 5984–5989, Nov. 2016, doi: 10.1016/j.vaccine.2016.09.042.

[7] J. N. Lim and A. A. Ojo, “Title: Barriers to utilization of cervical cancer screening in Sub Sahara Africa: a systematic review.”

[8] D. D. Atnafu, R. Khatri, and Y. Assefa, “Drivers of cervical cancer prevention and management in sub-Saharan Africa: a qualitative synthesis of mixed studies,” Dec. 01, 2024, *BioMed Central Ltd*. doi: 10.1186/s12961-023-01094-3.

[9] M. QUINN *et al.*, “Carcinoma of the Cervix Uteri,” *International Journal of Gynecology and Obstetrics*, vol. 95, no. SUPPL. 1, 2006, doi: 10.1016/S0020-7292(06)60030-1.

[10] S. Zhang, H. Xu, L. Zhang, and Y. Qiao, “Cervical cancer: Epidemiology, risk factors and screening,” *Chinese Journal of Cancer Research*, vol. 32, no. 6, pp. 720–728, 2020, doi: 10.21147/j.issn.1000-9604.2020.06.05.

[11] D. K. Gaffney, M. Hashibe, D. Kepka, K. A. Maurer, and T. L. Werner, “Too many women are dying from cervix cancer: Problems and solutions,” *Gynecol Oncol*, vol. 151, no. 3, pp. 547–554, Dec. 2018, doi: 10.1016/j.ygyno.2018.10.004.

[12] C. A. Burmeister *et al.*, “Cervical cancer therapies: Current challenges and future perspectives,” *Tumour Virus Res*, vol. 13, p. 200238, Jun. 2022, doi: 10.1016/j.tvr.2022.200238.

[13] G. Murewanhema, “The COVID-19 pandemic and its implications for cervical cancer treatment and prevention in Zimbabwe: perspectives and recommendations,” *Pan African Medical Journal*, vol. 39, 2021, doi: 10.11604/pamj.2021.39.149.26467.

[14] M. L. King, “How manufacturing won or lost the COVID-19 vaccine race,” *Vaccine*, vol. 42, no. 5, pp. 1004–1012, Feb. 2024, doi: 10.1016/j.vaccine.2023.12.031.

[15] “II. Complementary data on cervical cancer prevention.” [Online]. Available: www.hpvcentre.net

[16] W. Small *et al.*, “Cervical cancer: A global health crisis,” *Cancer*, vol. 123, no. 13, pp. 2404–2412, Jul. 2017, doi: 10.1002/cncr.30667.

[17] T. F. Akinyemiju, J. A. McDonald, and P. M. Lantz, “Health care access dimensions and cervical cancer screening in South Africa: Analysis of the world health survey,” *BMC Public Health*, vol. 15, no. 1, Apr. 2015, doi: 10.1186/s12889-015-1686-5.

[18] S. Finocchario-Kessler, C. Wexler, M. Maloba, N. Mabachi, F. Ndikum-Moffor, and E. Bukusi, “Cervical cancer prevention and treatment research in Africa: A systematic review from a public health perspective,” *BMC Womens Health*, vol. 16, no. 1, Jun. 2016, doi: 10.1186/s12905-016- 0306-6.

[19] S. P. Rautenbach *et al.*, “Future HIV epidemic trajectories in South Africa and projected long-term consequences of reductions in general population HIV testing: a mathematical modelling study,” *Lancet Public Health*, vol. 9, no. 4, pp. e218–e230, Apr. 2024, doi: 10.1016/S2468- 2667(24)00020-3.

[20] T. Dhokotera *et al.*, “The burden of cancers associated with HIV in the South African public health sector, 2004-2014: A record linkage study,” May 03, 2019, *BioMed Central Ltd.* doi: 10.1186/s13027-019-0228-7.

[21] E. Sinanovic, J. Moodley, M. A. Barone, S. Mall, S. Cleary, and J. Harries, “The potential cost-effectiveness of adding a human papillomavirus vaccine to the cervical cancer screening programme in South Africa,” *Vaccine*, vol. 27, no. 44, pp. 6196–6202, Oct. 2009, doi: 10.1016/j.vaccine.2009.08.004.

[22] C. Clendinen, Y. Zhang, R. N. Warburton, and D. W. Light, “Manufacturing costs of HPV vaccines for developing countries,” *Vaccine*, vol. 34, no. 48, pp. 5984–5989, Nov. 2016, doi: 10.1016/j.vaccine.2016.09.042.

[23] H. N. Nguyen and H. E. Averette, “Biology of cervical carcinoma,” *Semin Surg Oncol*, vol. 16, no. 3, pp. 212–216, Apr. 1999, doi: 10.1002/(SICI)1098-2388(199904/05)16:3<212::AID-SSU3>3.0.CO;2-B.

[24] W. M. J. Schoell, M. F. Janicek, and R. Mirhashemi, “Epidemiology and biology of cervical cancer,” *Semin Surg Oncol*, vol. 16, no. 3, pp. 203–211, Apr. 1999, doi: 10.1002/(SICI)1098-2388(199904/05)16:3<203::AID-SSU2>3.0.CO;2-C.

[25] T. Hagemann *et al.*, “Molecular profiling of cervical cancer progression,” *Br J Cancer*, vol. 96, no. 2, pp. 321–328, 2007, doi: 10.1038/sj.bjc.6603543.

[26] E. I. Obeagu and G. U. Obeagu, “An update on premalignant cervical lesions and cervical cancer screening An update on premalignant cervical

lesions and cervical cancer screening services among HIV positive women .," no. February, 2023, doi: 10.35841/aajphn-6.2.141.

[27] H. Kubitschke *et al.*, "Roadmap to Local Tumour Growth: Insights from Cervical Cancer," *Sci Rep*, vol. 9, no. 1, Dec. 2019, doi: 10.1038/s41598-019-49182-1.

[28] K. . K. Okunade., "Human papilomavirus and cervical cancer, "Journal of Obstetrics and Gynaecology. May. 2020, doi: 10.1080/01443615.2019.1634030. r.

[29] Y. Wu, Y. Chen, L. Li, G. Yu, Y. Zhang, and Y. He, "Associations of high-risk HPV types and viral load with cervical cancer in China," *Journal of Clinical Virology*, vol. 35, no. 3, pp. 264–269, Mar. 2006, doi: 10.1016/j.jcv.2005.07.011.

[30] S. D. Balasubramaniam, V. Balakrishnan, C. E. Oon, and G. Kaur, "Key molecular events in cervical cancer development," 2019, *MDPI AG*. doi: 10.3390/medicina55070384.

[31] D. D. Atnafu, R. Khatri, and Y. Assefa, "Drivers of cervical cancer prevention and management in sub-Saharan Africa: a qualitative synthesis of mixed studies," Dec. 01, 2024, *BioMed Central Ltd*. doi: 10.1186/s12961-023-01094-3.

[32] S. Shanmugasundaram and J. You, "Targeting persistent human papillomavirus infection," Feb. 18, 2017, *MDPI AG*. doi: 10.3390/v9080229.

[33] E. M. Burd, "Human papillomavirus and cervical cancer," Jan. 2003. doi: 10.1128/CMR.16.1.1-17.2003.

[34] J. Doorbar *et al.*, “The biology and life-cycle of human papillomaviruses,” 2012, *Elsevier Ltd*. doi: 10.1016/j.vaccine.2012.06.083.

[35] J. Proulx, M. Ghaly, I.-W. Park, and K. Borgmann, “HIV-1-Mediated Acceleration of Oncovirus-Related Non-AIDS-Defining Cancers,” *Biomedicines*, vol. 10, no. 4, p. 768, Mar. 2022, doi: 10.3390/biomedicines10040768.

[36] K. Baisley *et al.*, “Comparing one dose of HPV vaccine in girls aged 9–14 years in Tanzania (DoRIS) with one dose of HPV vaccine in historical cohorts: an immunobridging analysis of a randomised controlled trial,” *Lancet Glob Health*, vol. 10, no. 10, pp. e1485–e1493, Oct. 2022, doi: 10.1016/S2214-109X(22)00306-0.

[37] C.-S. Yoon, K.-D. Kim, S.-N. Park, and S.-W. Cheong, “α6 Integrin Is the Main Receptor of Human Papillomavirus Type 16 VLP,” *Biochem Biophys Res Commun*, vol. 283, no. 3, pp. 668–673, May 2001, doi: 10.1006/bbrc.2001.4838.

[38] S. Hong and L. A. Laimins, “Regulation of the Life Cycle of HPVs by Differentiation and the DNA Damage Response,” *Future Microbiol*, vol. 8, no. 12, pp. 1547–1557, Dec. 2013, doi: 10.2217/fmb.13.127.

[39] E. Albert and L. Laimins, “Regulation of the human papillomavirus life cycle by DNA damage repair pathways and epigenetic factors,” Jul. 01, 2020, *MDPI AG*. doi: 10.3390/v12070744.

[40] E. Albert and L. Laimins, “Regulation of the human papillomavirus life cycle by DNA damage repair pathways and epigenetic factors,” Jul. 01, 2020, *MDPI AG*. doi: 10.3390/v12070744.

[41] K. Strati and P. F. Lambert, “Role of Rb-dependent and Rb-independent functions of papillomavirus E7 oncogene in head and neck cancer,” *Cancer Res*, vol. 67, no. 24, pp. 11585–11593, Dec. 2007, doi: 10.1158/0008-5472.CAN-07-3007.

[42] A. A. McBride and A. Warburton, “The role of integration in oncogenic progression of HPV-associated cancers,” Apr. 01, 2017, *Public Library of Science*. doi: 10.1371/journal.ppat.1006211.

[43] J. Doorbar *et al.*, “The biology and life-cycle of human papillomaviruses,” 2012, *Elsevier Ltd*. doi: 10.1016/j.vaccine.2012.06.083.

[44] R. Jonsson, “The Nobel prize in physiology or medicine for 2008,” Dec. 2008. doi: 10.1111/j.1365-3083.2008.02189.x.

[45] P. Kaur *et al.*, “Human papillomavirus vaccine for cancer cervix prevention: Rationale & recommendations for implementation in India,” *Indian Journal of Medical Research*, vol. 146, no. 2, p. 153, 2017, doi: 10.4103/ijmr.IJMR_1906_16.

[46] S. Kamolratanakul and P. Pitisuttithum, “Human Papillomavirus Vaccine Efficacy and Effectiveness against Cancer.,” *Vaccines (Basel)*, vol. 9, no. 12, Nov. 2021, doi: 10.3390/vaccines9121413.

[47] M. Fawzy, E. Nofal, N. Abdelkhalek, and R. Ehab, “Intralesional bivalent and quadrivalent human papillomavirus vaccines didn’t significantly

enhance the response of multiple anogenital warts when co-administered with intralesional Candida antigen immunotherapy. A randomized controlled trial," *Arch Dermatol Res*, vol. 315, no. 10, pp. 2813–2823, Dec. 2023, doi: 10.1007/s00403-023-02698-z.

[48] J. W. Wang and R. B. Roden, "Virus-like particles for the prevention of human papillomavirus-associated malignancies," *Expert Rev Vaccines*, vol. 12, no. 2, pp. 129–141, Feb. 2013, doi: 10.1586/erv.12.151.

[49] S. Chairunnisa *et al.*, "Expression and scale-up production of recombinant human papillomavirus type 52 L1 protein in methylotrophic yeast Hansenula polymorpha," *Journal of Genetic Engineering and Biotechnology*, vol. 22, no. 1, p. 100342, Mar. 2024, doi: 10.1016/j.jgeb.2023.100342.

[50] S. Mroz, X. Zhang, M. Williams, A. Conlon, and N. K. LoConte, "Working to Increase Vaccination for Human Papillomavirus: A Survey of Wisconsin Stakeholders, 2015," *Prev Chronic Dis*, vol. 14, p. 160610, Sep. 2017, doi: 10.5888/pcd14.160610.

[51] P. Di Bonito, L. Accardi, L. Galati, F. Ferrantelli, and M. Federico, "Anti-cancer vaccine for HPV-associated neoplasms: Focus on a therapeutic HPV vaccine based on a novel tumor antigen delivery method using endogenously engineered exosomes," *Cancers (Basel)*, vol. 11, no. 2, Jan. 2019, doi: 10.3390/cancers11020138.

[52] E. Altobelli, G. Scarselli, A. Lattanzi, C. Fortunato, and V. F. Profeta, "A comparison between Pap and HPV screening tests and screening

methods," *Mol Clin Oncol*, vol. 5, no. 2, pp. 348–354, Aug. 2016, doi: 10.3892/mco.2016.909.

[53] H. Ashtarian, E. Mirzabeigi, E. Mahmoodi, and M. Khezeli, "Knowledge about Cervical Cancer and Pap Smear and the Factors Influencing the Pap test Screening among Women.," *Int J Community Based Nurs Midwifery*, vol. 5, no. 2, pp. 188–195, Apr. 2017.

[54] H. M. Shingleton, R. L. Patrick, W. W. Johnston, and R. A. Smith, "The current status of the Papanicolaou smear," *CA Cancer J Clin*, vol. 45, no. 5, pp. 305–320, Sep. 1995, doi: 10.3322/canjclin.45.5.305.

[55] S. Nassiri, S. Aminimoghaddam, M. R. Sadaghian, M. Nikandish, N. Jamshidnezhad, and E. Saffarieh, "Evaluation of the diagnostic accuracy of the cervical biopsy under colposcopic vision," *Eur J Transl Myol*, Oct. 2022, doi: 10.4081/ejtm.2022.10670.

[56] N. Wentzensen *et al.*, "Multiple Biopsies and Detection of Cervical Cancer Precursors at Colposcopy," *Journal of Clinical Oncology*, vol. 33, no. 1, pp. 83–89, Jan. 2015, doi: 10.1200/JCO.2014.55.9948.

[57] S. H. Liyanage, C. A. Roberts, and A. G. Rockall, "MRI and PET Scans for Primary Staging and Detection of Cervical Cancer Recurrence," *Women's Health*, vol. 6, no. 2, pp. 251–269, Mar. 2010, doi: 10.2217/WHE.10.7.

[58] J. Kusmirek, J. Robbins, H. Allen, L. Barroilhet, B. Anderson, and E. A. Sadowski, "PET/CT and MRI in the imaging assessment of cervical

cancer," Oct. 29, 2015, *Springer New York LLC*. doi: 10.1007/s00261-015-0363-6.

[59] J. Kusmirek, J. Robbins, H. Allen, L. Barroilhet, B. Anderson, and E. A. Sadowski, "PET/CT and MRI in the imaging assessment of cervical cancer," Oct. 29, 2015, *Springer New York LLC*. doi: 10.1007/s00261-015-0363-6.

[60] S. Finocchario-Kessler, C. Wexler, M. Maloba, N. Mabachi, F. Ndikum-Moffor, and E. Bukusi, "Cervical cancer prevention and treatment research in Africa: A systematic review from a public health perspective," *BMC Womens Health*, vol. 16, no. 1, Jun. 2016, doi: 10.1186/s12905-016- 0306-6.

[61] P. T. Ramirez, R. Pareja, G. J. Rendón, C. Millan, M. Frumovitz, and K. M. Schmeler, "Management of low-risk early-stage cervical cancer: Should conization, simple trachelectomy, or simple hysterectomy replace radical surgery as the new standard of care?," 2014, *Academic Press Inc.* doi: 10.1016/j.ygyno.2013.09.004.

[62] D. R. Roque, W. Z. Wysham, and J. T. Soper, "The Surgical Management of Cervical Cancer," *Obstet Gynecol Surv*, vol. 69, no. 7, pp. 426–441, Jul. 2014, doi: 10.1097/OGX.0000000000000089.

[63] Y. Li, Q. Kong, H. Wei, and Y. Wang, "Comparison of the complications between minimally invasive surgery and open surgical treatments for early-stage cervical cancer: A systematic review and meta-analysis," Jul. 01, 2021, *Public Library of Science*. doi: 10.1371/journal.pone.0253143.

[64] K. Willows, G. Lennox, and A. Covens, “Fertility-sparing management in cervical cancer: balancing oncologic outcomes with reproductive success,” *Gynecol Oncol Res Pract*, vol. 3, no. 1, p. 9, Dec. 2016, doi: 10.1186/s40661-016-0030-9.

[65] W. Zhang *et al.*, “Clinical Outcomes and Prognostic Factors in Stage III C Cervical Cancer Patients Treated with Radical Radiotherapy or Radiochemotherapy,” *Technol Cancer Res Treat*, vol. 23, Jan. 2024, doi: 10.1177/15330338241254075.

[66] P. G. Rose, “Chemoradiotherapy for cervical cancer,” *Eur J Cancer*, vol. 38, no. 2, pp. 270–278, Jan. 2002, doi: 10.1016/S0959-8049(01)00352-5.

[67] S. Chopra *et al.*, “Late Toxicity After Adjuvant Conventional Radiation Versus Image-Guided Intensity-Modulated Radiotherapy for Cervical Cancer (PARCER): A Randomized Controlled Trial,” *Journal of Clinical Oncology*, vol. 39, no. 33, pp. 3682–3692, Nov. 2021, doi: 10.1200/JCO.20.02530.

[68] R. Thirumaran, G. C. Prendergast, and P. B. Gilman, “Cytotoxic Chemotherapy in Clinical Treatment of Cancer,” in *Cancer Immunotherapy*, Elsevier, 2007, pp. 101–116. doi: 10.1016/B978-012372551-6/50071-7.

[69] A. Llanos, M. Savignano, and G. Cinat, “Maintenance treatment with chemotherapy and immunotherapy in non-small cell lung cancer: a case report,” *Front Oncol*, vol. 2, 2012, doi: 10.3389/fonc.2012.00152.

[70] M. Sahu and H. Suryawanshi, “Immunotherapy: The future of cancer treatment,” May 01, 2021, *Wolters Kluwer Medknow Publications*. doi: 10.4103/0973-029X.325257.

[71] F. Ye *et al.*, “Advancements in clinical aspects of targeted therapy and immunotherapy in breast cancer,” *Mol Cancer*, vol. 22, no. 1, p. 105, Jul. 2023, doi: 10.1186/s12943-023-01805-y.

[72] A. D. Waldman, J. M. Fritz, and M. J. Lenardo, “A guide to cancer immunotherapy: from T cell basic science to clinical practice,” Nov. 01, 2020, *Nature Research*. doi: 10.1038/s41577-020-0306-5.

[73] A. B. Apolo *et al.*, “Adjuvant Pembrolizumab versus Observation in Muscle-Invasive Urothelial Carcinoma,” *New England Journal of Medicine*, Sep. 2024, doi: 10.1056/NEJMoa2401726.

[74] L. Lertsumitkul *et al.*, “EphA3-targeted chimeric antigen receptor T cells are effective in glioma and generate curative memory T cell responses,” *J Immunother Cancer*, vol. 12, no. 8, p. e009486, Aug. 2024, doi: 10.1136/jitc-2024-009486.

[75] Hu. Yixuan., Zhu,Qi,D. *et al*., “Trop2-targeted therapy in breast cancer,” Biomark Res 12, 82 (2024). https://doi.org/10.1186/s40364-024-00633-6.

[76] D. Stefanoudakis *et al.*, “Immunotherapy in Cervical and Endometrial Cancer: Current Landscape and Future Directions,” Mar. 01, 2024, *Multidisciplinary Digital Publishing Institute (MDPI)*. doi: 10.3390/life14030344.

[77] L. Galluzzi *et al.*, “Classification of current anticancer immunotherapies,” *Oncotarget*, vol. 5, no. 24, pp. 12472–12508, Dec. 2014, doi: 10.18632/oncotarget.2998.

[78] S. P. Kang *et al.*, “Pembrolizumab KEYNOTE-001: an adaptive study leading to accelerated approval for two indications and a companion diagnostic,” *Annals of Oncology*, vol. 28, no. 6, pp. 1388–1398, Jun. 2017, doi: 10.1093/annonc/mdx076.

[79] G. Kwok, T. C. C. Yau, J. W. Chiu, E. Tse, and Y.-L. Kwong, “Pembrolizumab (Keytruda),” *Hum Vaccin Immunother*, vol. 12, no. 11, pp. 2777–2789, Nov. 2016, doi: 10.1080/21645515.2016.1199310.

[80] A. Marabelle and J. Gray, “Tumor-targeted and immune-targeted monoclonal antibodies: Going from passive to active immunotherapy,” Aug. 01, 2015, *John Wiley and Sons Inc.* doi: 10.1002/pbc.25508.

[81] W. P. Skelton, J. Castagno, J. Cardenas-Goicoechea, K. Daily, A. Yeung, and M. J. Markham, “Bevacizumab Eligibility in Patients with Metastatic and Recurrent Cervical Cancer: A Retrospective Review,” *Clin Med Insights Oncol*, vol. 12, Jan. 2018, doi: 10.1177/1179554918779587.

[82] K. Strebhardt and A. Ullrich, “Paul Ehrlich’s magic bullet concept: 100 years of progress,” *Nat Rev Cancer*, vol. 8, no. 6, pp. 473–480, Jun. 2008, doi: 10.1038/nrc2394.

[83] D. Ribatti, “From the discovery of monoclonal antibodies to their therapeutic application: An historical reappraisal,” *Immunol Lett*, vol. 161, no. 1, pp. 96–99, Sep. 2014, doi: 10.1016/j.imlet.2014.05.010.

[84] A. Ravelli *et al.*, “Breast cancer circulating biomarkers: advantages, drawbacks, and new insights,” *Tumor Biology*, vol. 36, no. 9, pp. 6653–6665, 2015, doi: 10.1007/s13277-015-3944-7.

[85] A. M. Scott, J. P. Allison, J. D. Wolchok, and H. Hughes, “Monoclonal antibodies in cancer therapy,” vol. 12, no. May, pp. 1–8, 2012.

[86] R. Rouet, K. J. L. Jackson, D. B. Langley, and D. Christ, “Next-Generation Sequencing of Antibody Display Repertoires,” *Front Immunol*, vol. 9, Feb. 2018, doi: 10.3389/fimmu.2018.00118.

[87] I. Pastan and R. Hassan, “Discovery of Mesothelin and Exploiting It as a Target for Immunotherapy,” *Cancer Res*, vol. 74, no. 11, pp. 2907–2912, Jun. 2014, doi: 10.1158/0008-5472.CAN-14-0337.

[88] S. Takamizawa *et al.*, “High mesothelin expression is correlated with non-squamous cell histology and poor survival in cervical cancer: a retrospective study,” *BMC Cancer*, vol. 22, no. 1, Dec. 2022, doi: 10.1186/s12885-022-10277-0.

[89] V. Ramundo, G. Zanirato, and E. Aldieri, “The epithelial-to-mesenchymal transition (Emt) in the development and metastasis of malignant pleural mesothelioma,” *Int J Mol Sci*, vol. 22, no. 22, Nov. 2021, doi: 10.3390/ijms222212216.

[90] K. Jöhrens, L. Lazzerini, J. Barinoff, J. Sehouli, and G. Cichon, “Mesothelin as a target for cervical cancer therapy,” *Arch Gynecol Obstet*, vol. 299, no. 1, pp. 211–216, Jan. 2019, doi: 10.1007/s00404-018-4933-z.

[91] S. S. Kachala *et al.*, “Mesothelin Overexpression Is a Marker of Tumor Aggressiveness and Is Associated with Reduced Recurrence-Free and Overall Survival in Early-Stage Lung Adenocarcinoma,” *Clinical Cancer Research*, vol. 20, no. 4, pp. 1020–1028, Feb. 2014, doi: 10.1158/1078-0432.CCR-13-1862.

[92] O. Kaneko *et al.*, “A Binding Domain on Mesothelin for CA125/MUC16,” *Journal of Biological Chemistry*, vol. 284, no. 6, pp. 3739–3749, Feb. 2009, doi: 10.1074/jbc.M806776200.

[93] I. Pastan and R. Hassan, “Discovery of mesothelin and exploiting it as a target for immunotherapy.,” *Cancer Res*, vol. 74, no. 11, pp. 2907–12, Jun. 2014, doi: 10.1158/0008-5472.CAN-14-0337.

[94] B. Zeybek *et al.*, “Cervical carcinomas that overexpress human trophoblast cell-surface marker (Trop-2) are highly sensitive to the antibody-drug conjugate sacituzumab govitecan,” *Sci Rep*, vol. 10, no. 1, Dec. 2020, doi: 10.1038/s41598-020-58009-3.

[95] X. Liu *et al.*, “Advances in Trop2-targeted therapy: Novel agents and opportunities beyond breast cancer,” Nov. 01, 2022, *Elsevier Inc.* doi: 10.1016/j.pharmthera.2022.108296.

[96] R. Cubas, S. Zhang, M. Li, C. Chen, and Q. Yao, “Trop2 expression contributes to tumor pathogenesis by activating the ERK MAPK pathway.,” *Mol Cancer*, vol. 9, p. 253, 2010, doi: 10.1186/1476-4598-9- 253.

[97] S. Lenárt, P. Lenárt, J. Šmarda, J. Remšík, K. Souček, and P. Beneš, “Trop2: Jack of all trades, master of none,” Nov. 01, 2020, *MDPI AG*. doi: 10.3390/cancers12113328.

[98] A. Shvartsur and B. Bonavida, “Trop2 and its overexpression in cancers: regulation and clinical/ therapeutic implications,” 2015. [Online]. Available: www.impactjournals.com/Genes&Cancer

[99] E. Bignotti *et al.*, “Trop-2 Overexpression in Poorly Differentiated Endometrial Endometrioid Carcinoma: Implications for Immunotherapy With hRS7, a Humanized Anti–Trop-2 Monoclonal Antibody,” *International Journal of Gynecologic Cancer*, vol. 21, no. 9, pp. 1613–1621, Nov. 2011, doi: 10.1097/IGC.0b013e318228f6da.

[100] S. Qiu *et al.*, “Targeting Trop-2 in cancer: Recent research progress and clinical application,” *Biochimica et Biophysica Acta (BBA) - Reviews on Cancer*, vol. 1878, no. 4, p. 188902, Jul. 2023, doi: 10.1016/j.bbcan.2023.188902.

[101] D. Liu, T. M. Cardillo, Y. Wang, E. A. Rossi, D. M. Goldenberg, and C.-H. Chang, “Trop-2-targeting tetrakis-ranpirnase has potent antitumor activity against triple-negative breast cancer,” *Mol Cancer*, vol. 13, no. 1, p. 53, 2014, doi: 10.1186/1476-4598-13-53.

[102] M. Reinisch *et al.*, “Safety and effectiveness of sacituzumab govitecan in patients with metastatic triple-negative breast cancer in real-world settings: first observations from an interdisciplinary breast cancer centre in Germany.,” *Ther Adv Med Oncol*, vol. 15, p. 17588359231200454, 2023, doi: 10.1177/17588359231200454.

[103] T. Manso, A. Kushwaha, N. Abdollahi, P. Duroux, V. Giudicelli, and S. Kossida, “Mechanisms of action of monoclonal antibodies in oncology integrated in IMGT/mAb-DB,” *Front Immunol*, vol. 14, May 2023, doi: 10.3389/fimmu.2023.1129323.

[104] A. I. Bhat and G. P. Rao, “Production of Monoclonal Antibody,” 2020, pp. 223–237. doi: 10.1007/978-1-0716-0334-5_29.

[105] S. Mitra and P. C. Tomar, “Hybridoma technology; advancements, clinical significance, and future aspects,” *Journal of Genetic Engineering and Biotechnology*, vol. 19, no. 1, p. 159, Dec. 2021, doi: 10.1186/s43141-021-00264-6.

[106] H. R. Hoogenboom, A. P. De Bruı̈nebruı̈ne, S. E. Hufton, R. M. Hoet, J.-W. Arends, and R. C. Roovers, “Antibody phage display technology and its applications,” 1998.

[107] S. Choudhary, S. Barth, and R. S. Verma, “SNAP-Tag Technology: A Promising Tool for Ex Vivo Immunophenotyping,” *Mol Diagn Ther*, vol. 21, no. 3, pp. 315–326, Jun. 2017, doi: 10.1007/s40291-017-0263-2.

[108] C. M. M. and N. Sivakumaran, “Detailed Review of Monoclonal Antibody Production and Its Advantage as a Role in Malignancy and Transplant Rejection,” *International Journal of Scientific and Research Publications (IJSRP)*, vol. 8, no. 11, Nov. 2018, doi: 10.29322/IJSRP.8.11.2018.p8337.

[109] G. KÖHLER and C. MILSTEIN, “Continuous cultures of fused cells secreting antibody of predefined specificity,” *Nature*, vol. 256, no. 5517, pp. 495–497, Aug. 1975, doi: 10.1038/256495a0.

[110] T. P. W. M. et al. Janeway CA Jr, “The Immune System in Health and Disease. ,” in *Immunobiology*, 5th edition., New York: Garland Science;, 2001.

[111] R. Dominguez and K. C. Holmes, “Antibody structure and function,” *Immunology*, vol. 40, no. 1, pp. 58–78, 2011, doi: 10.1146/annurev-biophys-042910-155359.

[112] M. L. Chiu, D. R. Goulet, A. Teplyakov, and G. L. Gilliland, “Antibody structure and function: The basis for engineering therapeutics,” Dec. 01, 2019, *MDPI*. doi: 10.3390/antib8040055.

[113] A. Kretschmer, R. Schwanbeck, T. Valerius, and T. Rösner, “Antibody Isotypes for Tumor Immunotherapy,” *Transfusion Medicine and Hemotherapy*, vol. 44, no. 5, pp. 320–326, 2017, doi: 10.1159/000479240.

[114] S. B. Petkova *et al.*, “Enhanced half-life of genetically engineered human IgG1 antibodies in a humanized FcRn mouse model: potential application in humorally mediated autoimmune disease,” *Int Immunol*, vol. 18, no. 12, pp. 1759–1769, Sep. 2006, doi: 10.1093/intimm/dxl110.

[115] J. Hazin, G. Moldenhauer, P. Altevogt, and N. R. Brady, “A novel method for measuring cellular antibody uptake using imaging flow cytometry reveals distinct uptake rates for two different monoclonal antibodies targeting L1,” *J Immunol Methods*, vol. 423, pp. 70–77, Aug. 2015, doi: 10.1016/j.jim.2015.04.024.

[116] J. H. Kim and H. J. Hong, “Humanization by CDR Grafting and Specificity-Determining Residue Grafting,” 2012, pp. 237–245. doi: 10.1007/978-1-61779-974-7_13.

[117] F. J. WARD, B. MESHI, and N. A. STAINES, “Framework and CDR structures of anti-DNA antibodies are implicated in antigen binding,” *Biochem Soc Trans*, vol. 25, no. 2, pp. 310S-310S, May 1997, doi: 10.1042/bst025310s.

[118] M. Toride King and C. L. Brooks, “Epitope Mapping of Antibody-Antigen Interactions with X-Ray Crystallography.,” *Methods Mol Biol*, vol. 1785, pp. 13–27, 2018, doi: 10.1007/978-1-4939-7841-0_2.

[119] F. A. Harding, M. M. Stickler, J. Razo, and R. B. DuBridge, “The immunogenicity of humanized and fully human antibodies: residual immunogenicity resides in the CDR regions.,” *MAbs*, vol. 2, no. 3, pp. 256–65, 2010, doi: 10.4161/mabs.2.3.11641.

[120] S. J. Kim, Y. Park, and H. J. Hong, “Antibody Engineering for the Development of Therapeutic Antibodies,” *Mol Cells*, vol. 20, no. 1, pp. 17–29, Aug. 2005, doi: 10.1016/S1016-8478(23)25245-0.

[121] E. Mason-Osann, K. Hollevoet, G. Niederfellner, and I. Pastan, “Quantification of recombinant immunotoxin delivery to solid tumors allows for direct comparison of in vivo and in vitro results,” *Sci Rep*, vol. 5, Jun. 2015, doi: 10.1038/srep10832.

[122] A.-C. C. R. Arn, M. F.-C. K. J. Halla, and R. (Hons), S. Gill, “Tisotumab Vedotin Safety and Tolerability in Clinical Practice: Managing Adverse

Events," *J Adv Pract Oncol*, vol. 14, no. 2, pp. 139–152, Mar. 2023, doi: 10.6004/jadpro.2023.14.2.4.

[123] R. F. Marshall, H. Xu, and M. Berkenstock, "Ocular toxicities associated with antibody drug conjugates," *Curr Opin Ophthalmol*, vol. 35, no. 6, pp. 494–498, Nov. 2024, doi: 10.1097/ICU.0000000000001063.

[124] C. Liu *et al.*, "Convenient method of producing cyclic single-chain Fv antibodies by split-intein-mediated protein ligation and chaperone co-expression," *The Journal of Biochemistry*, vol. 168, no. 3, pp. 257–263, Sep. 2020, doi: 10.1093/jb/mvaa042.

[125] P. Muñoz-López *et al.*, "Single-Chain Fragment Variable: Recent Progress in Cancer Diagnosis and Therapy," *Cancers (Basel)*, vol. 14, no. 17, p. 4206, Aug. 2022, doi: 10.3390/cancers14174206.

[126] A. Antignani and D. FitzGerald, "Immunotoxins: The Role of the Toxin," *Toxins (Basel)*, vol. 5, no. 8, pp. 1486–1502, Aug. 2013, doi: 10.3390/toxins5081486.

[127] C. Peters and S. Brown, "Antibody–drug conjugates as novel anti-cancer chemotherapeutics," *Biosci Rep*, vol. 35, no. 4, Aug. 2015, doi: 10.1042/BSR20150089.

[128] C. Rodríguez-Nava *et al.*, "Mechanisms of Action and Limitations of Monoclonal Antibodies and Single Chain Fragment Variable (scFv) in the Treatment of Cancer," *Biomedicines*, vol. 11, no. 6, p. 1610, Jun. 2023, doi: 10.3390/biomedicines11061610.

[129] C. F. McDonagh *et al.*, “Engineered antibody-drug conjugates with defined sites and stoichiometries of drug attachment,” *Protein Eng. Des. Sel.*, vol. 19, p. 299, 2006.

[130] C. A. Adebamowo *et al.*, “Challenges in the Detection, Prevention, and Treatment of HIV-Associated Malignancies in Low- and Middle-Income Countries in Africa,” *JAIDS Journal of Acquired Immune Deficiency Syndromes*, vol. 67, no. Supplement 1, pp. S17–S26, Sep. 2014, doi: 10.1097/QAI.0000000000000255.

[131] B. Kiss and J. Borbély, “Business Risk Mitigation in the Development Process of New Monoclonal Antibody Drug Conjugates for Cancer Treatment,” *Pharmaceutics*, vol. 15, no. 6, p. 1761, Jun. 2023, doi: 10.3390/pharmaceutics15061761.

[132] E. D. Lobo, R. J. Hansen, and J. P. Balthasar, “Antibody pharmacokinetics and pharmacodynamics,” 2004, *John Wiley and Sons Inc.* doi: 10.1002/jps.20178.

[133] N. Becker and I. Benhar, “Antibody-based immunotoxins for the treatment of cancer,” *Antibodies*, vol. 1, no. 1, pp. 39–69, Jun. 2012, doi: 10.3390/antib1010039.

[134] H. Allahyari, S. Heidari, M. Ghamgosha, P. Saffarian, and J. Amani, “Immunotoxin: A new tool for cancer therapy,” *Tumor Biology*, vol. 39, no. 2, pp. 1–11, 2017, doi: 10.1177/1010428317692226.

[135] H. G. Haggerty *et al.*, “BR96 sFv-PE40 Immunotoxin: Nonclinical Safety Assessment,” *Toxicol Pathol*, vol. 27, no. 1, pp. 87–94, Jan. 1999, doi: 10.1177/019262339902700116.

[136] I. Pastan, R. Hassan, D. J. FitzGerald, and R. J. Kreitman, “Immunotoxin therapy of cancer,” *Nat Rev Cancer*, vol. 6, no. 7, pp. 559–565, Jul. 2006, doi: 10.1038/nrc1891.

[137] R. Mazor, M. Onda, and I. Pastan, “Immunogenicity of therapeutic recombinant immunotoxins,” Mar. 01, 2016, *Blackwell Publishing Ltd*. doi: 10.1111/imr.12390.

[138] C. Gottstein, U. Winkler, H. Bohlen, V. Diehl, and A. Engert, “Immunotoxins:Is there a clinical value?,” *Annals of Oncology*, vol. 5, pp. S97–S103, 1994, doi: 10.1093/annonc/5.suppl_1.S97.

[139] E. S. Vitetta, R. J. Fulton, R. D. May, M. Till, and J. W. Uhr, “Redesigning Nature’s Poisons to Create Anti-Tumor Reagents,” *Science (1979)*, vol. 238, no. 4830, pp. 1098–1104, Nov. 1987, doi: 10.1126/science.3317828.

[140] R. N. Morgan, S. E. Saleh, H. A. Farrag, and K. M. Aboshanab, “New Insights on *Pseudomonas Aeruginosa* Exotoxin A-based Immunotoxins in Targeted Cancer Therapeutic Delivery,” *Ther Deliv*, vol. 14, no. 1, pp. 31–60, Jan. 2023, doi: 10.4155/tde-2022-0055.

[141] R. J. Kelly, E. Sharon, I. Pastan, and R. Hassan, “Mesothelin-Targeted Agents in Clinical Trials and in Preclinical Development,” *Mol Cancer Ther*, vol. 11, no. 3, pp. 517–525, Mar. 2012, doi: 10.1158/1535- 7163.MCT-11-0454.

[142] R. Mazor, M. Onda, and I. Pastan, “Immunogenicity of therapeutic recombinant immunotoxins,” *Immunol Rev*, vol. 270, no. 1, pp. 152–164, Mar. 2016, doi: 10.1111/imr.12390.

[143] S. Srivastava and S. Luqman, “Immune-O-Toxins as the magic bullet for therapeutic purposes,” *Biomedical Research and Therapy*, vol. 2, no. 1, p. 2, Jan. 2015, doi: 10.7603/s40730-015-0002-4.

[144] M. J. Bjorn, M. L. Vasil, J. C. Sadoff, and B. H. Iglewski, “Incidence of exotoxin production by Pseudomonas species,” *Infect Immun*, vol. 16, no. 1, pp. 362–366, Apr. 1977, doi: 10.1128/iai.16.1.362-366.1977.

[145] M. Ogata, I. Pastan, and D. FitzGerald, “Analysis of Pseudomonas exotoxin activation and conformational changes by using monoclonal antibodies as probes,” *Infect Immun*, vol. 59, no. 1, pp. 407–414, Jan. 1991, doi: 10.1128/iai.59.1.407-414.1991.

[146] N. ENTNER and A. P. GROLLMAN, “Inhibition of Protein Synthesis: A Mechanism of Amebicide Action of Emetine and Other Structurally Related Compounds*,” *J Protozool*, vol. 20, no. 1, pp. 160–163, Feb. 1973, doi: 10.1111/j.1550-7408.1973.tb06025.x.

[147] R. N. Morgan, S. E. Saleh, H. A. Farrag, and K. M. Aboshanab, “New Insights on *Pseudomonas Aeruginosa* Exotoxin A-based Immunotoxins in Targeted Cancer Therapeutic Delivery,” *Ther Deliv*, vol. 14, no. 1, pp. 31–60, Jan. 2023, doi: 10.4155/tde-2022-0055.

[148] A. Gholami, D. Minai-Tehrani, S. J. Mahdizadeh, P. Saenz-Mendez, and L. A. Eriksson, “Structural Insights into *Pseudomonas aeruginosa*

Exotoxin A–Elongation Factor 2 Interactions: A Molecular Dynamics Study," *J Chem Inf Model*, vol. 63, no. 5, pp. 1578–1591, Mar. 2023, doi: 10.1021/acs.jcim.3c00064.

[149] J. E. Weldon and I. Pastan, "A guide to taming a toxin – recombinant immunotoxins constructed from *Pseudomonas* exotoxin A for the treatment of cancer," *FEBS J*, vol. 278, no. 23, pp. 4683–4700, Dec. 2011, doi: 10.1111/j.1742-4658.2011.08182.x.

[150] R. N. Morgan, S. E. Saleh, H. A. Farrag, and K. M. Aboshanab, "New Insights on *Pseudomonas Aeruginosa* Exotoxin A-based Immunotoxins in Targeted Cancer Therapeutic Delivery," *Ther Deliv*, vol. 14, no. 1, pp. 31–60, Jan. 2023, doi: 10.4155/tde-2022-0055.

[151] M. Bottosso *et al.*, "Moving toward precision medicine to predict drug sensitivity in patients with metastatic breast cancer," *ESMO Open*, vol. 9, no. 3, p. 102247, Mar. 2024, doi: 10.1016/j.esmoop.2024.102247.

[152] A. Antignani and D. FitzGerald, "Immunotoxins: The Role of the Toxin," *Toxins (Basel)*, vol. 5, no. 8, pp. 1486–1502, Aug. 2013, doi: 10.3390/toxins5081486.

[153] M. Li, F. Dyda, I. Benhar, I. Pastan, and D. R. Davies, "The crystal structure of Pseudomonas aeruginosa exotoxin domain III with nicotinamide and AMP: conformational differences with the intact exotoxin.," *Proceedings of the National Academy of Sciences*, vol. 92, no. 20, pp. 9308–9312, Sep. 1995, doi: 10.1073/pnas.92.20.9308.

[154] W. J. Iglewski, H. Lee, and P. Muller, “A Cellular Mono(ADP-Ribosyl)Transferase which Modifies the Diphthamide Residue of Elongation Factor-2,” 1985, pp. 536–543. doi: 10.1007/978-3-642-70589-2_76.

[155] M. K. Mateyak and T. G. Kinzy, “ADP-ribosylation of Translation Elongation Factor 2 by Diphtheria Toxin in Yeast Inhibits Translation and Cell Separation,” *Journal of Biological Chemistry*, vol. 288, no. 34, pp. 24647–24655, Aug. 2013, doi: 10.1074/jbc.M113.488783.

[156] T. Shimazu *et al.*, “NBK/BIK antagonizes MCL-1 and BCL-X $_L$ and activates BAK-mediated apoptosis in response to protein synthesis inhibition,” *Genes Dev*, vol. 21, no. 8, pp. 929–941, Apr. 2007, doi: 10.1101/gad.1522007.

[157] D. Fernández-Lázaro, B. Sanz, and J. Seco-Calvo, “Mechanisms of programmed cell death: structural and functional pathways. A narrative review.,” *Invest Clin*, vol. 65, no. 2, pp. 230–252, May 2024, doi: 10.54817/IC.v65n2a09.

[158] M. Dieffenbach and I. Pastan, “Mechanisms of Resistance to Immunotoxins Containing Pseudomonas Exotoxin A in Cancer Therapy,” *Biomolecules*, vol. 10, no. 7, p. 979, Jun. 2020, doi: 10.3390/biom10070979.

[159] A. Y. Lin and S. N. Dinner, “Moxetumomab pasudotox for hairy cell leukemia: preclinical development to FDA approval,” *Blood Adv*, vol. 3, no. 19, pp. 2905–2910, Oct. 2019, doi: 10.1182/bloodadvances.2019000507.

[160] R. J. Kreitman, E. Arons, M. Stetler-Stevenson, D. J. P. Fitzgerald, W. H. Wilson, and I. Pastan, “Recombinant immunotoxins and other therapies for relapsed/refractory hairy cell leukemia,” *Leuk Lymphoma*, vol. 52, no. sup2, pp. 82–86, Jun. 2011, doi: 10.3109/10428194.2011.565843.

[161] R. J. Kreitman, E. Arons, M. Stetler-Stevenson, D. J. P. Fitzgerald, W. H. Wilson, and I. Pastan, “Recombinant immunotoxins and other therapies for relapsed/refractory hairy cell leukemia,” *Leuk Lymphoma*, vol. 52, no. sup2, pp. 82–86, Jun. 2011, doi: 10.3109/10428194.2011.565843.

[162] R. Hassan *et al.*, “Phase I Study of SS1P, a Recombinant Anti-Mesothelin Immunotoxin Given as a Bolus I.V. Infusion to Patients with Mesothelin-Expressing Mesothelioma, Ovarian, and Pancreatic Cancers,” *Clinical Cancer Research*, vol. 13, no. 17, pp. 5144–5149, Sep. 2007, doi: 10.1158/1078-0432.CCR-07-0869.

[163] R. J. Kreitman, R. Hassan, D. J. FitzGerald, and I. Pastan, “Phase I Trial of Continuous Infusion Anti-Mesothelin Recombinant Immunotoxin SS1P,” *Clinical Cancer Research*, vol. 15, no. 16, pp. 5274–5279, Aug. 2009, doi: 10.1158/1078-0432.CCR-09-0062.

[164] R. J. Kreitman, R. Hassan, D. J. FitzGerald, and I. Pastan, “Phase I Trial of Continuous Infusion Anti-Mesothelin Recombinant Immunotoxin SS1P,” *Clinical Cancer Research*, vol. 15, no. 16, pp. 5274–5279, Aug. 2009, doi: 10.1158/1078-0432.CCR-09-0062.

[165] R. Mazor and I. Pastan, “Immunogenicity of Immunotoxins Containing Pseudomonas Exotoxin A: Causes, Consequences, and Mitigation,” *Front Immunol*, vol. 11, Jun. 2020, doi: 10.3389/fimmu.2020.01261.

[166] L.-Y. Xie *et al.*, “Immunotoxin Therapy for Lung Cancer,” *Chin Med J (Engl)*, vol. 130, no. 5, pp. 607–612, Mar. 2017, doi: 10.4103/0366-6999.200540.

[167] X. Hu *et al.*, “Removal of B-cell epitopes for decreasing immunogenicity in recombinant immunotoxin against B-cell malignancies.,” *J BUON*, vol. 21, no. 6, pp. 1374–1378, 2016.

[168] J. E. Weldon *et al.*, “Designing the Furin-Cleavable Linker in Recombinant Immunotoxins Based on *Pseudomonas* Exotoxin A,” *Bioconjug Chem*, vol. 26, no. 6, pp. 1120–1128, Jun. 2015, doi: 10.1021/acs.bioconjchem.5b00190.

[169] W. Liu *et al.*, “Recombinant immunotoxin engineered for low immunogenicity and antigenicity by identifying and silencing human B-cell epitopes,” *Proceedings of the National Academy of Sciences*, vol. 109, no. 29, pp. 11782–11787, Jul. 2012, doi: 10.1073/pnas.1209292109.

[170] J. E. Weldon *et al.*, “A Recombinant Immunotoxin against the Tumor-Associated Antigen Mesothelin Reengineered for High Activity, Low Off-Target Toxicity, and Reduced Antigenicity,” *Mol Cancer Ther*, vol. 12, no. 1, pp. 48–57, Jan. 2013, doi: 10.1158/1535-7163.MCT-12-0336.

[171] “Removal of B-cell epitopes in B-cell malignancies.”

[172] J. Ruiz-de-la-Herrán, J. Tomé-Amat, R. Lázaro-Gorines, J. Gavilanes, and J. Lacadena, “Inclusion of a Furin Cleavage Site Enhances Antitumor Efficacy against Colorectal Cancer Cells of Ribotoxin α-Sarcin- or RNase

T1-Based Immunotoxins," *Toxins (Basel)*, vol. 11, no. 10, p. 593, Oct. 2019, doi: 10.3390/toxins11100593.

[173] Ø. Garred, B. van Deurs, and K. Sandvig, "Furin-induced Cleavage and Activation of Shiga Toxin," *Journal of Biological Chemistry*, vol. 270, no. 18, pp. 10817–10821, May 1995, doi: 10.1074/jbc.270.18.10817.

[174] R. Mazor *et al.*, "Recombinant immunotoxin for cancer treatment with low immunogenicity by identification and silencing of human T-cell epitopes," *Proceedings of the National Academy of Sciences*, vol. 111, no. 23, pp. 8571–8576, Jun. 2014, doi: 10.1073/pnas.1405153111.

[175] W. Liu *et al.*, "Recombinant immunotoxin engineered for low immunogenicity and antigenicity by identifying and silencing human B-cell epitopes," *Proceedings of the National Academy of Sciences*, vol. 109, no. 29, pp. 11782–11787, Jul. 2012, doi: 10.1073/pnas.1209292109.

[176] C. Alewine, L. Xiang, T. Yamori, G. Niederfellner, K. Bosslet, and I. Pastan, "Efficacy of RG7787, a Next-Generation Mesothelin-Targeted Immunotoxin, against Triple-Negative Breast and Gastric Cancers," *Mol Cancer Ther*, vol. 13, no. 11, pp. 2653–2661, Nov. 2014, doi: 10.1158/1535-7163.MCT-14-0132.

[177] K. Hollevoet, E. Mason-Osann, X. Liu, S. Imhof-Jung, G. Niederfellner, and I. Pastan, "*In Vitro* and *In Vivo* Activity of the Low-Immunogenic Antimesothelin Immunotoxin RG7787 in Pancreatic Cancer," *Mol Cancer Ther*, vol. 13, no. 8, pp. 2040–2049, Aug. 2014, doi: 10.1158/1535-7163.MCT-14-0089-T.

[178] A. Kemi Daramola, “Selective elimination of allergen-reactive B-cells in allergic asthma,” 2022.

[179] H. Lin *et al.*, “A novel human Fab antibody for Trop2 inhibits breast cancer growth *in vitro* and *in vivo*,” *Int J Cancer*, vol. 134, no. 5, pp. 1239–1249, Mar. 2014, doi: 10.1002/ijc.28451.

[180] P. M. (US); P. S. C. R. M. (US) Ira H. Pastan, “(12) United States Patent,” 2004.

[181] S. Barth, M. Huhn, B. Matthey, A. Klimka, E. A. Galinski, and A. A. Engert, “Compatible-Solute-Supported Periplasmic Expression of Functional Recombinant Proteins under Stress Conditions,” 2000. [Online]. Available: https://journals.asm.org/journal/aem

[182] tzhang not provided, “Copy of Determination of viable cells by XTT v1,” Mar. 22, 2021. doi: 10.17504/protocols.io.btiwnkfe.

[183] J. Wang, S. R. MacEwan, and A. Chilkoti, “Quantitative Mapping of the Spatial Distribution of Nanoparticles in Endo-Lysosomes by Local pH,” *Nano Lett*, vol. 17, no. 2, pp. 1226–1232, Feb. 2017, doi: 10.1021/acs.nanolett.6b05041.

[184] L. J. Shearer and N. O. Petersen, “Distribution and Co-localization of endosome markers in cells,” *Heliyon*, vol. 5, no. 9, p. e02375, Sep. 2019, doi: 10.1016/j.heliyon.2019.e02375.

[185] A. W. LaVigne, S. A. Triedman, T. C. Randall, E. L. Trimble, and A. N. Viswanathan, “Cervical cancer in low and middle income countries:

Addressing barriers to radiotherapy delivery," Nov. 01, 2017, *Elsevier B.V.* doi: 10.1016/j.gore.2017.08.004.

[186] H. Li, X. Wu, and X. Cheng, "Advances in diagnosis and treatment of metastatic cervical cancer," *J Gynecol Oncol*, vol. 27, no. 4, 2016, doi: 10.3802/jgo.2016.27.e43.

[187] A. Farthing, "Future fertility after conservation surgery for cervical cancer," *Br J Hosp Med*, vol. 67, no. 5, pp. 250–252, May 2006, doi: 10.12968/hmed.2006.67.5.21064.

[188] V. Makker, A. K. Green, R. M. Wenham, D. Mutch, B. Davidson, and D. S. Miller, "New therapies for advanced, recurrent, and metastatic endometrial cancers," *Gynecol Oncol Res Pract*, vol. 4, no. 1, Dec. 2017, doi: 10.1186/s40661-017-0056-7.

[189] M. Kangwa, V. Yelemane, A. N. Polat, K. D. D. Gorrepati, M. Grasselli, and M. Fernández-Lahore, "High-level fed-batch fermentative expression of an engineered Staphylococcal protein A based ligand in E. coli: purification and characterization," *AMB Express*, vol. 5, no. 1, p. 70, Dec. 2015, doi: 10.1186/s13568-015-0155-y.

[190] M. N. Baeshen *et al.*, "Production of Biopharmaceuticals in E. coli: Current Scenario and Future Perspectives," *J Microbiol Biotechnol*, vol. 25, no. 7, pp. 953–962, Jul. 2015, doi: 10.4014/jmb.1412.12079.

[191] L. Strandberg and S. O. Enfors, "Factors influencing inclusion body formation in the production of a fused protein in Escherichia coli," *Appl*

Environ Microbiol, vol. 57, no. 6, pp. 1669–1674, Jun. 1991, doi: 10.1128/aem.57.6.1669-1674.1991.

[192] C. H. Schein, “Soluble Protein Expression in Bacteria,” in *Encyclopedia of Industrial Biotechnology*, Wiley, 2010, pp. 1–20. doi: 10.1002/9780470054581.eib505.

[193] M. Lebendiker and T. Danieli, “Production of prone-to-aggregate proteins,” *FEBS Lett*, vol. 588, no. 2, pp. 236–246, Jan. 2014, doi: 10.1016/j.febslet.2013.10.044.

[194] I. Vyrides and D. C. Stuckey, “Compatible solute addition to biological systems treating waste/wastewater to counteract osmotic and other environmental stresses: a review,” *Crit Rev Biotechnol*, vol. 37, no. 7, pp. 865–879, Oct. 2017, doi: 10.1080/07388551.2016.1266460.

[195] D. L. Atroshenko, E. P. Sergeev, D. I. Golovina, and A. A. Pometun, “Additivities for Soluble Recombinant Protein Expression in Cytoplasm of Escherichia coli,” *Fermentation*, vol. 10, no. 3, p. 120, Feb. 2024, doi: 10.3390/fermentation10030120.

[196] S. Prasad, P. B. Khadatare, and I. Roy, “Effect of Chemical Chaperones in Improving the Solubility of Recombinant Proteins in Escherichia coli,” *Appl Environ Microbiol*, vol. 77, no. 13, pp. 4603–4609, Jul. 2011, doi: 10.1128/AEM.05259-11.

[197] N. Oganesyan, I. Ankoudinova, S.-H. Kim, and R. Kim, “Effect of osmotic stress and heat shock in recombinant protein overexpression and

crystallization," *Protein Expr Purif*, vol. 52, no. 2, pp. 280–285, Apr. 2007, doi: 10.1016/j.pep.2006.09.015.

[198] M. Mühlmann, E. Forsten, S. Noack, and J. Büchs, "Optimizing recombinant protein expression via automated induction profiling in microtiter plates at different temperatures," *Microb Cell Fact*, vol. 16, no. 1, p. 220, Dec. 2017, doi: 10.1186/s12934-017-0832-4.

[199] C. A. Galloway, M. P. Sowden, and H. C. Smith, "Increasing the Yield of Soluble Recombinant Protein Expressed in *E. coli* by Induction during Late Log Phase," *Biotechniques*, vol. 34, no. 3, pp. 524–530, Mar. 2003, doi: 10.2144/03343st04.

[200] T. San-Miguel, P. Pérez-Bermúdez, and I. Gavidia, "Production of soluble eukaryotic recombinant proteins in E. coli is favoured in early log-phase cultures induced at low temperature," *Springerplus*, vol. 2, no. 1, p. 89, Dec. 2013, doi: 10.1186/2193-1801-2-89.

[201] J. Kaur, A. Kumar, and J. Kaur, "Strategies for optimization of heterologous protein expression in E. coli: Roadblocks and reinforcements," *Int J Biol Macromol*, vol. 106, pp. 803–822, Jan. 2018, doi: 10.1016/j.ijbiomac.2017.08.080.

[202] L. Khalef, R. Lydia, K. Filicia, and B. Moussa, "Cell viability and cytotoxicity assays: Biochemical elements and cellular compartments," *Cell Biochem Funct*, vol. 42, no. 3, Apr. 2024, doi: 10.1002/cbf.4007.

[203] E. R. Padayachee *et al.*, “Applications of SNAP-tag technology in skin cancer therapy,” *Health Sci Rep*, vol. 2, no. 2, Feb. 2019, doi: 10.1002/hsr2.103.

[204] E. Adebowale Fajemisin Supervisor, S. Barth Co-Supervisor, and O. Alex Akinrinmade, “GENERATION AND THERAPEUTIC EVALUATION OF CD64-TARGETING IMMUNOTHERAPEUTICS ON CD64+ CELL LINES AND EX VIVO DIFFERENTIATED HUMAN MACROPHAGES,” 2023.

[205] J. Singh and S. Barth, “The Development of Recombinant Fusion Proteins for Immunotherapy of Human TNBC,” 2024.

[206] T. Ngwenya and S. Barth, “Development of recombinant immunodiagnostics and therapeutics for Triple Negative Breast Cancer (TNBC),” 2023.

[207] J. M. Lambert and W. A. Blättler, “Purification and biochemical characterization of immunotoxins,” 1988, pp. 323–348. doi: 10.1007/978-1-4613-1083-9_18.

[208] A. Eon-Duval, H. Broly, and R. Gleixner, “Quality attributes of recombinant therapeutic proteins: An assessment of impact on safety and efficacy as part of a quality by design development approach,” *Biotechnol Prog*, vol. 28, no. 3, pp. 608–622, May 2012, doi: 10.1002/btpr.1548.

[209] S. Zhu, Y. Liu, P. C. Wang, X. Gu, and L. Shan, “Recombinant Immunotoxin Therapy of Glioblastoma: Smart Design, Key Findings, and Specific Challenges,” *Biomed Res Int*, vol. 2017, pp. 1–18, 2017, doi: 10.1155/2017/7929286.

[210] S. Barth, M. Huhn, B. Matthey, A. Klimka, E. A. Galinski, and A. Engert, “Compatible-solute-supported periplasmic expression of functional recombinant proteins under stress conditions,” *Appl. Environ. Microbiol.*, vol. 66, p. 1572, 2000.

[211] V. Riguero *et al.*, “Immobilized metal affinity chromatography optimization for poly-histidine tagged proteins,” *J Chromatogr A*, vol. 1629, p. 461505, Oct. 2020, doi: 10.1016/j.chroma.2020.461505.

[212] A. S. Pina, Í. L. Batalha, and A. C. A. Roque, “Affinity Tags in Protein Purification and Peptide Enrichment: An Overview,” 2014, pp. 147–168. doi: 10.1007/978-1-62703-977-2_14.

[213] J. T. Mooney *et al.*, “Purification of a recombinant human growth hormone by an integrated IMAC procedure,” *Protein Expr Purif*, vol. 94, pp. 85–94, Feb. 2014, doi: 10.1016/j.pep.2013.11.002.

[214] D. G. Bracewell *et al.*, “Impact of clarification strategy on chromatographic separations: Pre-processing of cell homogenates,” *Biotechnol Bioeng*, vol. 100, no. 5, pp. 941–949, Aug. 2008, doi: 10.1002/bit.21823.

[215] W. Jiang and M. T. W. Hearn, “Protein Interaction with Immobilized Metal Ion Affinity Ligands under High Ionic Strength Conditions,” *Anal Biochem*, vol. 242, no. 1, pp. 45–54, Nov. 1996, doi: 10.1006/abio.1996.0426.

[216] W.-H. K. Kuo and H. A. Chase, “Exploiting the interactions between poly-histidine fusion tags and immobilized metal ions,” *Biotechnol Lett*, vol. 33, no. 6, pp. 1075–1084, Jun. 2011, doi: 10.1007/s10529-011-0554-3.

[217] J. Overnell, “Use of 2-mercaptoethanol during chromatography of crab (Cancer pagurus) metallothionein on deae cellulose,” *Comparative Biochemistry and Physiology Part C: Comparative Pharmacology*, vol. 77, no. 2, pp. 245–248, Jan. 1984, doi: 10.1016/0742-8413(84)90008-2.

[218] A. E. Voinescu, P. Bauduin, M. C. Pinna, D. Touraud, B. W. Ninham, and W. Kunz, “Similarity of Salt Influences on the pH of Buffers, Polyelectrolytes, and Proteins,” *J Phys Chem B*, vol. 110, no. 17, pp. 8870–8876, May 2006, doi: 10.1021/jp0600209.

[219] K. L. Brogan, J. H. Shin, and M. H. Schoenfisch, “Influence of Surfactants and Antibody Immobilization Strategy on Reducing Nonspecific Protein Interactions for Molecular Recognition Force Microscopy,” *Langmuir*, vol. 20, no. 22, pp. 9729–9735, Oct. 2004, doi: 10.1021/la048437y.

[220] S. A. Berkowitz, “Role of analytical ultracentrifugation in assessing the aggregation of protein biopharmaceuticals,” *AAPS J*, vol. 8, no. 3, pp. E590–E605, Sep. 2006, doi: 10.1208/aapsj080368.

[221] S. Fekete, V. D’Atri, and D. Guillarme, “Chromatographic Strategies for the Successful Characterization of Protein Biopharmaceuticals,” in *Optimization in HPLC*, Wiley, 2021, pp. 57–71. doi: 10.1002/9783527837489.ch1-4.

[222] G. J. Acton and S. Gupta, “A releationship between protein-degradation rates *in vivo* , isoelectric points, and molecular weights obtained by using density labelling,” *Biochemical Journal*, vol. 184, no. 2, pp. 367–377, Nov. 1979, doi: 10.1042/bj1840367.

[223] S. Fekete, A. Beck, J.-L. Veuthey, and D. Guillarme, “Theory and practice of size exclusion chromatography for the analysis of protein aggregates,” *J Pharm Biomed Anal*, vol. 101, pp. 161–173, Dec. 2014, doi: 10.1016/j.jpba.2014.04.011.

[224] E. Rapani, A. Sacchetti, D. Corda, and S. Alberti, “Human TROP-2 is a tumor-associated calcium signal transducer,” *Int J Cancer*, vol. 76, no. 5, pp. 671–676, May 1998, doi: 10.1002/(SICI)1097-0215(19980529)76:5<671::AID-IJC10>3.0.CO;2-7.

[225] K. Hirano and S. Sueda, “A fluorescence-based binding assay for proteins using the cell surface as a sensing platform,” *Analytical Sciences*, vol. 40, no. 3, pp. 563–571, Mar. 2024, doi: 10.1007/s44211-023-00476-5.

[226] T. Liu, Y. Liu, X. Bao, J. Tian, Y. Liu, and X. Yang, “Overexpression of TROP2 Predicts Poor Prognosis of Patients with Cervical Cancer and Promotes the Proliferation and Invasion of Cervical Cancer Cells by Regulating ERK Signaling Pathway,” *PLoS One*, vol. 8, no. 9, p. e75864, Sep. 2013, doi: 10.1371/journal.pone.0075864.

[227] Y.-T. Hsu, Q. Hou, H. Zhou, S. Mohanty, and A. Litvinchuk, “Differential Immunoscreening Identifies a Glycosylation Variant of the Epidermal Growth Factor Receptor in ME-180 Cervical Carcinoma Cells,” *Hybridoma*, vol. 24, no. 5, pp. 225–230, Oct. 2005, doi: 10.1089/hyb.2005.24.225.

[228] N. J. Bevan, T. J. Dale, and D. J. Trezise, “Abstract 749: Antibody internalization assays for cancer drug discovery,” *Cancer Res*, vol. 78, no.

13_Supplement, pp. 749–749, Jul. 2018, doi: 10.1158/1538-7445.AM2018-749.

[229] F. Invrea, R. Rovito, E. Torchiaro, C. Petti, C. Isella, and E. Medico, “Patient-derived xenografts (PDXs) as model systems for human cancer,” *Curr Opin Biotechnol*, vol. 63, pp. 151–156, Jun. 2020, doi: 10.1016/j.copbio.2020.01.003.

[230] D. Obinata *et al.*, “Patient-derived castration-resistant prostate cancer model revealed CTBP2 upregulation mediated by OCT1 and androgen receptor,” *BMC Cancer*, vol. 24, no. 1, p. 554, May 2024, doi: 10.1186/s12885-024-12298-3.

[231] L. Pompili, M. Porru, C. Caruso, A. Biroccio, and C. Leonetti, “Patient-derived xenografts: a relevant preclinical model for drug development,” *Journal of Experimental & Clinical Cancer Research*, vol. 35, no. 1, p. 189, Dec. 2016, doi: 10.1186/s13046-016-0462-4.

[232] D. J. FitzGerald, R. Kreitman, W. Wilson, D. Squires, and I. Pastan, “Recombinant immunotoxins for treating cancer,” *International Journal of Medical Microbiology*, vol. 293, no. 7–8, pp. 577–582, 2004, doi: 10.1078/1438-4221-00302.

[233] P. Awuah, T. K. Bera, M. Folivi, O. Chertov, and I. Pastan, “Reduced Shedding of Surface Mesothelin Improves Efficacy of Mesothelin-Targeting Recombinant Immunotoxins,” *Mol Cancer Ther*, vol. 15, no. 7, pp. 1648–1655, Jul. 2016, doi: 10.1158/1535-7163.MCT-15-0863.

[234] M. K. Tur *et al.*, “Recombinant CD64-Specific Single Chain Immunotoxin Exhibits Specific Cytotoxicity against Acute Myeloid Leukemia Cells,” 2003. [Online]. Available: http://aacrjournals.org/cancerres/article-pdf/63/23/8414/2510954/zch02303008414.pdf

[235] B. J. Moss, Y. Kim, M. P. Nandakumar, and M. R. Marten, “Quantifying Metabolic Activity of Filamentous Fungi Using a Colorimetric XTT Assay,” *Biotechnol Prog*, vol. 24, no. 3, pp. 780–783, May 2008, doi: 10.1021/bp070334t.

[236] N. W. Roehm, G. H. Rodgers, S. M. Hatfield, and A. L. Glasebrook, “An improved colorimetric assay for cell proliferation and viability utilizing the tetrazolium salt XTT,” *J Immunol Methods*, vol. 142, no. 2, pp. 257–265, Sep. 1991, doi: 10.1016/0022-1759(91)90114-U.

[237] M. Henry and S. Barth, “Masters Thesis Development and Characterization of Recombinant Immunotoxins for Cervical Carcinoma Plagiarism Declaration,” 2023.

[238] I. Pastan and R. Hassan, “Cancer Resea,” vol. 74, no. 11, pp. 2907–2912, 2014, doi: 10.1086/498510.Parasitic.

[239] R. Hassan *et al.*, “Phase 1 study of the antimesothelin immunotoxin SS1P in combination with pemetrexed and cisplatin for front-line therapy of pleural mesothelioma and correlation of tumor response with serum mesothelin, megakaryocyte potentiating factor, and cancer antigen 125,” *Cancer*, vol. 120, no. 21, pp. 3311–3319, Nov. 2014, doi: 10.1002/cncr.28875.

[240] G. Niederfellner *et al.*, “Abstract 4510: RG7787 - a novel de-immunized PE based fusion protein for therapy of mesothelin-positive solid tumors,” *Cancer Res*, vol. 74, no. 19_Supplement, pp. 4510–4510, Oct. 2014, doi: 10.1158/1538-7445.AM2014-4510.

[241] R. Hull1 *et al.*, “Cervical cancer in low and middle.income countries (Review),” *Oncol Lett*, vol. 20, no. 3, pp. 2058–2074, 2020, doi: 10.3892/ol.2020.11754.

[242] M. Li *et al.*, “Clinical targeting recombinant immunotoxins for cancer therapy,” Jul. 20, 2017, *Dove Medical Press Ltd.* doi: 10.2147/OTT.S134584.

[243] S. Zuppone, M. S. Fabbrini, and R. Vago, “Hosts for Hostile Protein Production: The Challenge of Recombinant Immunotoxin Expression,” *Biomedicines*, vol. 7, no. 2, p. 38, May 2019, doi: 10.3390/biomedicines7020038.

APPENDIX

7.1 Materials

This chapter provides information on the materials and equipment used as standard operating procedures and protocols at the MB&I Research Unit. It outlines the reagents, buffers, and other solutions employed in the experimental procedures described in Chapter 2 to produce functional recombinant immunotoxins (rITs).

7.2 Consumable

Consumables used in this study were purchased from the following companies: Roche (Switzerland), Beckham Coulter (California, USA), Qiagen (Hilden, Germany), Sigma Aldrich (Missouri, USA), Inqaba Biotechnological Industries (Pretoria, South Africa), Thermo Fisher Scientific (Waltham, USA), Zymo Research (USA), GE Healthcare (USA), Bio-Rad (California, USA), GenScript Biotech (Piscataway, USA), Macherey-Nagel (Nordrhein-Westfalen, Germany), Glentham Life Sciences (UK), New England Biolabs® (Massachusetts, USA), Cytiva (USA), Nebraska (USA), and Gibco (New York, USA).

7.3 Equipment

Table 7.1: Equipment used for the experimental process of this study

Equipment	**Manufacturer**
Agarose Gel electrophoresis system	Bio-Rad (Sub-cell GT mini and widemini)
Autoclave	Equitron® (Autoclave SLEFA)
BSLII Cabinet	ESCO Life Technologies (Airstream AC2-458)
Cell counter	Bio-Rad (TC20 automated cell counter)
Centrifuge	Beckman Coulter (Allegra X-30R)
CO2 Incubator	NuAire (NU-5800E)
Confocal microscope	Carl Zeiss (LSM-880 Airyscan
Deep-well plates	faCellitate (P-DW-20-C-S)

Electrophoresis power supply	Bio-Rad (PowerPac™ HC)
Gel documentation	Bio-Rad (Molecular Imager® Gel Doc™ XR+ Imaging System)
Heating block	Eppendorf (Thermomixer Comfort)
Hot plate and magnetic stirrer	Fried Electric (MH-4)
Immobilized Metal Affinity Chromatography (IMAC) system	GE Healthcare (ÄKTA Avant 25)
Microcentrifuge	Labnet (Prism C2500-230V)
Microplate reader	Star Lab (Microcentrifuge 24)
Microscope	Bio-Rad (iMark)
Microwave	Defy (DMO 390)
Multichannel pipette, 2-20 L	Gilson PIPETMAN® (P8X20)
pH meter	Dostmann Electronic (pH50+DHS)
Pipettes	Discovery Pro (Pipette starter kit)
Scale	RadWag (PS 600.R2
Shaking incubator	Yinder Co Ltd (LM-510RD)
Sonicator	Qsonica L.L.C (Qsonica)
Spectrophotometer for DNA/P	Denovix (Denovix Ds-11)
Spectrophotometer for optical density	Eppendorf (BioPhotometer plus)
SpeedVac drier	SP Scientific (miVAC DNA-23050-L00)
TC Hood	Labgard (BSC Class II biological safety cabinet)
Tissue culture incubator	Nuaire (In-VitroCell
Trans-Blot® transfer system	Bio-Rad (Turbo™)
UV Transilluminator for WB documentation	Syngene (G:Box Chemi XL
Vortex	Laboratory and Medical Supplies (VTX3000L)
Water purification system	Milli-Q (Direct-Q® 3UV)
Western Blot	Bio-Rad (Trans-Blot Cell)

7.4 Molecular Cloning Reagents

All Media and specific buffers were prepared following the manufacturer's instructions using de-ionized water. Media and specific buffers underwent autoclaving at 121ºC for 20 minutes to name the PBS, Luria Bertani Agar/ broth, and terrific broth IMAC buffers were sterile filtered using a 0.45µm filter and degassed. Antibiotics (ampicillin and kanamycin) (Sigma-Aldrich) and Isopropyl-ß-d-1- thi ogalactopyranoside (IPTG) were filter-sterilized and the stock solutions stored at -20ºC.The pH of the buffers was adjusted by titration using 1M HCl (acidic) or 10M NaOH(basic).

Table 7.2: The composition of media used for bacterial transformation in molecular cloning

REAGENT	**Composition**	**Concentration**
Luria Bertani (LB) broth	Yeast extract Peptone NaCl	0.5% (w/v) 1% (w/v) 1%(w/v)
LB agar	Yeast extract Peptone NaCl Agar	0.5%(w/v) 1% (w/v) 1% (w/v) 1.5%(w/v)
SOC	Peptone Yeast extract NaCl KCl MgCl2 MgSO4 Glucose	2% (w/v) 0.5% (w/v) 10mM 25mM 10mM 10mM 20Mm

Table 7.3: Restriction digestion of pUC57 and pMT-“x”(scFv)-dETA/ETA

Reagent	**Volume**
SfiI enzyme (2000 units/mL)	1µL
NotI enzyme (2000 units/mL)	1µL
Cut Smart Buffer®	1µL
Plasmid DNA (pUC57 or pMT-’x’(scFv)- dETA/ETA)	2µg
Nuclease free water	50µL

Table 7.4: Buffer recipes and composition for agarose gel electrophoresis

Reagents	**Composition**	**Concentration**
10x TAE (pH7.5)	Tris Base Glacial acetic acid EDTA	0.4M 1.14% (v/v) 10mM
1.2% agarose gel	agarose powder 1x TAE buffer SYBR™ Safe	1.2% w/v 100ml (Total volume) 10%

Table 7.5: Reaction reagents for ligation of the scFv inserted into the pMT-scFv-ETA/dETA vector.

	1:5	**1:3**	**1:1**	**1:0**
Vector DNA (backbone /pMT-(scFv)-dETA/ETA)	50ng	50ng	50ng	50ng
Insert DNA	Dependent on ratio and fragment size (calculated	Dependent on ratio and fragment size (calculated	Dependent on ratio and fragment size (calculated	-

	using NEB Calculator	using NEB Calculator	using NEB Calculator	
T4 DNA ligase	1µL	1µL	1µL	1µL
T4 DNA ligase buffer	2µL	2µL	2µL	2µL
DdH_2O	20µL	20µL	20µL	20µL

The materials required for the ligation reaction included the following: ice, Parafilm M® (catalogue number: PM996), a Zyppy Miniprep purification kit, T4 DNA ligase and buffer, a ligation reaction mixture, a heating block, SOC, LB broth (250 mL), 15 mL round-bottom tubes, Eppendorf® microtubes, LB agar plates supplemented with kanamycin (50 mg/mL), pipettes, pipette tips, and an incubator with a shaker.

Table 7.6: Restriction mapping reagents

Reagent	**Volume**
Restriction Enzyme (Maub1, XbaI, SacI and PvuII)	1µL (per enzyme)
Cut Smart Buffer®	1 µL (per enzyme)
Plasmid DNA from colonies	1µg
ddH2O	Topped up to 20µL

7.4.1 Bacterial strains

DH5 alpha and BL21 (DE3) *E. coli* were the two strains used in this study. The DH5 alpha strain was used for all the cloning steps and for the expression of the recombinant fusion protein BL21(DE3) strain was used. The two strains are described below in the table.

Table 7.7: *E.coli* strain used for the entire

Strain	Genotype	Source
Escherichia coli (*E. coli*) DH5 alpha	*supE44 ΔlacU169 (F80 lacZΔM15) hsdR17 recA1 endA1gyrA96 thi-1 relA1*	New England Biolabs, USA
Escherichia coli (E. coli) BL21(DE3)	*F- ompT hsdSB (rB- mB-) gal dcm- lon*	New England Biolabs, USA

7.5 Protein expression

Table 7.8: Buffer recipes for bacterial expression

Reagent	Composition	Quantity/ Concentration
Terrific broth (Autoclaved at 121 °C for 20 minutes (stored at 4 °C)	Peptone Yeast Extract NaCl	47.6g
	Glycerol	8mL
	ddH_2O	Topped up to 1L
Isopropyl-ß-d-1-thiogalactopyranoside (IPTG) (1M) (stored at -20 °C	IPTG powder	1.19 g
	ddH_2O	5mL
Compatible solute		
Compatible solute	Betaine monohydrate (4 °C)	40 mM
	D-glucose	35 g/L (35 mg/ml)
	D-sorbitol	0.5 M
	NaCl	4% (w/v)
	$ZnCl_2$	0.5 mM
	Terrific broth media	Topped up to 100 mL

Lysis buffer		
Lysis buffer	DL-Dithiothreitol (DTT)	5 mM
	Glycerol	10% (v/v)
	NaCl	300 mM
	Protease inhibitor tablet	1 tablet/100 mL
	Tris-HCl pH 8.0	75 mM
	ddH_2O	Topped up to 200 mL

7.6 Protein purification

Table 7.9: First IMAC purification buffers recipes.

Buffer weight	**Reagent**	**Molecular**	**Concentration**
Loading/wash buffer (pH 8.0)	Tris-base	121 g/mol	100mM
	NaCl	58.5g/mol	1M
	Type 1 Water		1L
Elution buffer (pH 8.0	Tris Base	121 g/mol	100mM
	NaCl	58.5 g/mol	1M
	Imidazole	68.08 g/mol	250mM
	Type 1 Water		1L
Buffer exchange			
Buffer exchange buffer (pH 8.0)	Tris-base	121 g/mol	20mM
	NaCl	58.5g/mol	1M
	Type 1 Water		1L

Table 7.10: Second IMAC purification buffer recipes.

Buffer	Reagent	Molecular weight	Concentration
Loading buffer (pH 8.0)	Tris-base	121 g/mol	20mM
	NaCl	58.5g/mol	500M
	Imidazole	68.08 g/mol	10mM
	Type 1 Water		1L
Wash buffer	Tris-base	121 g/mol	20mM
	NaCl	58.5g/mol	500M
	Imidazole	68.08 g/mol	30mM
	Type 1 Water		1L
Elution Buffer (pH 8.0)	Tris-base	121 g/mol	20mM
	NaCl	58.5g/mol	500M
	Imidazole	68.08 g/mol	250mM
	Type 1 Water		1L

All the buffers used for purification were degassed using Vacuum Degassing to prevent issues like air bubbles and ensure the accuracy of chemical reactions. They were then filtered using a 0.22/0.45 µm PVDF membrane.

7.7 Functionality assay

Table 7.11: Cell lines for in vitro studies.

Cell line	The American Type Culture Collection (ATCC)	Origin
Ca Ski	CRL-1550	The cervix of a White, 40-year-old female patient with epidermoid carcinoma, American Type Culture Collection (ATCC, USA)

HeLa	CCL-2	Cervical carcinoma derived from a 31-year-old patient, American Type Culture Collection (ATCC, USA)
ME-180	HTB-33	The uterus of a 66-year-old, White female patient with epidermoid carcinoma, American Type Culture Collection (ATCC, USA)
SiHa	HTB-35	Fragments of a primary uterine tissue sample from a 55-year-old female Japanese patient with squamous cell carcinoma, American Type Culture Collection (ATCC, USA)
HEK293t	CRL-3216	An epithelial-like cell that was isolated from the kidney of a patient

Table 7.12: Reagents for conjugation of the anti-His PE antibody Fluorophore to an rIT.

Reagent	**Concentration**
PBS	1x
DTT	1 mM
anti-His-Tag PE	10 µM
Recombinant immunotoxin (ETA/dETA	5 µM
Total	50 µl

Table 7.13: Reagent and equipment for rIT functionality testing.

Equipment / Reagent	**Source**
RPMI 1640 Medium	Gibco (52400-025)
DMEM	Gibco (41965-039)
T25 culture flask	SPL Life Sciences (70012)
Penicillin-Streptomycin	Gibco (15140122)
10X Trypsin /EDTA	Sigma-Aldrich (T4174

Mowiol	Merck (475904)
0.4% Trypan blue solution	Thermo Fisher (15250061)
Anti-fade (propyl-gallate)	Sigma Aldrich (P3130)
4% PFA	Thermo Fisher (J19943.K2)
6-Well plate	SPL Life Sciences (30006)
Anti-His PE conjugate /fluorophore	RnD Systems (IC050P)
DL-Dithiothreitol (DTT	Sigma-Aldrich (43819-25G)
Cell proliferation kit II (XTT)	Roche (11465015001
Zeocin™ Selection Reagen	Gibco (R25005)
Reagent Reservoirs	Thermo Fisher (95128095)